ESAIM: M2AN 51 (2017) 1429–1471
DOI: 10.1051/m2an/2016069

ESAIM: Mathematical Modelling and Numerical Analysis
www.esaim-m2an.org

DIMENSIONAL MODEL REDUCTION FOR FLOW THROUGH FRACTURES IN POROELASTIC MEDIA

Martina Bukač[1,*], Ivan Yotov[2,**] and Paolo Zunino[3,4,***]

Abstract. We study the interaction between a poroelastic medium and a fracture filled with fluid. The flow in the fracture is described by the Brinkman equations for an incompressible fluid and the poroelastic medium by the quasi-static Biot model. The two models are fully coupled *via* the kinematic and dynamic conditions. The Brinkman equations are then averaged over the cross-sections, giving rise to a reduced flow model on the fracture midline. We derive suitable interface and closure conditions between the Biot system and the dimensionally reduced Brinkman model that guarantee solvability of the resulting coupled problem. We design and analyze a numerical discretization scheme based on finite elements in space and the Backward Euler in time, and perform numerical experiments to compare the behavior of the reduced model to the full-dimensional formulation and study the response of the model with respect to its parameters.

Mathematics Subject Classification. 76S05, 76D07, 74F10, 65M60, 65M12.

Received October 21, 2015. Accepted November 7, 2016.

1. Introduction

Computational modeling of flows in fractured oil and gas reservoirs is increasingly attracting the attention of the scientific community. Naturally occurring fractures may affect significantly the effective flow rates. Furthermore, an increasing fraction of hydrocarbon supply for western countries is coming from shale oil and gas. Hydraulic fracturing is the main technology for extraction of these natural resources. Efficient exploitation of trapped hydrocarbons requires careful reservoir management.

The problem of modeling fluid injection, flow and fracture propagation through reservoirs is challenging. Typical fractures are only 10−100 μm thin and they extend for 10−100 m. In the process of creating new fractures or opening existing ones, the injected flow rate in wells can exceed 10^{-3} m^3/s, namely one liter per

Keywords and phrases. Reduced model, fracture flow, poroelasticity.

[1] Department of Applied and Computational Mathematics and Statistics, University of Notre Dame, Indiana 46556, USA.
[2] Department of Mathematics, University of Pittsburgh, Pittsburgh, PA 15260, USA.
[3] MOX, Department of Mathematics, Politecnico di Milano, 20133 Milano, Italy.
[4] Department of Mechanical Engineering and Materials Science, University of Pittsburgh, PA 15260, USA.
paolo.zunino@polimi.it

* Partially supported by NSF grants DMS-1318763 and DMS-1619993.
** Partially supported by DOE grant DE-FG02-04ER25618 and NSF grant DMS 1418947.
*** Partially supported by DOE grant DE-FG02-04ER25618.

Article published by EDP Sciences

second, which induces a significant fracture front propagation speed, up to one meter per second. These numbers outline a complex dynamic scenario, where fluid flow and solid mechanics are tightly coupled.

Models that employ Darcy's law in the fracture and the reservoir have been developed in [1, 2, 12, 15, 26, 30, 34, 35], see also extensions to two-phase flow in [17, 25]. More recently, models that account for faster flow within the fracture have been investigated, including Forchheimer [16], Brinkman [28], and Reynolds lubrication equations [18, 19, 21]. Attention has also been given to development of partitioned non-iterative or iterative algorithms. For example, in [8], a non-iterative Nitsche's coupling approach is developed for the Stokes–Biot system using the mixed formulation for Darcy flow, while an operator-splitting method for a coupled Navier–Stokes - Biot model has been developed in [9]. The Biot system can be further split into elasticity and flow sub-problems using either non-iterative [8] or iterative coupling [32].

Geometrical model reduction techniques for coupled flow through fractures and porous media are commonly used in the literature [2, 26, 28, 30]. In this approach the fractures are modeled as manifolds of one dimension less than the reservoir. This is done by averaging of the flow equation along the fracture aperture, in order to reduce the computational cost of coupling the flow through a reservoir with the one in the fractures, because this approach avoids fine meshing of the fracture domain, which becomes technically challenging in those cases where the aperture is small. The main issue of this approach consists in the determination of appropriate interface conditions between reservoir and fracture, which may depend on the models used in each region.

The objective of this work is to develop a reduced model for coupled flow through fractured reservoirs while accounting for the deformation of the porous media. As mentioned above, during the hydraulic fracturing process, fluid flow and rock mechanics are tightly coupled. Our model is based on coupling the Brinkman equations in the fracture with the Biot system of poroelasticity [6, 45] in the reservoir. Our approach is similar to the one in [28], where a reduced model for the interaction between porous medium and Brinkman model is developed, but no poroelastic effects are considered. The resulting reduced Brinkman–Biot model is an alternative to the lubrication-Biot model studied in [18,19,21]. A notable difference between the two approaches is in the continuity condition between the poroelastic stress in the reservoir and the fluid stress in the fracture. In particular, the Brinkman model allows for full continuity between the two stress tensors, see (2.11), while with the lubrication equation the normal poroelastic stress vector is balanced with the normal vector to the interface scaled by the fluid pressure in the fracture. Furthermore, the Brinkman model requires an additional interface condition for the tangential fluid stress. While in [28] zero tangential stress was imposed, here we employ the Beavers–Joseph–Saffman condition [5, 42], which is widely accepted in modeling coupled Stokes–Darcy flows [13,20,27]. We note that full-dimensional Stokes–Biot models have been studied in [4, 8, 31, 44].

To discretize the problem in time, we employ the Backward Euler method for time discretization, which results in solving a coupled Brinkman–Biot system at each time step. In this work we treat stationary fractures. Fracture propagation has been modeled using level set methods [10, 22], phase-field methods [33], or boundary element methods [41]. Incorporating some of these techniques into the Brinkman–Biot model is a topic of future research.

The rest of the paper is organized as follows. In Section 2 we introduce the governing equations of the problem. Without loss of generality, but with considerable simplification of the notation, we present the problem in two spatial dimensions. In Section 3 we present the topological model reduction technique that enables us to represent the fracture as a curve embedded into the reservoir. Particular attention is given to the derivation of interface conditions based on closure assumptions for the pressure and velocity profiles in the fracture cross sections. To our knowledge, this is the first time this issue is addressed for the case of Brinkman flow coupled with the Biot model for the reservoir. The variational formulation and its numerical discretization based on finite elements in space and the Backward Euler in time is presented in Section 4, where the well posedness of the latter is also discussed. The numerical error of the proposed scheme is analyzed in Section 4.2 following the general approach in the sequence of works for the Biot system [37–39], extended here to the coupled reservoir/fracture problem. Numerical results that validate the correct behavior of the mathematical model and of the numerical scheme are presented in Section 5. In particular, we verify the convergence rate of the spatial discretization error, compare

the results to the full dimensional model and analyze the model response to variations of the fluid and rock parameters.

2. Description of the problem

Consider a bounded, two-dimensional domain $\Omega = \Omega_p \cup \Omega_f$. Region Ω_p is occupied by a fully-saturated poroelastic matrix and region Ω_f represents a fracture filled with fluid. We assume that Ω_f is a non self-intersecting strip with a constant aperture, which is *small* with respect to the size of the surrounding poroelastic media. We denote the two long edges of the fracture with Γ_1 and Γ_2, see Figure 1. Let $\Gamma_f = \partial\Omega_f \setminus (\Gamma_1 \cup \Gamma_2)$ be the union of the two short edges of the fracture. We allow for none, one, or both of the short edges to be on the outside boundary $\partial\Omega$, corresponding to the fracture being entirely confined in the poroelastic domain, having one confined end, or splitting the poroelastic domain in two parts. The dynamics in the poroelastic domain Ω_p is described by the Biot model. The stress tensor of the poroelastic medium is given by $\boldsymbol{\sigma}_p = \boldsymbol{\sigma}_E - \alpha p \boldsymbol{I}$, where $\boldsymbol{\sigma}_E$ denotes the elasticity stress tensor, p is the fluid pressure, and the Biot–Willis constant α is the pressure-storage coupling coefficient. With the assumption that the displacement $\boldsymbol{\eta} = (\eta_x, \eta_y)$ of the skeleton is connected to stress tensor $\boldsymbol{\sigma}_E$ *via* the linear elastic model, we have $\boldsymbol{\sigma}_E(\boldsymbol{\eta}) = 2\mu \boldsymbol{D}(\boldsymbol{\eta}) + \lambda \mathrm{tr}(\boldsymbol{D}(\boldsymbol{\eta}))\boldsymbol{I}$, where μ and λ denote the Lamé coefficients for the skeleton. Furthermore, we assume that the domain Ω_p does not change in time and with the hypothesis of infinitesimal deformations, we have $\boldsymbol{D}(\boldsymbol{\eta}) = (\nabla\boldsymbol{\eta} + (\nabla\boldsymbol{\eta})^T)/2$. Then, the Biot equations read as follows:

$$-\nabla \cdot \boldsymbol{\sigma}_p = \boldsymbol{f}_p \qquad \text{in} \quad \Omega_p \times (0,T], \tag{2.1}$$

$$\boldsymbol{K}^{-1}\boldsymbol{q} = -\nabla p \qquad \text{in} \quad \Omega_p \times (0,T], \tag{2.2}$$

$$\frac{\partial}{\partial t}(s_0 p + \alpha \nabla \cdot \boldsymbol{\eta}) + \nabla \cdot \boldsymbol{q} = g \qquad \text{in} \quad \Omega_p \times (0,T]. \tag{2.3}$$

System (2.1)–(2.3) consists of the momentum equation for the balance of total forces (2.1), the Darcy law (2.2), and the storage equation (2.3) for the fluid mass conservation in the pores of the matrix, where $\boldsymbol{q}$ is the Darcy velocity. The coefficient $s_0 > 0$ is the storage coefficient and $\boldsymbol{K}$ denotes a symmetric uniformly positive definite hydraulic conductivity tensor satisfying, for some constants $0 < k_0 \le k_1$,

$$k_0 \boldsymbol{\xi}^T\boldsymbol{\xi} \le \boldsymbol{\xi}^T \boldsymbol{K} \boldsymbol{\xi} \le k_1 \boldsymbol{\xi}^T\boldsymbol{\xi}, \quad \forall\, \boldsymbol{\xi}(\boldsymbol{x}) \in \mathbb{R}^2,\ \forall \boldsymbol{x} \in \Omega_p. \tag{2.4}$$

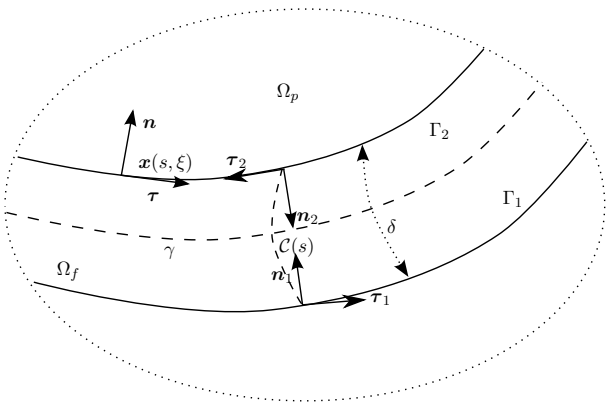

FIGURE 1. Configuration of the fluid and porous domains, Ω_p and Ω_f respectively, and of the curvilinear coordinate system introduced for the definition of the topological model reduction in the fracture.

Let $\Gamma_p = \Gamma_p^D \cup \Gamma_p^N = \Gamma_p^p \cup \Gamma_p^q$ be two partitions of $\Gamma_p = \partial\Omega_p \cap \partial\Omega$. We prescribe the following boundary conditions on Γ_p,

$$\begin{aligned} &\boldsymbol{\eta} = 0 && \text{on } \Gamma_p^D \times (0,T], \\ &\boldsymbol{\sigma}_p \boldsymbol{n}_p = \boldsymbol{s}_p^N && \text{on } \Gamma_p^N \times (0,T], \\ &p = p^D && \text{on } \Gamma_p^p \times (0,T], \\ &\boldsymbol{q} \cdot \boldsymbol{n}_p = 0 && \text{on } \Gamma_p^q \times (0,T], \end{aligned}$$

where $\boldsymbol{n}_p$ is the outward unit normal on Γ_p. In order to guarantee uniqueness of the solution, we assume that $|\Gamma_p^D| > 0$ and $|\Gamma_p^p| > 0$. If Ω_p is split by Ω_f in two parts, we assume that each part has a piece of Γ_p^D and Γ_p^p. We also prescribe the pressure and the displacement fields at the initial time:

$$p(0) = p_0, \quad \boldsymbol{\eta}(0) = \boldsymbol{\eta}_0 \text{ in } \Omega_p.$$

To model the flow in the fracture, we use the Brinkman model, which is a valid approximation of the Navier–Stokes equations for incompressible fluids at low Reynolds numbers in presence of friction due to debris in the fracture bed,

$$\boldsymbol{K}_f^{-1}\boldsymbol{u} - \mu_f \Delta \boldsymbol{u} + \nabla p_f = \boldsymbol{f}_f \quad \text{in} \quad \Omega_f \times (0,T], \tag{2.5}$$

$$\nabla \cdot \boldsymbol{u} = h \quad \text{in} \quad \Omega_f \times (0,T]. \tag{2.6}$$

Here $\boldsymbol{u} = (u_x, u_y)$ is the fluid velocity, p_f is the fluid pressure, $\boldsymbol{K}_f$ is a symmetric uniformly positive definite hydraulic conductivity tensor (sometimes called *drag coefficient*, see for example [40]), and μ_f is the Brinkman viscosity. We assume that there exist constants $0 < k_{f,0} \le k_{f,1}$ such that

$$k_{f,0}\boldsymbol{\xi}^T\boldsymbol{\xi} \le \boldsymbol{\xi}^T \boldsymbol{K}_f \boldsymbol{\xi} \le k_{f,1}\boldsymbol{\xi}^T\boldsymbol{\xi}, \quad \forall\, \boldsymbol{\xi}(\boldsymbol{x}) \in \mathbb{R}^2,\ \forall \boldsymbol{x} \in \Omega_f. \tag{2.7}$$

For simplicity of notation, we introduce

$$\boldsymbol{\sigma}_f = \mu_f \nabla \boldsymbol{u} - p_f \boldsymbol{I}.$$

We note that $\boldsymbol{\sigma}_f$ is not a physical stress tensor, but we may call it that, abusing notation. Furthermore, because we are using $\nabla \boldsymbol{u}$, the coupling conditions below are an approximation. A similar simplification has been made in [28]. Handling the symmetric gradient would lead to additional problems in derivation of the closure conditions, which is outside the scope of the paper.

The boundary conditions on $\Gamma_f = \Gamma_f^D \cup \Gamma_f^N$ are

$$\begin{aligned} &\boldsymbol{u} = \boldsymbol{u}^D && \text{on} \quad \Gamma_f^D \times (0,T], \\ &\boldsymbol{\sigma}_f \boldsymbol{n}_f = 0 && \text{on} \quad \Gamma_f^N \times (0,T], \end{aligned}$$

where $\boldsymbol{n}_f$ is the outward unit normal vector on $\partial\Omega_f$. If an edge from Γ_f is not on the boundary $\partial\Omega$, a physically reasonable boundary condition is $\boldsymbol{u} = 0$, which is motivated by the fact that the aperture is very small and the flux across a short edge is negligible relative to the flux across the transversal edges. Similar condition is considered in [2]. Alternatively, one can assign the stress-free outflow condition $\boldsymbol{\sigma}_f \boldsymbol{n}_f = 0$. To guarantee uniqueness of the fluid pressure, we assume that $|\Gamma_f^N| > 0$. Let $\boldsymbol{\tau}_f$ be the unit tangential vector on $\partial\Omega_f$ such that $\boldsymbol{\tau}_f$ and $\boldsymbol{n}_f$ form a positively oriented coordinate system. To couple the Biot problem (2.1)–(2.3) with the Brinkman equations (2.5)–(2.6), we prescribe the following coupling conditions on Γ_i, $i = 1, 2$.

Mass conservation: the continuity of normal flux yields

$$\boldsymbol{u} \cdot \boldsymbol{n}_f = \left(\frac{\partial \boldsymbol{\eta}}{\partial t} + \boldsymbol{q} \right) \cdot \boldsymbol{n}_f \quad \text{on } \Gamma_i \times (0,T]. \tag{2.8}$$

Beavers–Joseph–Saffman condition: the tangential component of the fluid stress is proportional to the slip velocity

$$\boldsymbol{\tau}_f \cdot \boldsymbol{\sigma}_f \boldsymbol{n}_f = -c_{BJS}(\boldsymbol{u} - \frac{\partial \boldsymbol{\eta}}{\partial t}) \cdot \boldsymbol{\tau}_f \quad \text{on } \Gamma_i \times (0,T]. \tag{2.9}$$

Balance of normal components of the stress in the fluid phase

$$\boldsymbol{n}_f \cdot \boldsymbol{\sigma}_f \boldsymbol{n}_f = -p \quad \text{on } \Gamma_i \times (0,T]. \tag{2.10}$$

Conservation of momentum: the sum of contact forces at the fracture-poroelastic medium interface is equal to zero:

$$\boldsymbol{\sigma}_f \boldsymbol{n}_f = \boldsymbol{\sigma}_p \boldsymbol{n}_f \quad \text{on } \Gamma_i \times (0,T]. \tag{2.11}$$

3. Derivation of a dimensionally reduced model for the fracture

We assume that Ω_f admits a curvilinear, orthogonal coordinate system (see Fig. 1) defined by the arc length $s \in [0, L]$ and by a transversal coordinate ξ. For any fixed $s \in [0, L]$, let the cross-section $\mathcal{C}(s)$ be the locus of points obtained by varying ξ, and let the length of $\mathcal{C}(s)$ be δ, *i.e.*, the aperture of Ω_f. The orthogonal coordinate system is then $(s, \xi) \in [0, L] \times \frac{\delta}{2}[-1, 1]$ with an orthonormal local basis $\boldsymbol{\tau}, \boldsymbol{n}$. Let γ be the *midline* of Ω_f defined as the isoline $\xi = 0$. More precisely we have,

$$\gamma = \{(s,0)\},\ \Gamma_1 = \left\{ \left(\frac{-\delta}{2} \right) \right\},\ \Gamma_2 = \left\{ \left(\frac{+\delta}{2} \right) \right\},\ \mathcal{C} = \left\{ (s,\xi) : \xi \in \frac{\delta}{2}[-1,1] \right\},\quad s \in [0,L].$$

Let us denote with $\boldsymbol{n}_1$ and $\boldsymbol{n}_2$ the outward unit normal vectors to Ω_p on Γ_1 and Γ_2, respectively. According to the notation above (*e.g.* Fig. 1) we also have

$$\boldsymbol{n}_1 = \boldsymbol{n} = -\boldsymbol{n}_f,\ \boldsymbol{\tau}_1 = \boldsymbol{\tau} = -\boldsymbol{\tau}_f \ \text{ on } \ \Gamma_1; \quad \boldsymbol{n}_2 = -\boldsymbol{n} = -\boldsymbol{n}_f,\ \boldsymbol{\tau}_2 = -\boldsymbol{\tau} = -\boldsymbol{\tau}_f \ \text{ on } \ \Gamma_2.$$

Then, we rewrite the coupling conditions (2.8)–(2.11) using the notation of Figure 1:

$$\boldsymbol{u} \cdot \boldsymbol{n}_i = \left(\frac{\partial \boldsymbol{\eta}_i}{\partial t} + \boldsymbol{q}_i \right) \cdot \boldsymbol{n}_i \qquad \text{on } \Gamma_i \times (0,T], \tag{3.1}$$

$$\boldsymbol{\tau}_i \cdot \boldsymbol{\sigma}_f \boldsymbol{n}_i = c_{BJS}(\boldsymbol{u} - \frac{\partial \boldsymbol{\eta}_i}{\partial t}) \cdot \boldsymbol{\tau}_i \qquad \text{on } \Gamma_i \times (0,T], \tag{3.2}$$

$$\boldsymbol{n}_i \cdot \boldsymbol{\sigma}_f \boldsymbol{n}_i = -p_i \qquad \text{on } \Gamma_i \times (0,T], \tag{3.3}$$

$$\boldsymbol{\sigma}_f \boldsymbol{n}_i = \boldsymbol{\sigma}_p \boldsymbol{n}_i \qquad \text{on } \Gamma_i \times (0,T]. \tag{3.4}$$

In the Cartesian reference frame $\boldsymbol{x}$, we denote by $\mathrm{d}\boldsymbol{\tau}, \mathrm{d}\boldsymbol{n}$ the differentials in the direction orthogonal and tangential to $\mathcal{C}$, respectively, which correspond to $ds, \mathrm{d}\xi$ in the local reference frame (s, ξ). Furthermore, there exists a bijective mapping between points on γ and Γ_i. As a result, any function trace on Γ_i $(i = 1, 2)$ can be mapped onto Γ_j $(i \neq j)$ and onto γ. For notational convenience, we denote this class of three equivalent functions as $(\cdot)|^*_{\Gamma_i}$ where $|_{\Gamma_i}$ denotes where the trace is defined and $|^*$ denotes that it can be mapped on γ and Γ_j. In this way, in the derivation of the reduced model we will be able to formally combine traces on Γ_1, Γ_2, and γ. Furthermore, we only adopt this notation for variables defined on Γ_i, while it is implicitly assumed that the variables of the reduced model for the fracture flow are defined on γ.

For the derivation of the reduced model, we will exploit the following property of integrals along the curve $\mathcal{C}$,

$$f\left(\frac{+\delta}{2} \right) - f\left(\frac{-\delta}{2} \right) = \int_{\mathcal{C}} \frac{\partial f(s,\xi)}{\partial \xi} \mathrm{d}\xi = \int_{\mathcal{C}} \frac{\partial f(\boldsymbol{x})}{\partial \boldsymbol{n}} \mathrm{d}\boldsymbol{n}. \tag{3.5}$$

To derive a reduced model, we project the Brinkman equations in the fracture on the local orthogonal system, and then we average the resulting equations over the corresponding $\mathcal{C}-$curves in Ω_f. We start by projecting the mass conservation equation (2.6) in Ω_f on the local orthogonal reference system:

$$\nabla \cdot \boldsymbol{u} = \frac{\partial \boldsymbol{u}}{\partial \boldsymbol{n}} \cdot \boldsymbol{n} + \frac{\partial \boldsymbol{u}}{\partial \boldsymbol{\tau}} \cdot \boldsymbol{\tau} = h.$$

Integrating the latter equation over the corresponding curve $\mathcal{C}$, we get

$$(\boldsymbol{u} \cdot \boldsymbol{n}) \left(\frac{+\delta}{2} \right) - (\boldsymbol{u} \cdot \boldsymbol{n}) \left(\frac{-\delta}{2} \right) + \frac{\partial}{\partial s} \int_{\mathcal{C}} \boldsymbol{u}(s,\xi) \cdot \boldsymbol{\tau} \mathrm{d}\xi = \int_{\mathcal{C}} h \mathrm{d}\xi.$$

Recalling that $\boldsymbol{u} \left(\frac{+\delta}{2} \right) \cdot \boldsymbol{n} = -\boldsymbol{u} \cdot \boldsymbol{n}_2|^*_{\Gamma_2}$ and that $-\boldsymbol{u} \left(\frac{-\delta}{2} \right) \cdot \boldsymbol{n} = -\boldsymbol{u} \cdot \boldsymbol{n}_1|^*_{\Gamma_1}$ and employing the kinematic coupling condition (3.1) we obtain a one-dimensional mass conservation equation on γ:

$$\delta \left(\frac{\partial U_\tau}{\partial \boldsymbol{\tau}} - H \right) = \left(\frac{\partial \boldsymbol{\eta}_1}{\partial t} \cdot \boldsymbol{n}_1 + \boldsymbol{q}_1 \cdot \boldsymbol{n}_1 \right) \Big|^*_{\Gamma_1} + \left(\frac{\partial \boldsymbol{\eta}_2}{\partial t} \cdot \boldsymbol{n}_2 + \boldsymbol{q}_2 \cdot \boldsymbol{n}_2 \right) \Big|^*_{\Gamma_2} \quad \text{on } \gamma, \tag{3.6}$$

where we have defined mean values as follows,

$$U_\tau = \frac{1}{\delta} \int_{\mathcal{C}} \boldsymbol{u} \cdot \boldsymbol{\tau} \mathrm{d}\boldsymbol{n} \quad \text{and} \quad H = \frac{1}{\delta} \int_{\mathcal{C}} h \mathrm{d}\boldsymbol{n}. \tag{3.7}$$

Let R be the orthonormal matrix mapping the canonical basis $[\boldsymbol{e}_1, \boldsymbol{e}_2]$ onto the local basis $[\boldsymbol{n}, \boldsymbol{\tau}]$

$$R = \begin{bmatrix} \boldsymbol{n}^T \\ \boldsymbol{\tau}^T \end{bmatrix} = \begin{bmatrix} \boldsymbol{n}^T \\ 0 \end{bmatrix} + \begin{bmatrix} 0 \\ \boldsymbol{\tau}^T \end{bmatrix}.$$

To project equation (2.5) on the local orthogonal system, we apply matrix R to (2.5)

$$R \boldsymbol{K}_f^{-1} R^T R \boldsymbol{u} - \mu_f R \Delta \boldsymbol{u} + R \nabla p_f = R \boldsymbol{f}_f. \tag{3.8}$$

For two vectors $\boldsymbol{a}$ and $\boldsymbol{b} \in \mathbb{R}^2$ we define $M(\boldsymbol{a}, \boldsymbol{b}) = \boldsymbol{a}^T \boldsymbol{K}_f^{-1} \boldsymbol{b}$. Using this notation and relation

$$\Delta \boldsymbol{u} = \frac{\partial^2 \boldsymbol{u}}{\partial \boldsymbol{n}^2} + \frac{\partial^2 \boldsymbol{u}}{\partial \boldsymbol{\tau}^2},$$

we split equation (3.8) as follows

$$M(\boldsymbol{n}, \boldsymbol{n}) \boldsymbol{u} \cdot \boldsymbol{n} + M(\boldsymbol{n}, \boldsymbol{\tau}) \boldsymbol{u} \cdot \boldsymbol{\tau} - \mu_f \left(\frac{\partial^2 \boldsymbol{u}}{\partial \boldsymbol{n}^2} + \frac{\partial^2 \boldsymbol{u}}{\partial \boldsymbol{\tau}^2} \right) \cdot \boldsymbol{n} + \frac{\partial p_f}{\partial \boldsymbol{n}} = \boldsymbol{f}_f \cdot \boldsymbol{n}, \tag{3.9}$$

$$M(\boldsymbol{\tau}, \boldsymbol{n}) \boldsymbol{u} \cdot \boldsymbol{n} + M(\boldsymbol{\tau}, \boldsymbol{\tau}) \boldsymbol{u} \cdot \boldsymbol{\tau} - \mu_f \left(\frac{\partial^2 \boldsymbol{u}}{\partial \boldsymbol{n}^2} + \frac{\partial^2 \boldsymbol{u}}{\partial \boldsymbol{\tau}^2} \right) \cdot \boldsymbol{\tau} + \frac{\partial p_f}{\partial \boldsymbol{\tau}} = \boldsymbol{f}_f \cdot \boldsymbol{\tau}. \tag{3.10}$$

Integrating equations (3.9) and (3.10) over s-curves $\mathcal{C}$ we get

$$\delta M(\boldsymbol{n}, \boldsymbol{n}) U_n + \delta M(\boldsymbol{n}, \boldsymbol{\tau}) U_\tau - \mu_f \left(\frac{\partial \boldsymbol{u}}{\partial \boldsymbol{n}} \cdot \boldsymbol{n} \Big|^*_{\Gamma_2} - \frac{\partial \boldsymbol{u}}{\partial \boldsymbol{n}} \cdot \boldsymbol{n} \Big|^*_{\Gamma_1} \right) - \delta \mu_f \frac{\partial^2 U_n}{\partial \boldsymbol{\tau}^2} + p_f|^*_{\Gamma_2} - p_f|^*_{\Gamma_1} = \delta F^f_n, \tag{3.11}$$

$$\delta M(\boldsymbol{\tau}, \boldsymbol{n}) U_n + \delta M(\boldsymbol{\tau}, \boldsymbol{\tau}) U_\tau - \mu_f \left(\frac{\partial \boldsymbol{u}}{\partial \boldsymbol{n}} \cdot \boldsymbol{\tau} \Big|^*_{\Gamma_2} - \frac{\partial \boldsymbol{u}}{\partial \boldsymbol{n}} \cdot \boldsymbol{\tau} \Big|^*_{\Gamma_1} \right) - \delta \mu_f \frac{\partial^2 U_\tau}{\partial \boldsymbol{\tau}^2} + \delta \frac{\partial P}{\partial \boldsymbol{\tau}} = \delta F^f_\tau, \tag{3.12}$$

where

$$U_n = \frac{1}{\delta}\int_{\mathcal{C}} \boldsymbol{u}\cdot\boldsymbol{n}\mathrm{d}\boldsymbol{n},\ P = \frac{1}{\delta}\int_{\mathcal{C}} p_f\mathrm{d}\boldsymbol{n},\ \text{and } F_r^f = \frac{1}{\delta}\int_{\mathcal{C}} \boldsymbol{f}_f\cdot\boldsymbol{r}\mathrm{d}\boldsymbol{n},\ \boldsymbol{r}\in\{\boldsymbol{n},\boldsymbol{\tau}\}.$$

Since the definition of $\boldsymbol{\sigma}_f$ implies that $\mu_f\dfrac{\partial \boldsymbol{u}}{\partial \boldsymbol{n}}\cdot\boldsymbol{n} - p_f = \boldsymbol{n}\cdot\boldsymbol{\sigma}_f\boldsymbol{n}$, employing condition (3.3), equation (3.11) can be seen as a one-dimensional law for the flow through the fracture,

$$\delta\left(M(\boldsymbol{n},\boldsymbol{n})U_n + M(\boldsymbol{n},\boldsymbol{\tau})U_\tau - \mu_f\frac{\partial^2 U_n}{\partial\boldsymbol{\tau}^2} - F_n^f\right) = p_1\big|_{\Gamma_1}^* - p_2\big|_{\Gamma_2}^*. \tag{3.13}$$

Equation (3.12) gives a one-dimensional momentum balance law on γ

$$\delta\left(M(\boldsymbol{\tau},\boldsymbol{n})U_n + M(\boldsymbol{\tau},\boldsymbol{\tau})U_\tau - \mu_f\frac{\partial^2 U_\tau}{\partial\boldsymbol{\tau}^2} + \frac{\partial P}{\partial\boldsymbol{\tau}} - F_\tau^f\right) = \mu_f\left(\frac{\partial\boldsymbol{u}}{\partial\boldsymbol{n}}\cdot\boldsymbol{\tau}\Big|_{\Gamma_2}^* - \frac{\partial\boldsymbol{u}}{\partial\boldsymbol{n}}\cdot\boldsymbol{\tau}\Big|_{\Gamma_1}^*\right). \tag{3.14}$$

Finally, we average the boundary conditions on the external boundaries of the fracture. Without loss of generality, we consider a Dirichlet boundary condition at $s=0$ and a Neumann boundary condition at $s=L$. In particular, letting $\gamma^D = \gamma\cap\Gamma_f^D = (0,0)$ and $\gamma^N = \gamma\cap\Gamma_f^N = (L,0)$, we have

$$U_n = U_n^D = \frac{1}{|\Gamma_f^D|}\int_{\Gamma_f^D}\boldsymbol{u}^D\cdot\boldsymbol{n}\,\mathrm{d}\boldsymbol{n},\quad U_\tau = U_\tau^D = \frac{1}{|\Gamma_f^D|}\int_{\Gamma_f^D}\boldsymbol{u}^D\cdot\boldsymbol{\tau}\,\mathrm{d}\boldsymbol{n}\ \text{ on }\gamma^D, \tag{3.15}$$

$$\mu_f\frac{\partial U_n}{\partial s} = 0,\quad \mu_f\frac{\partial U_\tau}{\partial s} - P = 0\ \text{ on }\gamma^N. \tag{3.16}$$

3.1. Interface conditions for problem closure

In order to couple the Biot system with the reduced model for flow in the fracture, described by equations (3.6), (3.13) and (3.14), additional interface conditions are necessary. More precisely, the goal is to derive interface conditions using the averaged quantities P, U_n, U_τ. This issue has already been studied for example in [28,30], and it will be addressed here for a more advanced mathematical model. More precisely, we formulate hypotheses on the cross sectional profiles of pressure, and normal and tangential components of the velocity in Ω_f. Then, we use the mappings identified by $(\cdot)|_{\Gamma_i}^*$ to combine traces of the Biot variables on Γ_i with the average values P, U_n, U_τ, in order to obtain suitable interface conditions that couple equations on Ω_p with the reduced fracture model. To close the system, we need to prescribe the interface conditions for the shear stress $\boldsymbol{\tau}_i\cdot\boldsymbol{\sigma}_p\boldsymbol{n}_i$ and the conditions for the fluid pressure and Darcy velocity in Ω_p.

The basis for the derivation of new interface conditions for the Biot problem in terms of the variables of the reduced model is the following set of equations, obtained by rearranging (3.1), (3.3) and (3.4):

$$p_1 = -\boldsymbol{n}_1\cdot\boldsymbol{\sigma}_f\boldsymbol{n}_1 = p_f - \mu_f\frac{\partial(\boldsymbol{u}\cdot\boldsymbol{n})}{\partial\boldsymbol{n}} \quad \text{on}\quad \Gamma_1, \tag{3.17}$$

$$p_2 = -\boldsymbol{n}_2\cdot\boldsymbol{\sigma}_f\boldsymbol{n}_2 = p_f - \mu_f\frac{\partial(\boldsymbol{u}\cdot\boldsymbol{n})}{\partial\boldsymbol{n}} \quad \text{on}\quad \Gamma_2, \tag{3.18}$$

$$\left(\frac{\partial\boldsymbol{\eta}_1}{\partial t}\cdot\boldsymbol{n}_1 + \boldsymbol{q}_1\cdot\boldsymbol{n}_1\right) = \boldsymbol{u}\cdot\boldsymbol{n} \quad \text{on}\quad \Gamma_1, \tag{3.19}$$

$$-\left(\frac{\partial\boldsymbol{\eta}_2}{\partial t}\cdot\boldsymbol{n}_2 + \boldsymbol{q}_2\cdot\boldsymbol{n}_2\right) = \boldsymbol{u}\cdot\boldsymbol{n} \quad \text{on}\quad \Gamma_2, \tag{3.20}$$

$$\boldsymbol{\tau}_1\cdot\boldsymbol{\sigma}_p\boldsymbol{n}_1 = \boldsymbol{\tau}_1\cdot\boldsymbol{\sigma}_f\boldsymbol{n}_1 = \mu_f\frac{\partial(\boldsymbol{u}\cdot\boldsymbol{\tau})}{\partial\boldsymbol{n}} \quad \text{on}\quad \Gamma_1, \tag{3.21}$$

$$\boldsymbol{\tau}_2\cdot\boldsymbol{\sigma}_p\boldsymbol{n}_2 = \boldsymbol{\tau}_2\cdot\boldsymbol{\sigma}_f\boldsymbol{n}_2 = \mu_f\frac{\partial(\boldsymbol{u}\cdot\boldsymbol{\tau})}{\partial\boldsymbol{n}} \quad \text{on}\quad \Gamma_2. \tag{3.22}$$

We also have

$$p_1 = -\boldsymbol{n}_1 \cdot \boldsymbol{\sigma}_f \boldsymbol{n}_1 = -\boldsymbol{n}_1 \cdot \boldsymbol{\sigma}_p \boldsymbol{n}_1 \qquad \text{on } \Gamma_1, \tag{3.23}$$

$$p_2 = -\boldsymbol{n}_2 \cdot \boldsymbol{\sigma}_f \boldsymbol{n}_2 = -\boldsymbol{n}_2 \cdot \boldsymbol{\sigma}_p \boldsymbol{n}_2 \qquad \text{on } \Gamma_2. \tag{3.24}$$

Closure assumptions will be used to relate the fluid velocity $\boldsymbol{u}$ and pressure p_f to the averaged values U_n, U_τ and P. Note that (3.23)–(3.24) are normal stress interface conditions that are expressed in terms of the variables on Ω_p and do not require closure assumptions. In the following we consider four cases of closure assumptions that allow us to derive Robin-type conditions interface for the fluid pressure and the normal component of the Darcy velocity, as well as interface conditions for the tangential stress in Ω_p. We note that the normal interface conditions depend on the closure assumption for the fracture pressure p_f and normal velocity $\boldsymbol{u} \cdot \boldsymbol{n}$, while the tangential interface conditions depend on the closure assumption for the fracture tangential velocity $\boldsymbol{u} \cdot \boldsymbol{\tau}$. The new interface conditions will be used in the weak formulation to couple the Biot equations with the averaged model for the flow in fracture.

3.1.1. Cases $P0 - U_n0$ and $U_\tau 0$: constant p_f, $\boldsymbol{u} \cdot \boldsymbol{n}$, $\boldsymbol{u} \cdot \boldsymbol{\tau}$ with respect to ξ along $\mathcal{C}$.

In this case we have $p_f(s, \xi) = P$, $\boldsymbol{u} \cdot \boldsymbol{n}(s, \xi) = U_n$, and $\boldsymbol{u} \cdot \boldsymbol{\tau}(s, \xi) = U_\tau$ for any $\xi \in [-1, 1]$. As a result we have

$$p_1|^*_{\Gamma_1} = p_2|^*_{\Gamma_2} = P, \quad \boldsymbol{u} \cdot \boldsymbol{n}|^*_{\Gamma_1} = \boldsymbol{u} \cdot \boldsymbol{n}|^*_{\Gamma_2} = U_n, \quad \boldsymbol{u} \cdot \boldsymbol{\tau}|^*_{\Gamma_1} = \boldsymbol{u} \cdot \boldsymbol{\tau}|^*_{\Gamma_2} = U_\tau, \tag{3.25}$$

where we have used (3.17)–(3.18) in the first set of equalities, and (3.19)–(3.22) imply

$$\left(\frac{\partial \boldsymbol{\eta}_1}{\partial t} \cdot \boldsymbol{n}_1 + \boldsymbol{q}_1 \cdot \boldsymbol{n}_1 \right) \Big|^*_{\Gamma_1} = \boldsymbol{u} \cdot \boldsymbol{n}_1|^*_{\Gamma_1} = U_n, \tag{3.26}$$

$$-\left(\frac{\partial \boldsymbol{\eta}_2}{\partial t} \cdot \boldsymbol{n}_2 + \boldsymbol{q}_2 \cdot \boldsymbol{n}_2 \right) \Big|^*_{\Gamma_2} = -\boldsymbol{u} \cdot \boldsymbol{n}_2|^*_{\Gamma_2} = U_n, \tag{3.27}$$

$$\boldsymbol{\tau}_1 \cdot \boldsymbol{\sigma}_p \boldsymbol{n}_1|^*_{\Gamma_1} = 0, \tag{3.28}$$

$$\boldsymbol{\tau}_2 \cdot \boldsymbol{\sigma}_p \boldsymbol{n}_2|^*_{\Gamma_2} = 0. \tag{3.29}$$

3.1.2. Cases $P0 - U_n1$ and $U_\tau 1$: constant p_f and linear $\boldsymbol{u} \cdot \boldsymbol{n}$, $\boldsymbol{u} \cdot \boldsymbol{\tau}$ with respect to ξ along $\mathcal{C}$.

Again we have $p_f(s, \xi) = P$. With the hypothesis of linear $\boldsymbol{u} \cdot \boldsymbol{n}(\cdot, \xi)$ we have, using (3.19)–(3.20),

$$\frac{\partial (\boldsymbol{u} \cdot \boldsymbol{n})}{\partial \boldsymbol{n}} = \frac{\boldsymbol{u} \cdot \boldsymbol{n}|^*_{\Gamma_2} - \boldsymbol{u} \cdot \boldsymbol{n}|^*_{\Gamma_1}}{\delta} = -\frac{\left(\frac{\partial \boldsymbol{\eta}_1}{\partial t} \cdot \boldsymbol{n}_1 + \boldsymbol{q}_1 \cdot \boldsymbol{n}_1 \right) \Big|^*_{\Gamma_1} + \left(\frac{\partial \boldsymbol{\eta}_2}{\partial t} \cdot \boldsymbol{n}_2 + \boldsymbol{q}_2 \cdot \boldsymbol{n}_2 \right) \Big|^*_{\Gamma_2}}{\delta}, \tag{3.30}$$

$$U_n = \frac{\boldsymbol{u} \cdot \boldsymbol{n}|^*_{\Gamma_1} + \boldsymbol{u} \cdot \boldsymbol{n}|^*_{\Gamma_2}}{2} = \frac{\left(\frac{\partial \boldsymbol{\eta}_1}{\partial t} \cdot \boldsymbol{n}_1 + \boldsymbol{q}_1 \cdot \boldsymbol{n}_1 \right) |^*_{\Gamma_1} - \left(\frac{\partial \boldsymbol{\eta}_2}{\partial t} \cdot \boldsymbol{n}_2 + \boldsymbol{q}_2 \cdot \boldsymbol{n}_2 \right) |^*_{\Gamma_2}}{2}. \tag{3.31}$$

Similarly, with $\boldsymbol{u} \cdot \boldsymbol{\tau}(\cdot, \xi)$ linear, we have

$$\begin{aligned} \frac{\partial (\boldsymbol{u} \cdot \boldsymbol{\tau})}{\partial \boldsymbol{n}} &= \frac{\boldsymbol{u} \cdot \boldsymbol{\tau}|^*_{\Gamma_2} - \boldsymbol{u} \cdot \boldsymbol{\tau}|^*_{\Gamma_1}}{\delta}, \\ U_\tau &= \frac{\boldsymbol{u} \cdot \boldsymbol{\tau}|^*_{\Gamma_1} + \boldsymbol{u} \cdot \boldsymbol{\tau}|^*_{\Gamma_2}}{2}. \end{aligned} \tag{3.32}$$

Adding and subtracting equations (3.17) and (3.18) gives, using (3.30),

$$p_2|^*_{\Gamma_2} - p_1|^*_{\Gamma_1} = 0, \tag{3.33}$$

$$p_2|^*_{\Gamma_2} + p_1|^*_{\Gamma_1} = 2P + \frac{2\mu_f}{\delta} \left(\left(\frac{\partial \boldsymbol{\eta}_1}{\partial t} \cdot \boldsymbol{n}_1 + \boldsymbol{q}_1 \cdot \boldsymbol{n}_1 \right) \Big|^*_{\Gamma_1} + \left(\frac{\partial \boldsymbol{\eta}_2}{\partial t} \cdot \boldsymbol{n}_2 + \boldsymbol{q}_2 \cdot \boldsymbol{n}_2 \right) \Big|^*_{\Gamma_2} \right). \tag{3.34}$$

Now, combining (3.31) and (3.34), we get

$$\left(\frac{\partial \boldsymbol{\eta}_1}{\partial t}\cdot\boldsymbol{n}_1+\boldsymbol{q}_1\cdot\boldsymbol{n}_1\right)\Big|^*_{\Gamma_1}=U_n+\frac{\delta}{4\mu_f}(p_2|^*_{\Gamma_2}+p_1|^*_{\Gamma_1}-2P),$$
$$\left(\frac{\partial \boldsymbol{\eta}_2}{\partial t}\cdot\boldsymbol{n}_2+\boldsymbol{q}_2\cdot\boldsymbol{n}_2\right)\Big|^*_{\Gamma_2}=-U_n+\frac{\delta}{4\mu_f}(p_2|^*_{\Gamma_2}+p_1|^*_{\Gamma_1}-2P),$$

which can be rewritten as

$$\delta p_1|^*_{\Gamma_1}-4\mu_f\left(\frac{\partial \boldsymbol{\eta}_1}{\partial t}\cdot\boldsymbol{n}_1+\boldsymbol{q}_1\cdot\boldsymbol{n}_1\right)\Big|^*_{\Gamma_1}=\delta P-4\mu_f U_n+\delta(P-p_2|^*_{\Gamma_2}), \tag{3.35}$$
$$\delta p_2|^*_{\Gamma_2}-4\mu_f\left(\frac{\partial \boldsymbol{\eta}_2}{\partial t}\cdot\boldsymbol{n}_2+\boldsymbol{q}_2\cdot\boldsymbol{n}_2\right)\Big|^*_{\Gamma_2}=\delta P+4\mu_f U_n+\delta(P-p_1|^*_{\Gamma_1}). \tag{3.36}$$

Due to (3.33), the above equations can be further simplified as

$$-2\mu_f\left(\frac{\partial \boldsymbol{\eta}_1}{\partial t}\cdot\boldsymbol{n}_1+\boldsymbol{q}_1\cdot\boldsymbol{n}_1\right)\Big|^*_{\Gamma_1}=-2\mu_f U_n+\delta(P-p_2|^*_{\Gamma_2}), \tag{3.37}$$
$$-2\mu_f\left(\frac{\partial \boldsymbol{\eta}_2}{\partial t}\cdot\boldsymbol{n}_2+\boldsymbol{q}_2\cdot\boldsymbol{n}_2\right)\Big|^*_{\Gamma_2}=2\mu_f U_n+\delta(P-p_1|^*_{\Gamma_1}). \tag{3.38}$$

To derive the conditions on the tangential stress, we first note that conditions (3.2) and (3.4) yield

$$(\boldsymbol{u}\cdot\boldsymbol{\tau})|^*_{\Gamma_1}=\frac{1}{c_{BJS}}(\boldsymbol{\tau}_1\cdot\boldsymbol{\sigma}_p\boldsymbol{n}_1)|^*_{\Gamma_1}+\frac{\partial \boldsymbol{\eta}_1}{\partial t}\cdot\boldsymbol{\tau}_1\Big|^*_{\Gamma_1} \tag{3.39}$$
$$(\boldsymbol{u}\cdot\boldsymbol{\tau})|^*_{\Gamma_2}=-\frac{1}{c_{BJS}}(\boldsymbol{\tau}_2\cdot\boldsymbol{\sigma}_p\boldsymbol{n}_2)|^*_{\Gamma_2}-\frac{\partial \boldsymbol{\eta}_2}{\partial t}\cdot\boldsymbol{\tau}_2\Big|^*_{\Gamma_2}. \tag{3.40}$$

Now, starting from (3.21)–(3.22) and using (3.32) and (3.39)–(3.40), we obtain

$$\boldsymbol{\tau}_1\cdot\boldsymbol{\sigma}_p\boldsymbol{n}_1|^*_{\Gamma_1}=-\frac{\mu_f}{\delta}\left(\frac{\boldsymbol{\tau}_2\cdot\boldsymbol{\sigma}_p\boldsymbol{n}_2|^*_{\Gamma_2}}{c_{BJS}}+\frac{\partial \boldsymbol{\eta}_2}{\partial t}\cdot\boldsymbol{\tau}_2\Big|^*_{\Gamma_2}+\frac{\boldsymbol{\tau}_1\cdot\boldsymbol{\sigma}_p\boldsymbol{n}_1|^*_{\Gamma_1}}{c_{BJS}}+\frac{\partial \boldsymbol{\eta}_1}{\partial t}\cdot\boldsymbol{\tau}_1\Big|^*_{\Gamma_1}\right),$$
$$\boldsymbol{\tau}_2\cdot\boldsymbol{\sigma}_p\boldsymbol{n}_2|^*_{\Gamma_2}=-\frac{\mu_f}{\delta}\left(\frac{\boldsymbol{\tau}_2\cdot\boldsymbol{\sigma}_p\boldsymbol{n}_2|^*_{\Gamma_2}}{c_{BJS}}+\frac{\partial \boldsymbol{\eta}_2}{\partial t}\cdot\boldsymbol{\tau}_2\Big|^*_{\Gamma_2}+\frac{\boldsymbol{\tau}_1\cdot\boldsymbol{\sigma}_p\boldsymbol{n}_1|^*_{\Gamma_1}}{c_{BJS}}+\frac{\partial \boldsymbol{\eta}_1}{\partial t}\cdot\boldsymbol{\tau}_1\Big|^*_{\Gamma_1}\right).$$

Solving the system we get

$$\left(\frac{\delta}{\mu_f}+\frac{2}{c_{BJS}}\right)(\boldsymbol{\tau}_1\cdot\boldsymbol{\sigma}_p\boldsymbol{n}_1)|^*_{\Gamma_1}=-\frac{\partial \boldsymbol{\eta}_2}{\partial t}\cdot\boldsymbol{\tau}_2\Big|^*_{\Gamma_2}-\frac{\partial \boldsymbol{\eta}_1}{\partial t}\cdot\boldsymbol{\tau}_1\Big|^*_{\Gamma_1}, \tag{3.41}$$
$$\left(\frac{\delta}{\mu_f}+\frac{2}{c_{BJS}}\right)(\boldsymbol{\tau}_2\cdot\boldsymbol{\sigma}_p\boldsymbol{n}_2)|^*_{\Gamma_2}=-\frac{\partial \boldsymbol{\eta}_2}{\partial t}\cdot\boldsymbol{\tau}_2\Big|^*_{\Gamma_2}-\frac{\partial \boldsymbol{\eta}_1}{\partial t}\cdot\boldsymbol{\tau}_1\Big|^*_{\Gamma_1}. \tag{3.42}$$

3.1.3. Cases $P1-U_n1$ and $U_\tau 1$: linear p_f, $\boldsymbol{u}\cdot\boldsymbol{n}$, $\boldsymbol{u}\cdot\boldsymbol{\tau}$ with respect to ξ along $\mathcal{C}$.

For linear pressure along $\mathcal{C}$, we have

$$P=\frac{p_f|^*_{\Gamma_1}+p_f|^*_{\Gamma_2}}{2}.$$

The derivation of the interface conditions is similar to the case of constant p_f and linear $\boldsymbol{u}\cdot\boldsymbol{n}$, $\boldsymbol{u}\cdot\boldsymbol{\tau}$, with the exception that (3.33) does not hold, so the conditions (3.35)–(3.36) cannot be simplified. Therefore the conditions in this case are (3.35)–(3.36) and (3.41)–(3.42).

3.1.4. Cases $P0-U_n2$ and $U_\tau 2$: constant p_f and quadratic $\boldsymbol{u}\cdot\boldsymbol{n}$, $\boldsymbol{u}\cdot\boldsymbol{\tau}$ with respect to ξ along $\mathcal{C}$.

A quadratic $\boldsymbol{u}\cdot\boldsymbol{n}$ along $\mathcal{C}$ can be written as

$$(\boldsymbol{u}\cdot\boldsymbol{n})(\xi) = a\xi^2 + b\xi + c,$$

where to determine a, b, and c for any $s \in [0, L]$, we have to solve the following system of equations:

$$\begin{aligned}
(\boldsymbol{u}\cdot\boldsymbol{n})\left(\frac{-\delta}{2}\right) &= a\frac{\delta^2}{4} - b\frac{\delta}{2} + c = \boldsymbol{u}\cdot\boldsymbol{n}|^*_{\Gamma_1},\\
(\boldsymbol{u}\cdot\boldsymbol{n})\left(\frac{+\delta}{2}\right) &= a\frac{\delta^2}{4} + b\frac{\delta}{2} + c = \boldsymbol{u}\cdot\boldsymbol{n}|^*_{\Gamma_2},\\
U_n &= \frac{1}{\delta}\int_{\mathcal{C}}(a\xi^2 + b\xi + c)\mathrm{d}\xi.
\end{aligned}$$

The solution is given by

$$\begin{aligned}
a &= 3\frac{\boldsymbol{u}\cdot\boldsymbol{n}|^*_{\Gamma_1} + \boldsymbol{u}\cdot\boldsymbol{n}|^*_{\Gamma_2} - 2U_n}{\delta^2},\\
b &= \frac{\boldsymbol{u}\cdot\boldsymbol{n}|^*_{\Gamma_2} - \boldsymbol{u}\cdot\boldsymbol{n}|^*_{\Gamma_1}}{\delta},\\
c &= \frac{6U_n - \boldsymbol{u}\cdot\boldsymbol{n}|^*_{\Gamma_1} - \boldsymbol{u}\cdot\boldsymbol{n}|^*_{\Gamma_2}}{4}.
\end{aligned}$$

In a similar way we can find coefficients for $\boldsymbol{u}\cdot\boldsymbol{\tau}$. Now we can write

$$\begin{aligned}
\frac{\partial(\boldsymbol{u}\cdot\boldsymbol{n})}{\partial\boldsymbol{n}}\bigg|^*_{\Gamma_1} &= -2a\frac{\delta}{2} + b = -2\frac{\boldsymbol{u}\cdot\boldsymbol{n}|^*_{\Gamma_2} + 2(\boldsymbol{u}\cdot\boldsymbol{n})|^*_{\Gamma_1} - 3U_n}{\delta},\\
\frac{\partial(\boldsymbol{u}\cdot\boldsymbol{n})}{\partial\boldsymbol{n}}\bigg|^*_{\Gamma_2} &= 2a\frac{\delta}{2} + b = 2\frac{\boldsymbol{u}\cdot\boldsymbol{n}|^*_{\Gamma_1} + 2(\boldsymbol{u}\cdot\boldsymbol{n})|^*_{\Gamma_2} - 3U_n}{\delta}.
\end{aligned}$$

Adding and subtracting equations (3.17) and (3.18) gives

$$\begin{aligned}
p_2|^*_{\Gamma_2} - p_1|^*_{\Gamma_1} &= -6\mu_f\frac{\boldsymbol{u}\cdot\boldsymbol{n}|^*_{\Gamma_2} + \boldsymbol{u}\cdot\boldsymbol{n}|^*_{\Gamma_1} - 2U_n}{\delta},\\
p_2|^*_{\Gamma_2} + p_1|^*_{\Gamma_1} &= 2P + 2\mu_f\frac{\boldsymbol{u}\cdot\boldsymbol{n}|^*_{\Gamma_1} - \boldsymbol{u}\cdot\boldsymbol{n}|^*_{\Gamma_2}}{\delta}.
\end{aligned}$$

Solving this system to obtain Robin boundary conditions, we have

$$\begin{aligned}
\left(\frac{\partial\boldsymbol{\eta}_1}{\partial t}\cdot\boldsymbol{n}_1 + \boldsymbol{q}_1\cdot\boldsymbol{n}_1\right)\bigg|^*_{\Gamma_1} &= \boldsymbol{u}\cdot\boldsymbol{n}|^*_{\Gamma_1} = U_n + \frac{\delta}{6\mu_f}(2p_1|^*_{\Gamma_1} + p_2|^*_{\Gamma_2} - 3P),\\
-\left(\frac{\partial\boldsymbol{\eta}_2}{\partial t}\cdot\boldsymbol{n}_2 + \boldsymbol{q}_2\cdot\boldsymbol{n}_2\right)\bigg|^*_{\Gamma_2} &= \boldsymbol{u}\cdot\boldsymbol{n}|^*_{\Gamma_2} = U_n + \frac{\delta}{6\mu_f}(-p_1|^*_{\Gamma_1} - 2p_2|^*_{\Gamma_2} + 3P),
\end{aligned}$$

which can be rewritten as

$$2\delta p_1|^*_{\Gamma_1} - 6\mu_f\left(\frac{\partial\boldsymbol{\eta}_1}{\partial t}\cdot\boldsymbol{n}_1 + \boldsymbol{q}_1\cdot\boldsymbol{n}_1\right)\bigg|^*_{\Gamma_1} = 2\delta P - 6\mu_f U_n + \delta(P - p_2|^*_{\Gamma_2}), \tag{3.43}$$

$$2\delta p_2|^*_{\Gamma_2} - 6\mu_f\left(\frac{\partial\boldsymbol{\eta}_2}{\partial t}\cdot\boldsymbol{n}_2 + \boldsymbol{q}_2\cdot\boldsymbol{n}_2\right)\bigg|^*_{\Gamma_2} = 2\delta P + 6\mu_f U_n + \delta(P - p_1|^*_{\Gamma_1}). \tag{3.44}$$

To derive the conditions on the tangential stress, we note that

$$\left.\frac{\partial(\boldsymbol{u}\cdot\boldsymbol{\tau})}{\partial \boldsymbol{n}}\right|_{\Gamma_1}^{*} = -2\frac{\boldsymbol{u}\cdot\boldsymbol{\tau}|_{\Gamma_2}^{*} + 2(\boldsymbol{u}\cdot\boldsymbol{\tau})|_{\Gamma_1}^{*} - 3U_\tau}{\delta},$$
$$\left.\frac{\partial(\boldsymbol{u}\cdot\boldsymbol{\tau})}{\partial \boldsymbol{n}}\right|_{\Gamma_2}^{*} = 2\frac{\boldsymbol{u}\cdot\boldsymbol{\tau}|_{\Gamma_1}^{*} + 2(\boldsymbol{u}\cdot\boldsymbol{\tau})|_{\Gamma_2}^{*} - 3U_\tau}{\delta},$$

which, combined with (3.21)–(3.22), and using conditions (3.2) and (3.4), imply

$$\boldsymbol{\tau}_1\cdot\boldsymbol{\sigma}_p\boldsymbol{n}_1|_{\Gamma_1}^{*} = -\frac{2\mu_f}{\delta}\left(-\frac{\partial\boldsymbol{\eta}_2}{\partial t}\cdot\boldsymbol{\tau}_2\Big|_{\Gamma_2}^{*} - \frac{1}{c_{BJS}}(\boldsymbol{\tau}_2\cdot\boldsymbol{\sigma}_p\boldsymbol{n}_2)|_{\Gamma_2}^{*} + 2\frac{1}{c_{BJS}}(\boldsymbol{\tau}_1\cdot\boldsymbol{\sigma}_p\boldsymbol{n}_1)|_{\Gamma_1}^{*} + 2\frac{\partial\boldsymbol{\eta}_1}{\partial t}\cdot\boldsymbol{\tau}_1\Big|_{\Gamma_1}^{*} - 3U_\tau\right),$$
$$\boldsymbol{\tau}_2\cdot\boldsymbol{\sigma}_p\boldsymbol{n}_2|_{\Gamma_2}^{*} = \frac{2\mu_f}{\delta}\left(\frac{\partial\boldsymbol{\eta}_1}{\partial t}\cdot\boldsymbol{\tau}_1\Big|_{\Gamma_1}^{*} + \frac{1}{c_{BJS}}(\boldsymbol{\tau}_1\cdot\boldsymbol{\sigma}_p\boldsymbol{n}_1)|_{\Gamma_1}^{*} - 2\frac{\partial\boldsymbol{\eta}_2}{\partial t}\cdot\boldsymbol{\tau}_2\Big|_{\Gamma_2}^{*} - 2\frac{1}{c_{BJS}}(\boldsymbol{\tau}_2\cdot\boldsymbol{\sigma}_p\boldsymbol{n}_2)|_{\Gamma_2}^{*} - 3U_\tau\right).$$

Solving for $\boldsymbol{\tau}_1\cdot\boldsymbol{\sigma}_p\boldsymbol{n}_1|_{\Gamma_1}^{*}$ and $\boldsymbol{\tau}_2\cdot\boldsymbol{\sigma}_p\boldsymbol{n}_2|_{\Gamma_2}^{*}$ we get

$$\left(\frac{\delta}{2\mu_f} + \frac{4}{c_{BJS}} + \frac{6\mu_f}{c_{BJS}^2\delta}\right)(\boldsymbol{\tau}_1\cdot\boldsymbol{\sigma}_p\boldsymbol{n}_1)|_{\Gamma_1}^{*} = \frac{\partial\boldsymbol{\eta}_2}{\partial t}\cdot\boldsymbol{\tau}_2\Big|_{\Gamma_2}^{*} - \left(2 + \frac{6\mu_f}{c_{BJS}\delta}\right)\frac{\partial\boldsymbol{\eta}_1}{\partial t}\cdot\boldsymbol{\tau}_1\Big|_{\Gamma_1}^{*} + 3\left(1 + \frac{2\mu_f}{c_{BJS}\delta}\right)U_\tau, \tag{3.45}$$

$$\left(\frac{\delta}{2\mu_f} + \frac{4}{c_{BJS}} + \frac{6\mu_f}{c_{BJS}^2\delta}\right)(\boldsymbol{\tau}_2\cdot\boldsymbol{\sigma}_p\boldsymbol{n}_2)|_{\Gamma_2}^{*} = \frac{\partial\boldsymbol{\eta}_1}{\partial t}\cdot\boldsymbol{\tau}_1\Big|_{\Gamma_1}^{*} - \left(2 + \frac{6\mu_f}{c_{BJS}\delta}\right)\frac{\partial\boldsymbol{\eta}_2}{\partial t}\cdot\boldsymbol{\tau}_2\Big|_{\Gamma_2}^{*} - 3\left(1 + \frac{2\mu_f}{\delta c_{BJS}}\right)U_\tau. \tag{3.46}$$

3.2. Unified formulation of the closure conditions

In this section we present a parametrized unified formulation for the interface conditions derived in the previous sections. Since the normal and tangential closure assumptions can be made independently of each other, we use two different parameters to describe them. In the cases above, the Robin boundary conditions for the pressure in the Biot system (3.37)–(3.38), (3.35)–(3.36), and (3.43)–(3.44), can be written in a general form as

$$\delta\theta_n p_1|_{\Gamma_1}^{*} - 2\mu_f\left(\frac{\partial\boldsymbol{\eta}_1}{\partial t}\cdot\boldsymbol{n}_1 + \boldsymbol{q}_1\cdot\boldsymbol{n}_1\right)\Big|_{\Gamma_1}^{*} = \delta\theta_n P - 2\mu_f U_n + \delta(1-\theta_n)(P - p_2|_{\Gamma_2}^{*}), \tag{3.47}$$

$$\delta\theta_n p_2|_{\Gamma_2}^{*} - 2\mu_f\left(\frac{\partial\boldsymbol{\eta}_2}{\partial t}\cdot\boldsymbol{n}_2 + \boldsymbol{q}_2\cdot\boldsymbol{n}_2\right)\Big|_{\Gamma_2}^{*} = \delta\theta_n P + 2\mu_f U_n + \delta(1-\theta_n)(P - p_1|_{\Gamma_1}^{*}), \tag{3.48}$$

where for $\theta_n = 0$ we have the $P0 - U_n1$ case (3.37)–(3.38), for $\theta_n = \frac{1}{2}$ we have the $P1 - U_n1$ case (3.35)–(3.36), and for $\theta_n = \frac{2}{3}$ we have the $P0 - U_n2$ case (3.43)–(3.44). In addition, $\theta_n = 0$ also gives the $P0 - U_n0$ case (3.26)–(3.27) under the constraint $p_1|_{\Gamma_1}^{*} = p_2|_{\Gamma_2}^{*} = P$.

In a similar way, we write the general conditions for the tangential components of the normal stress (3.28)–(3.29), (3.41)–(3.42), and (3.45)–(3.46) as

$$\begin{aligned}
&\left(\frac{\delta(1-\theta_\tau)^2}{\mu_f}+\frac{2{\theta_\tau}^2}{c_{BJS}}+\frac{6\theta_\tau(2\theta_\tau-1)\mu_f}{c_{BJS}^2\delta}\right)(\boldsymbol{\tau}_1\cdot\boldsymbol{\sigma}_p\boldsymbol{n}_1)|^*_{\Gamma_1}\\
&=\left(\left(-1-\frac{6\mu_f}{c_{BJS}\delta}\right){\theta_\tau}^2+\frac{6\mu_f\theta_\tau(1-\theta_\tau)}{c_{BJS}\delta}\right)\frac{\partial\boldsymbol{\eta}_1}{\partial t}\cdot\boldsymbol{\tau}_1\Big|^*_{\Gamma_1}\\
&\quad+\theta_\tau(5\theta_\tau-3)\frac{\partial\boldsymbol{\eta}_2}{\partial t}\cdot\boldsymbol{\tau}_2\Big|^*_{\Gamma_2}+3\theta_\tau(2\theta_\tau-1)\left(1+\frac{2\mu_f}{c_{BJS}\delta}\right)U_\tau,
\end{aligned}\tag{3.49}$$

$$\begin{aligned}
&\left(\frac{\delta(1-\theta_\tau)^2}{\mu_f}+\frac{2{\theta_\tau}^2}{c_{BJS}}+\frac{6\theta_\tau(2\theta_\tau-1)\mu_f}{c_{BJS}^2\delta}\right)(\boldsymbol{\tau}_2\cdot\boldsymbol{\sigma}_p\boldsymbol{n}_2)|^*_{\Gamma_2}\\
&=\left(\left(-1-\frac{6\mu_f}{c_{BJS}\delta}\right){\theta_\tau}^2+\frac{6\mu_f\theta_\tau(1-\theta_\tau)}{c_{BJS}\delta}\right)\frac{\partial\boldsymbol{\eta}_2}{\partial t}\cdot\boldsymbol{\tau}_2\Big|^*_{\Gamma_2}\\
&\quad+\theta_\tau(5\theta_\tau-3)\frac{\partial\boldsymbol{\eta}_1}{\partial t}\cdot\boldsymbol{\tau}_1\Big|^*_{\Gamma_1}-3\theta_\tau(2\theta_\tau-1)\left(1+\frac{2\mu_f}{\delta c_{BJS}}\right)U_\tau,
\end{aligned}\tag{3.50}$$

where $\theta_\tau=0$ gives the $U_\tau 0$ case (3.28)–(3.29), $\theta_\tau=\frac{1}{2}$ gives the $U_\tau 1$ case (3.41)–(3.42), and $\theta_\tau=\frac{2}{3}$ gives the $U_\tau 2$ case (3.45)–(3.46). The relation between the parameters θ_n, θ_τ and the approximation of the variables p_f, $\boldsymbol{u}\cdot\boldsymbol{n}$, $\boldsymbol{u}\cdot\boldsymbol{\tau}$ inside the fracture is summarized in Table 1. We note that normal conditions part of the table is consistent with Table 1 in [28].

Using a simple calculation, which consists of inverting a 2×2 linear system, we can rewrite (3.49)–(3.50) as follows:

$$(\boldsymbol{\tau}_1\cdot\boldsymbol{\sigma}_p\boldsymbol{n}_1)|^*_{\Gamma_1}=(C^\tau\theta_\tau(5\theta_\tau-3)-C^\eta)\frac{\partial\boldsymbol{\eta}_1}{\partial t}\cdot\boldsymbol{\tau}_1\Big|^*_{\Gamma_1}+C^\tau\theta_\tau(5\theta_\tau-3)\frac{\partial\boldsymbol{\eta}_2}{\partial t}\cdot\boldsymbol{\tau}_2\Big|^*_{\Gamma_2}+C^\eta U_\tau,\tag{3.51}$$

$$(\boldsymbol{\tau}_2\cdot\boldsymbol{\sigma}_p\boldsymbol{n}_2)|^*_{\Gamma_2}=(C^\tau\theta_\tau(5\theta_\tau-3)-C^\eta)\frac{\partial\boldsymbol{\eta}_2}{\partial t}\cdot\boldsymbol{\tau}_2\Big|^*_{\Gamma_2}+C^\tau\theta_\tau(5\theta_\tau-3)\frac{\partial\boldsymbol{\eta}_1}{\partial t}\cdot\boldsymbol{\tau}_1\Big|^*_{\Gamma_1}-C^\eta U_\tau,\tag{3.52}$$

where

$$C^\tau=\left(\frac{\delta(1-\theta_\tau)^2}{\mu_f}+\frac{2{\theta_\tau}^2}{c_{BJS}}+\frac{6\theta_\tau(2\theta_\tau-1)\mu_f}{c_{BJS}^2\delta}\right)^{-1},\tag{3.53}$$

$$C^\eta=\begin{cases}\dfrac{6\mu_f c_{BJS}}{c_{BJS}\delta+6\mu_f}, & \theta_\tau=\dfrac{2}{3},\\ 0, & \theta_\tau\in\left\{\dfrac{1}{2},0\right\}.\end{cases}\tag{3.54}$$

Note that C^η is non-zero only when $\theta_\tau=\frac{2}{3}$. It is also helpful to analyze the asymptotic behavior of these constants when the parameters of the problem c_{BJS} and δ vanish (we implicitly assume here that the fluid viscosity in the fracture μ_f is a strictly positive parameter). Let us denote as $\mathcal{O}(x)$ any quantity that scales as Cx when $x\to 0$, C being a generic constant. Then, it is straightforward to show that

$$C^\tau=\mathcal{O}(c_{BJS}^2,\delta),\quad C^\eta=\mathcal{O}(c_{BJS}).\tag{3.55}$$

TABLE 1. Relation between the values of the parameters θ_n, θ_τ and the approximation of the variables p_f, $\boldsymbol{u}\cdot\boldsymbol{n}$, $\boldsymbol{u}\cdot\boldsymbol{\tau}$ inside the fracture. C denotes constant approximation of the variables across the interface aperture, L stands for linear approximation and Q for quadratic.

θ_n	p_f	$\boldsymbol{u}\cdot\boldsymbol{n}$	θ_τ	$\boldsymbol{u}\cdot\boldsymbol{\tau}$
0	C	L	0	C
1/2	L	L	1/2	L
2/3	C	Q	2/3	Q

From (3.53) and (3.54) it is easy to see that for $\theta_\tau = 2/3$,

$$C^\tau = \frac{3c_{BJS}\delta}{2c_{BJS}\delta + 4\mu_f} C^\eta, \tag{3.56}$$

$$C^\eta \leq c_{BJS}, \tag{3.57}$$

which will be utilized later in the stability analysis.

Recalling that $\frac{\partial}{\partial s} = \frac{\partial}{\partial \boldsymbol{\tau}}$ and using equations (3.47)–(3.48), we can write the mass conservation equation in the model for the fracture (3.6) as:

$$\delta\left(\frac{\partial U_\tau}{\partial s} - H\right) = \frac{\delta}{2\mu_f} p_1|^*_{\Gamma_1} + \frac{\delta}{2\mu_f} p_2|^*_{\Gamma_2} - \frac{\delta}{\mu_f} P \quad \text{on } \gamma. \tag{3.58}$$

Furthermore, the right hand side in equation (3.14) depends on the velocity profile. Employing conditions (3.21)–(3.22) and (3.51)–(3.52), we obtain

$$\delta\left(M(\boldsymbol{\tau},\boldsymbol{n})U_n + M(\boldsymbol{\tau},\boldsymbol{\tau})U_\tau - \mu_f \frac{\partial^2 U_\tau}{\partial s^2} + \frac{\partial P}{\partial s} + \frac{2}{\delta} C^\eta U_\tau - F^f_\tau\right) = C^\eta \left(\frac{\partial \boldsymbol{\eta}_1}{\partial t}\cdot\boldsymbol{\tau}_1\Big|^*_{\Gamma_1} - \frac{\partial \boldsymbol{\eta}_2}{\partial t}\cdot\boldsymbol{\tau}_2\Big|^*_{\Gamma_2}\right). \tag{3.59}$$

Remark 3.1. We note that the parameter θ_n in (3.47)–(3.48) can be interpreted as a quadrature weight and therefore any $\theta_n \in [0,1]$ results in a physically meaningful interface condition of Robin type. This feature is similar to the model in [28] and in the earlier work [30]. This is not however the case in (3.51)–(3.52), which are meaningful only for $\theta_\tau = 0, \frac{1}{2}, \frac{2}{3}$.

To summarize, in this section we derived a reduced model for the flow in the fracture based on four different profile assumptions. The assumptions were used together with the coupling conditions (3.1)–(3.4), giving rise to equations (3.47)–(3.48), (3.51)–(3.52), (3.58) and (3.59). We note that when $\theta_\tau = 0$, the Beavers–Joseph–Saffman condition is not being used.

4. WEAK FORMULATION OF THE COUPLED PROBLEM

In this section we couple the Biot system (2.1)–(2.3) with the reduced model for the flow in the fracture, derived in the previous sections with the suitable closure conditions. We remind the reader that after averaging across the aperture of the fracture Ω_f, the governing equations of the reduced model are set on the fluid domain midline γ, and depend only on the arc length along this curve, denoted by s. The coupled model is defined in domain Ω, with the fracture domain Ω_f collapsed to its midline γ, which is in contrast with the approach in [28]. In this case the fracture edges, denoted by Γ_i, $i = 1, 2$ in Figure 1, coincide with γ and Ω_p becomes a domain with a slit. Combining (2.1)–(2.3), (3.13), (3.59) and (3.58) we obtain the following coupled

problem: find $\boldsymbol{\eta}, \boldsymbol{q}, p, U_n, U_\tau$ and P such that

$$
\begin{aligned}
&-\nabla\cdot\boldsymbol{\sigma}_p(\boldsymbol{\eta},p) = \boldsymbol{f}_p && \text{in } \ \Omega_p\times(0,T], && (4.1)\\
&\boldsymbol{K}^{-1}\boldsymbol{q} = -\nabla p && \text{in } \ \Omega_p\times(0,T], && (4.2)\\
&\frac{\partial}{\partial t}(s_0 p + \alpha\nabla\cdot\boldsymbol{\eta}) + \nabla\cdot\boldsymbol{q} = g && \text{in } \ \Omega_p\times(0,T], && (4.3)\\
&\delta\left(M(\boldsymbol{n},\boldsymbol{n})U_n + M(\boldsymbol{n},\boldsymbol{\tau})U_\tau - \mu_f\frac{\partial^2 U_n}{\partial s^2} - F_n^f\right) = p_1\big|_{\Gamma_1}^* - p_2\big|_{\Gamma_2}^* && \text{on } \ \gamma\times(0,T], && (4.4)\\
&\delta\left(M(\boldsymbol{\tau},\boldsymbol{n})U_n + M(\boldsymbol{\tau},\boldsymbol{\tau})U_\tau - \mu_f\frac{\partial^2 U_\tau}{\partial s^2} + \frac{\partial P}{\partial s} + \frac{2}{\delta}C^\eta U_\tau - F_\tau^f\right) = \\
&\qquad C^\eta\left(\frac{\partial\boldsymbol{\eta}_1}{\partial t}\cdot\boldsymbol{\tau}_1\Big|_{\Gamma_1}^* - \frac{\partial\boldsymbol{\eta}_2}{\partial t}\cdot\boldsymbol{\tau}_2\Big|_{\Gamma_2}^*\right) && \text{on } \ \gamma\times(0,T], && (4.5)\\
&\delta\left(\frac{\partial U_\tau}{\partial s} + \frac{1}{\mu_f}P\right) = \delta H + \frac{\delta}{2\mu_f}p_1|_{\Gamma_1}^* + \frac{\delta}{2\mu_f}p_2|_{\Gamma_2}^* && \text{on } \ \gamma\times(0,T], && (4.6)
\end{aligned}
$$

with the following coupling conditions from (3.23)–(3.24), (3.51)–(3.52), and (3.47)–(3.48) for $i = 1, 2$,

$$
\begin{aligned}
&(\boldsymbol{n}_i\cdot\boldsymbol{\sigma}_p\boldsymbol{n}_i)|_{\Gamma_i}^* = -p_i|_{\Gamma_i}^*, && (4.7)\\
&(\boldsymbol{\tau}_1\cdot\boldsymbol{\sigma}_p\boldsymbol{n}_1)|_{\Gamma_1}^* = (C^\tau\theta_\tau(5\theta_\tau-3) - C^\eta)\frac{\partial\boldsymbol{\eta}_1}{\partial t}\cdot\boldsymbol{\tau}_1\big|_{\Gamma_1}^* + C^\tau\theta_\tau(5\theta_\tau-3)\frac{\partial\boldsymbol{\eta}_2}{\partial t}\cdot\boldsymbol{\tau}_2\big|_{\Gamma_2}^* + C^\eta U_\tau, && (4.8)\\
&(\boldsymbol{\tau}_2\cdot\boldsymbol{\sigma}_p\boldsymbol{n}_2)|_{\Gamma_2}^* = (C^\tau\theta_\tau(5\theta_\tau-3) - C^\eta)\frac{\partial\boldsymbol{\eta}_2}{\partial t}\cdot\boldsymbol{\tau}_2\big|_{\Gamma_2}^* + C^\tau\theta_\tau(5\theta_\tau-3)\frac{\partial\boldsymbol{\eta}_1}{\partial t}\cdot\boldsymbol{\tau}_1\big|_{\Gamma_1}^* - C^\eta U_\tau, && (4.9)\\
&\delta\theta_n p_1|_{\Gamma_1}^* - 2\mu_f\left(\frac{\partial\boldsymbol{\eta}_1}{\partial t}\cdot\boldsymbol{n}_1 + \boldsymbol{q}_1\cdot\boldsymbol{n}_1\right)\Big|_{\Gamma_1}^* = \delta\theta_n P - 2\mu_f U_n + \delta(1-\theta_n)(P - p_2|_{\Gamma_2}^*), && (4.10)\\
&\delta\theta_n p_2|_{\Gamma_2}^* - 2\mu_f\left(\frac{\partial\boldsymbol{\eta}_2}{\partial t}\cdot\boldsymbol{n}_2 + \boldsymbol{q}_2\cdot\boldsymbol{n}_2\right)\Big|_{\Gamma_2}^* = \delta\theta_n P + 2\mu_f U_n + \delta(1-\theta_n)(P - p_1|_{\Gamma_1}^*), && (4.11)
\end{aligned}
$$

boundary conditions

$$
\begin{aligned}
&\boldsymbol{\eta} = 0 && \text{on } \ \Gamma_p^D,\\
&\boldsymbol{\sigma}_p\boldsymbol{n} = \boldsymbol{s}_p^N && \text{on } \ \Gamma_p^N,\\
&p = p^D && \text{on } \ \Gamma_p^p,\\
&\boldsymbol{q}\cdot\boldsymbol{n} = 0 && \text{on } \ \Gamma_p^q,\\
&U_n = U_n^D, \ \ U_\tau = U_\tau^D, && \text{on } \ \gamma^D,\\
&\mu_f\frac{\partial U_n}{\partial s} = 0, \ \ \mu_f\frac{\partial U_\tau}{\partial s} - P = 0 && \text{on } \ \gamma^N,
\end{aligned}
$$

and initial conditions

$$p(0) = p_0, \quad \boldsymbol{\eta}(0) = \boldsymbol{\eta}_0 \text{ in } \Omega_p.$$

We note that in the case when $\delta \to 0$, we lose the equation for flow in the fracture and recover the continuity of Biot pressure, tangential component of displacement and the continuity of the normal flux.

Remark 4.1. In the following, for simplicity, we use notation corresponding to the case of a connected domain Ω_p. If Ω_p is split into two parts, spaces and integrals in Ω_p should be understood as defined in a piecewise fashion in $\Omega_{p,i}$, $i = 1, 2$.

Throughout the paper we use standard notation for Sobolev spaces, see *e.g.* [7, 11, 14]. To write the weak formulation, we start by introducing the test function spaces related to the Biot problem:

$$\begin{aligned}
\boldsymbol{\mathcal{V}}^{\eta} &= \{\boldsymbol{\xi} \in (H^1(\Omega_p))^2 : \ \boldsymbol{\xi} = 0 \text{ on } \Gamma_p^D\},\\
\boldsymbol{\mathcal{V}}^{p} &= \{\boldsymbol{r} \in H(\mathrm{div};\Omega_p) : \ \boldsymbol{r}\cdot\boldsymbol{n}|^*_{\Gamma_i} \in L^2(\Gamma_i),\ \boldsymbol{r}\cdot\boldsymbol{n} = 0 \text{ on } \Gamma_p^q\},\\
\mathcal{Q}^{p} &= \{\varphi \in L^2(\Omega_p) : \ \varphi|^*_{\Gamma_i} \in L^2(\Gamma_i)\}.
\end{aligned}$$

Then, the weak formulation of the Biot system (4.1)–(4.3) reads as follows: find $(\boldsymbol{\eta}(t), \boldsymbol{q}(t), p(t)) \in \boldsymbol{\mathcal{V}}^{\eta} \times \boldsymbol{\mathcal{V}}^{p} \times \mathcal{Q}^{p}$ such that for all $(\boldsymbol{\xi}, \boldsymbol{r}, \varphi) \in \boldsymbol{\mathcal{V}}^{\eta} \times \boldsymbol{\mathcal{V}}^{p} \times \mathcal{Q}^{p}$

$$\begin{aligned}
&\int_{\Omega_p} \boldsymbol{\sigma}_E : \nabla\boldsymbol{\xi}\mathrm{d}\boldsymbol{x} - \alpha\int_{\Omega_p} p\nabla\cdot\boldsymbol{\xi}\mathrm{d}\boldsymbol{x} + \int_{\Omega_p} \boldsymbol{K}^{-1}\boldsymbol{q}\cdot\boldsymbol{r}\mathrm{d}\boldsymbol{x} - \int_{\Omega_p} p\nabla\cdot\boldsymbol{r}\mathrm{d}\boldsymbol{x} + \int_{\Omega_p} s_0\frac{\partial p}{\partial t}\varphi\mathrm{d}\boldsymbol{x}\\
&+\alpha\int_{\Omega_p} \nabla\cdot\frac{\partial\boldsymbol{\eta}}{\partial t}\varphi\mathrm{d}\boldsymbol{x} + \int_{\Omega_p} \nabla\cdot\boldsymbol{q}\varphi\mathrm{d}\boldsymbol{x} = \overbrace{\int_{\partial\Omega_p\setminus\Gamma_p} \boldsymbol{\sigma}_p\boldsymbol{n}_p\cdot\boldsymbol{\xi}\mathrm{d}x}^{\mathrm{I}} \overbrace{- \int_{\partial\Omega_p\setminus\Gamma_p} p\boldsymbol{r}\cdot\boldsymbol{n}_p\mathrm{d}x}^{\mathrm{II}}\\
&\qquad + \int_{\Omega_p} \boldsymbol{f}_p\cdot\boldsymbol{\xi}\mathrm{d}\boldsymbol{x} + \int_{\Omega_p} g\varphi\mathrm{d}\boldsymbol{x} + \int_{\Gamma_p^N} \boldsymbol{s}_N^p\cdot\boldsymbol{\xi}\mathrm{d}x - \int_{\Gamma_p^p} p^D\boldsymbol{r}\cdot\boldsymbol{n}_p\mathrm{d}x.
\end{aligned} \tag{4.12}$$

Let us define $\boldsymbol{U} = [U_n, U_\tau]^T$, $\boldsymbol{V} = [V_n, V_\tau]^T$, $\boldsymbol{U}^D = [U_n^D, U_\tau^D]^T$ and the following test function spaces related to the flow in the fracture,

$$\begin{aligned}
\boldsymbol{\mathcal{V}}^{f} &= \{\boldsymbol{V} \in (H^1(\gamma))^2 : \ \boldsymbol{V} = 0 \text{ on } \gamma^D\},\\
\boldsymbol{\mathcal{V}}_D^{f} &= \{\boldsymbol{V} \in (H^1(\gamma))^2 : \ \boldsymbol{V} = \boldsymbol{U}^D \text{ on } \gamma^D\},\\
\mathcal{Q}^{f} &= L^2(\gamma).
\end{aligned}$$

The weak formulation of the flow in the fracture (4.4)–(4.6) is given as follows: find $(\boldsymbol{U}(t), P(t)) \in \boldsymbol{\mathcal{V}}_D^f \times \mathcal{Q}^f$, such that for all $(\boldsymbol{V}, R) \in \boldsymbol{\mathcal{V}}^f \times \mathcal{Q}^f$

$$\begin{aligned}
&\int_\gamma \delta\frac{\partial U_\tau}{\partial s}R\mathrm{d}s + \int_\gamma \frac{\delta}{\mu_f}PR\mathrm{d}s + \int_\gamma \delta\left(M(\boldsymbol{n},\boldsymbol{n})U_n + M(\boldsymbol{n},\boldsymbol{\tau})U_\tau - \mu_f\frac{\partial^2 U_n}{\partial s^2}\right)V_n\mathrm{d}s\\
&+\int_\gamma \delta\left(M(\boldsymbol{\tau},\boldsymbol{n})U_n + M(\boldsymbol{\tau},\boldsymbol{\tau})U_\tau - \mu_f\frac{\partial^2 U_\tau}{\partial s^2} + \frac{\partial P}{\partial s} + \frac{2}{\delta}C^\eta U_\tau\right)V_\tau\mathrm{d}s = \int_\gamma \delta HR\mathrm{d}s\\
&+\int_\gamma \frac{\delta}{2\mu_f}\left(p_1|^*_{\Gamma_1} + p_2|^*_{\Gamma_2}\right)R\mathrm{d}s + \int_\gamma \left(p_1|^*_{\Gamma_1} - p_2|^*_{\Gamma_2}\right)V_n\mathrm{d}s + \int_\gamma \delta F_n^f V_n\mathrm{d}s + \int_\gamma \delta F_\tau^f V_\tau\mathrm{d}s\\
&\qquad + \int_\gamma C^\eta\left(\frac{\partial\boldsymbol{\eta}_1}{\partial t}\cdot\boldsymbol{\tau}_1\Big|^*_{\Gamma_1} - \frac{\partial\boldsymbol{\eta}_2}{\partial t}\cdot\boldsymbol{\tau}_2\Big|^*_{\Gamma_2}\right)V_\tau\mathrm{d}s.
\end{aligned} \tag{4.13}$$

Introduce the matrix $\boldsymbol{M}$ and the vector $\boldsymbol{F}$ defined as

$$\boldsymbol{M} = \begin{bmatrix} M(\boldsymbol{n},\boldsymbol{n}) & M(\boldsymbol{n},\boldsymbol{\tau}) \\ M(\boldsymbol{\tau},\boldsymbol{n}) & M(\boldsymbol{\tau},\boldsymbol{\tau}) \end{bmatrix}, \quad \boldsymbol{F} = \begin{bmatrix} F_n^f \\ F_\tau^f \end{bmatrix}.$$

Then, we can write the equation (4.13) as

$$\begin{aligned}
&\int_\gamma \delta\frac{\partial U_\tau}{\partial s}R\mathrm{d}s + \int_\gamma \frac{\delta}{\mu_f}PR\mathrm{d}s + \int_\gamma \delta\boldsymbol{M}\boldsymbol{U}\cdot\boldsymbol{V}\mathrm{d}s - \int_\gamma \delta\mu_f\frac{\partial^2\boldsymbol{U}}{\partial s^2}\cdot\boldsymbol{V}\mathrm{d}s + \int_\gamma \delta\frac{\partial P}{\partial s}V_\tau\mathrm{d}s\\
&\quad + \int_\gamma 2C^\eta U_\tau V_\tau\mathrm{d}s = \int_\gamma \frac{\delta}{2\mu_f}\left(p_1|^*_{\Gamma_1} + p_2|^*_{\Gamma_2}\right)R\mathrm{d}s + \int_\gamma \left(p_1|^*_{\Gamma_1} - p_2|^*_{\Gamma_2}\right)V_n\mathrm{d}s\\
&\quad + \int_\gamma \delta\boldsymbol{F}\cdot\boldsymbol{V}\mathrm{d}s + \int_\gamma \delta HR\mathrm{d}s + \int_\gamma C^\eta\left(\frac{\partial\boldsymbol{\eta}_1}{\partial t}\cdot\boldsymbol{\tau}_1\Big|^*_{\Gamma_1} - \frac{\partial\boldsymbol{\eta}_2}{\partial t}\cdot\boldsymbol{\tau}_2\Big|^*_{\Gamma_2}\right)V_\tau\mathrm{d}s.
\end{aligned} \tag{4.14}$$

Integration by parts yields, using the boundary conditions on γ^D and γ^N,

$$\int_\gamma \delta\frac{\partial U_\tau}{\partial s}R\mathrm{d}s + \int_\gamma \frac{\delta}{\mu_f}PR\mathrm{d}s + \int_\gamma \delta\boldsymbol{MU}\cdot\boldsymbol{V}\mathrm{d}s + \int_\gamma \delta\mu_f\frac{\partial \boldsymbol{U}}{\partial s}\cdot\frac{\partial \boldsymbol{V}}{\partial s}\mathrm{d}s - \int_\gamma \delta\frac{\partial V_\tau}{\partial s}P\mathrm{d}s$$
$$+ \int_\gamma 2C^\eta U_\tau V_\tau \mathrm{d}s = \int_\gamma \frac{\delta}{2\mu_f}\left(p_1|^*_{\Gamma_1} + p_2|^*_{\Gamma_2}\right)R\mathrm{d}s \overbrace{+ \int_\gamma \left(p_1|^*_{\Gamma_1} - p_2|^*_{\Gamma_2}\right)V_n\mathrm{d}s}^{III}$$
$$+ \int_\gamma \delta\boldsymbol{F}\cdot\boldsymbol{V}\mathrm{d}s + \int_\gamma \delta HR\mathrm{d}s + \int_\gamma C^\eta\left(\frac{\partial\boldsymbol{\eta}_1}{\partial t}\cdot\boldsymbol{\tau}_1\Big|^*_{\Gamma_1} - \frac{\partial\boldsymbol{\eta}_2}{\partial t}\cdot\boldsymbol{\tau}_2\Big|^*_{\Gamma_2}\right)V_\tau\mathrm{d}s. \tag{4.15}$$

We observe, however, that sub-problems (4.12) and (4.15) are not fully coupled yet. More precisely (4.12) affects (4.15), but the latter does not induce any feedback on (4.12). For this reason, we need to plug equations (4.7)−(4.11) into (4.12). Decomposing the first two terms on the right hand side of (4.12), denoted as I, II respectively, into the normal and tangential components, employing condition (4.7), and combining it with term III from (4.15), we obtain

$$\begin{aligned}
I + II + III &= \int_\gamma (\boldsymbol{n}_1\cdot\boldsymbol{\sigma}_p\boldsymbol{n}_1)|^*_{\Gamma_1}(\boldsymbol{\xi}_1\cdot\boldsymbol{n}_1)|^*_{\Gamma_1}\mathrm{d}x + \int_\gamma (\boldsymbol{n}_2\cdot\boldsymbol{\sigma}_p\boldsymbol{n}_2)|^*_{\Gamma_2}(\boldsymbol{\xi}_2\cdot\boldsymbol{n}_2)|^*_{\Gamma_2}\mathrm{d}x\\
&+ \int_\gamma (\boldsymbol{\tau}_1\cdot\boldsymbol{\sigma}_p\boldsymbol{n}_1)|^*_{\Gamma_1}(\boldsymbol{\xi}_1\cdot\boldsymbol{\tau}_1)|^*_{\Gamma_1}\mathrm{d}x + \int_\gamma (\boldsymbol{\tau}_2\cdot\boldsymbol{\sigma}_p\boldsymbol{n}_2)|^*_{\Gamma_2}(\boldsymbol{\xi}_2\cdot\boldsymbol{\tau}_2)|^*_{\Gamma_2}\mathrm{d}x\\
&- \int_\gamma p_1|^*_{\Gamma_1}(\boldsymbol{r}_1\cdot\boldsymbol{n}_1)|^*_{\Gamma_1}\mathrm{d}x - \int_\gamma p_2|^*_{\Gamma_2}(\boldsymbol{r}_2\cdot\boldsymbol{n}_2)|^*_{\Gamma_2}\mathrm{d}x + \int_\gamma \left(p_1|^*_{\Gamma_1} - p_2|^*_{\Gamma_2}\right)V_n\mathrm{d}s\\
&= \int_\gamma (\boldsymbol{\tau}_1\cdot\boldsymbol{\sigma}_p\boldsymbol{n}_1)\big|^*_{\Gamma_1}(\boldsymbol{\xi}_1\cdot\boldsymbol{\tau}_1)\big|^*_{\Gamma_1}\mathrm{d}s + \int_\gamma (\boldsymbol{\tau}_2\cdot\boldsymbol{\sigma}_p\boldsymbol{n}_2)\big|^*_{\Gamma_2}(\boldsymbol{\xi}_2\cdot\boldsymbol{\tau}_2)\big|^*_{\Gamma_2}\mathrm{d}s\\
&+ \int_\gamma p_1\big|^*_{\Gamma_1}\left(V_n - (\boldsymbol{\xi}_1\cdot\boldsymbol{n}_1)\big|^*_{\Gamma_1} - (\boldsymbol{r}_1\cdot\boldsymbol{n}_1)\,\big|^*_{\Gamma_1}\right)\mathrm{d}s - \int_\gamma p_2\big|^*_{\Gamma_2}\left(V_n + (\boldsymbol{\xi}_2\cdot\boldsymbol{n}_2)\big|^*_{\Gamma_2} + (\boldsymbol{r}_2\cdot\boldsymbol{n}_2)\,\big|^*_{\Gamma_2}\right)\mathrm{d}s.
\end{aligned} \tag{4.16}$$

Employing conditions (4.8)−(4.9), the first two terms on the right hand side of equation (4.16) are given as follows

$$\begin{aligned}
&\int_\gamma (\boldsymbol{\tau}_1\cdot\boldsymbol{\sigma}_p\boldsymbol{n}_1)|^*_{\Gamma_1}(\boldsymbol{\xi}_1\cdot\boldsymbol{\tau}_1)|^*_{\Gamma_1}\mathrm{d}s + \int_\gamma (\boldsymbol{\tau}_2\cdot\boldsymbol{\sigma}_p\boldsymbol{n}_2)|^*_{\Gamma_2}(\boldsymbol{\xi}_2\cdot\boldsymbol{\tau}_2)|^*_{\Gamma_2}\mathrm{d}s\\
&= -\int_\gamma C^\tau\theta_\tau(3-5\theta_\tau)\left[\left(\frac{\partial\boldsymbol{\eta}_1}{\partial t}\cdot\boldsymbol{\tau}_1\right)\Big|^*_{\Gamma_1} + \left(\frac{\partial\boldsymbol{\eta}_2}{\partial t}\cdot\boldsymbol{\tau}_2\right)\Big|^*_{\Gamma_2}\right]\left[(\boldsymbol{\xi}_1\cdot\boldsymbol{\tau}_1)\,\big|^*_{\Gamma_1} + (\boldsymbol{\xi}_2\cdot\boldsymbol{\tau}_2)\,\big|^*_{\Gamma_2}\right]\mathrm{d}s\\
&- \int_\gamma C^\eta\left[\left(\frac{\partial\boldsymbol{\eta}_1}{\partial t}\cdot\boldsymbol{\tau}_1\right)\Big|^*_{\Gamma_1}(\boldsymbol{\xi}_1\cdot\boldsymbol{\tau}_1)\,\big|^*_{\Gamma_1} + \left(\frac{\partial\boldsymbol{\eta}_2}{\partial t}\cdot\boldsymbol{\tau}_2\right)\Big|^*_{\Gamma_2}(\boldsymbol{\xi}_2\cdot\boldsymbol{\tau}_2)\,\big|^*_{\Gamma_2}\right]\mathrm{d}s\\
&+ \int_\gamma C^\eta U_\tau\left((\boldsymbol{\xi}_1\cdot\boldsymbol{\tau}_1)\big|^*_{\Gamma_1} - (\boldsymbol{\xi}_2\cdot\boldsymbol{\tau}_2)\big|^*_{\Gamma_2}\right)\mathrm{d}s.
\end{aligned}$$

We impose (4.10)–(4.11) weakly as follows: for all $\varphi\in\mathcal{Q}^p$,

$$\int_\gamma \varphi_1|^*_{\Gamma_1}\left(\frac{\delta\theta_n}{2\mu_f}p_1|^*_{\Gamma_1} + \frac{\delta(1-\theta_n)}{2\mu_f}p_2|^*_{\Gamma_2} - \frac{\delta}{2\mu_f}P - \left(\frac{\partial\boldsymbol{\eta}_1}{\partial t}\cdot\boldsymbol{n}_1 + \boldsymbol{q}_1\cdot\boldsymbol{n}_1\right)\Big|^*_{\Gamma_1} + U_n\right)\mathrm{d}s$$
$$+ \int_\gamma \varphi_2|^*_{\Gamma_2}\left(\frac{\delta\theta_n}{2\mu_f}p_2|^*_{\Gamma_2} + \frac{\delta(1-\theta_n)}{2\mu_f}p_1|^*_{\Gamma_1} - \frac{\delta}{2\mu_f}P - \left(\frac{\partial\boldsymbol{\eta}_2}{\partial t}\cdot\boldsymbol{n}_2 + \boldsymbol{q}_2\cdot\boldsymbol{n}_2\right)\Big|^*_{\Gamma_2} - U_n\right)\mathrm{d}s = 0.$$

When $\theta_n < \frac{1}{2}$, a stabilization term is needed, which enforces weakly the condition $p_1\big|^*_{\Gamma_1} = p_2\big|^*_{\Gamma_2} = P$ through the following equation, for all $\varphi \in \mathcal{Q}^p$ and $R \in \mathcal{Q}^f$,

$$\chi_0 \sum_{i=1,2} \frac{\delta}{2\mu_f} \int_\gamma \left(p\big|^*_{\Gamma_i} - P\right)\left(\varphi\big|^*_{\Gamma_i} - R\right)\mathrm{d}s = 0,$$

where χ_0 is a function of θ_n such that

$$\chi_0 = \begin{cases} 1 - 2\theta_n & \text{if } \theta_n \in [0, 1/2), \\ 0 & \text{if } \theta_n \in [1/2, 1]. \end{cases}$$

Adding this equation guarantees the stability of the scheme, as shown in Theorem 4.5.

We define the following bilinear forms:

$$\begin{aligned}
a_e(\boldsymbol{\eta}, \boldsymbol{\xi}) &= 2\mu \int_{\Omega_p} \boldsymbol{D}(\boldsymbol{\eta}) : \boldsymbol{D}(\boldsymbol{\xi})\mathrm{d}\boldsymbol{x} + \lambda \int_{\Omega_p} (\nabla \cdot \boldsymbol{\eta})(\nabla \cdot \boldsymbol{\xi})\mathrm{d}\boldsymbol{x}, \\
a_e^\tau(\boldsymbol{\eta}, \boldsymbol{\xi}) &= \int_\gamma C^\tau \theta_\tau (3 - 5\theta_\tau) \left[(\boldsymbol{\eta}_1 \cdot \boldsymbol{\tau}_1)\,|^*_{\Gamma_1} + (\boldsymbol{\eta}_2 \cdot \boldsymbol{\tau}_2)\,|^*_{\Gamma_2}\right] \left[(\boldsymbol{\xi}_1 \cdot \boldsymbol{\tau}_1)\,\big|^*_{\Gamma_1} + (\boldsymbol{\xi}_2 \cdot \boldsymbol{\tau}_2)\,\big|^*_{\Gamma_2}\right] \mathrm{d}s, \\
a_e^\eta(\boldsymbol{\eta}, \boldsymbol{\xi}) &= \int_\gamma C^\eta \left[(\boldsymbol{\eta}_1 \cdot \boldsymbol{\tau}_1)\,|^*_{\Gamma_1} (\boldsymbol{\xi}_1 \cdot \boldsymbol{\tau}_1)\,|^*_{\Gamma_1} + (\boldsymbol{\eta}_2 \cdot \boldsymbol{\tau}_2)\,|^*_{\Gamma_2} (\boldsymbol{\xi}_2 \cdot \boldsymbol{\tau}_2)\,|^*_{\Gamma_2}\right] \mathrm{d}s, \\
a_q(\boldsymbol{q}, \boldsymbol{r}) &= \int_{\Omega_p} \boldsymbol{K}^{-1}\boldsymbol{q} \cdot \boldsymbol{r}\mathrm{d}\boldsymbol{x}, \\
a_f(\boldsymbol{U}, \boldsymbol{V}) &= \int_\gamma \delta \boldsymbol{M}\boldsymbol{U} \cdot \boldsymbol{V}\mathrm{d}s + \int_\gamma \delta\mu_f \frac{\partial \boldsymbol{U}}{\partial s} \cdot \frac{\partial \boldsymbol{V}}{\partial s}\mathrm{d}s, \\
a_f^\eta(\boldsymbol{U}, \boldsymbol{V}) &= \int_\gamma 2C^\eta U_\tau V_\tau \mathrm{d}s, \\
b_p(\boldsymbol{r}, \varphi) &= \int_{\Omega_p} \varphi \nabla \cdot \boldsymbol{r}\mathrm{d}\boldsymbol{x}, \\
b_f(\boldsymbol{V}, R) &= \int_\gamma \delta \frac{\partial V_\tau}{\partial s} R\mathrm{d}s, \\
b_\gamma^\eta(\boldsymbol{\xi}, \boldsymbol{V}) &= \int_\gamma C^\eta V_\tau \left((\boldsymbol{\xi}_1 \cdot \boldsymbol{\tau}_1)\big|^*_{\Gamma_1} - (\boldsymbol{\xi}_2 \cdot \boldsymbol{\tau}_2)\big|^*_{\Gamma_2}\right) \mathrm{d}s, \\
c_p(p, \varphi) &= \int_\gamma \left[\frac{(1-\theta_n)\delta}{2\mu_f} \left(p_1\big|^*_{\Gamma_1} + p_2\big|^*_{\Gamma_2}\right) \left(\varphi_1\big|^*_{\Gamma_1} + \varphi_2\big|^*_{\Gamma_2}\right)\right. \\
&\qquad \left. + (2\theta_n - 1 + \chi_0) \frac{\delta}{2\mu_f} \left((p_1\varphi_1)\,\big|^*_{\Gamma_1} + (p_2\varphi_2)\,\big|^*_{\Gamma_2}\right)\right] \mathrm{d}s \\
c_P(P, R) &= \int_\gamma (1 + \chi_0) \frac{\delta}{\mu_f} PR\,\mathrm{d}s, \\
c_\gamma(R, \varphi) &= \sum_{i=1,2} \int_\gamma (1 + \chi_0) \frac{\delta}{2\mu_f} \varphi\big|^*_{\Gamma_i} R\,\mathrm{d}s, \\
m_\gamma(\boldsymbol{\zeta}, \varphi) &= \sum_{i=1,2} \int_\gamma \varphi\big|^*_{\Gamma_i} (\boldsymbol{\zeta} \cdot \boldsymbol{n}_i)|^*_{\Gamma_i} \mathrm{d}s, \\
m_\gamma(\boldsymbol{V}, \varphi) &= \int_\gamma \left(\varphi_1\big|^*_{\Gamma_1} - \varphi_2\big|^*_{\Gamma_2}\right) V_n\,\mathrm{d}s \\
s_0(p, \varphi) &= \int_{\Omega_p} s_0 p\,\varphi\,\mathrm{d}\boldsymbol{x}.
\end{aligned}$$

Note that the bilinear form m_γ has a different definition depending on the type of its first component. Before proceeding, we substitute into $a_e^\tau(\boldsymbol{\eta},\boldsymbol{\xi})$, $a_e^\eta(\boldsymbol{\eta},\boldsymbol{\xi})$, $a_f^\eta(\boldsymbol{U},\boldsymbol{V})$ and $b_\gamma^\eta(\boldsymbol{\xi},\boldsymbol{U})$ the asymptotic expressions (3.55) for C^τ and C^η. It is straightforward to verify that all these bilinear forms are fully robust in the limit $c_{BJS},\delta\to 0$.

The variational form of equations (4.1)−(4.11) is given as follows: given initial conditions $p(0)=p_0$ and $\boldsymbol{\eta}(0)=\boldsymbol{\eta}_0$, for any $t\in(0,T]$, find $(\boldsymbol{\eta}(t),\boldsymbol{q}(t),\boldsymbol{U}(t),P(t),p(t))\in\mathcal{W}^D=\boldsymbol{\mathcal{V}}^\eta\times\boldsymbol{\mathcal{V}}^p\times\boldsymbol{\mathcal{V}}_D^f\times\mathcal{Q}^f\times\mathcal{Q}^p$ (displacement, Darcy velocity, fracture velocity, fracture pressure, and reservoir pressure, respectively) such that

$$
\begin{aligned}
&a_e(\boldsymbol{\eta},\boldsymbol{\xi})+a_e^\tau(\partial_t\boldsymbol{\eta},\boldsymbol{\xi})+a_e^\eta(\partial_t\boldsymbol{\eta},\boldsymbol{\xi})-b_\gamma^\eta(\boldsymbol{\xi},\boldsymbol{U})-\alpha b_p(\boldsymbol{\xi},p)+m_\gamma(\boldsymbol{\xi},p)=L_{\boldsymbol{\eta}}\boldsymbol{\xi},\quad\forall\boldsymbol{\xi}\in\boldsymbol{\mathcal{V}}^\eta,\\
&a_q(\boldsymbol{q},\boldsymbol{r})-b_p(\boldsymbol{r},p)+m_\gamma(\boldsymbol{r},p)=L_{\boldsymbol{q}}\boldsymbol{r},\quad\forall\boldsymbol{r}\in\boldsymbol{\mathcal{V}}^p,\\
&a_f(\boldsymbol{U},\boldsymbol{V})+a_f^\eta(\boldsymbol{U},\boldsymbol{V})-b_f(\boldsymbol{V},P)-b_\gamma^\eta(\partial_t\boldsymbol{\eta},\boldsymbol{V})-m_\gamma(\boldsymbol{V},p)=L_{\boldsymbol{U}}\boldsymbol{V},\quad\forall\boldsymbol{V}\in\boldsymbol{\mathcal{V}}^f,\\
&b_f(\boldsymbol{U},R)+c_P(P,R)-c_\gamma(R,p)=L_PR,\quad\forall R\in\mathcal{Q}^f,\\
&s_0(\partial_tp,\varphi)+c_p(p,\varphi)+\alpha b_p(\partial_t\boldsymbol{\eta},\varphi)+b_p(\boldsymbol{q},\varphi)-c_\gamma(P,\varphi)-m_\gamma(\partial_t\boldsymbol{\eta}+\boldsymbol{q}-\boldsymbol{U},\varphi)=L_p\varphi,\quad\forall\varphi\in\mathcal{Q}^p,
\end{aligned}
$$

where

$$
L_{\boldsymbol{\eta}}\boldsymbol{\xi}=\int_{\Omega_p}\boldsymbol{f}_p\cdot\boldsymbol{\xi}\mathrm{d}\boldsymbol{x}+\int_{\Gamma_p^N}\boldsymbol{s}_p^N\cdot\boldsymbol{\xi}\mathrm{d}x,\quad L_{\boldsymbol{q}}\boldsymbol{r}=-\int_{\Gamma_p^p}p^D\boldsymbol{r}\cdot\boldsymbol{n}_p\mathrm{d}x,
$$
$$
L_{\boldsymbol{U}}\boldsymbol{V}=\int_\gamma\delta\boldsymbol{F}\cdot\boldsymbol{V}ds,\quad L_PR=\int_\gamma\delta HR\mathrm{d}s,\quad L_p\varphi=\int_{\Omega_p}g\varphi\mathrm{d}\boldsymbol{x}.
$$

With a little abuse of notation the bilinear form $m_\gamma(\partial_t\boldsymbol{\eta}+\boldsymbol{q}-\boldsymbol{U},\varphi)$ has been combined, which prescribes the weak enforcement of normal flux continuity across the fracture interface. The coupled variational problem in the operator form is equivalent to the following equation,

$$
\begin{bmatrix}0\\0\\0\\0\\s_0\partial_tp\end{bmatrix}+\underbrace{\begin{bmatrix}\mathcal{A}_e+(\mathcal{A}_e^\tau+\mathcal{A}_e^\eta)\partial_t & 0 & -(\mathcal{B}_\gamma^\eta)^T & 0 & -(\alpha\mathcal{B}_p-\mathcal{M}_\gamma)^T\\ 0 & \mathcal{A}_q & 0 & 0 & -(\mathcal{B}_p-\mathcal{M}_\gamma)^T\\ -\mathcal{B}_\gamma^\eta\partial_t & 0 & \mathcal{A}_f+\mathcal{A}_f^\eta & -(\mathcal{B}_f)^T & -(\mathcal{M}_\gamma)^T\\ 0 & 0 & \mathcal{B}_f & \mathcal{C}_P & -(\mathcal{C}_\gamma)^T\\ (\alpha\mathcal{B}_p-\mathcal{M}_\gamma)\partial_t & \mathcal{B}_p-\mathcal{M}_\gamma & \mathcal{M}_\gamma & -\mathcal{C}_\gamma & \mathcal{C}_p\end{bmatrix}}_{\text{operator }\mathcal{A}}\begin{bmatrix}\boldsymbol{\eta}\\\boldsymbol{q}\\\boldsymbol{U}\\P\\p\end{bmatrix}=\underbrace{\begin{bmatrix}L_{\boldsymbol{\eta}}\\L_{\boldsymbol{q}}\\L_{\boldsymbol{U}}\\L_P\\L_p\end{bmatrix}}_{\mathcal{L}},\tag{4.17}
$$

where the matrix entries are the operators corresponding to the bilinear forms. For the terms containing time derivatives we have adopted the notation $a_e^\eta(\partial_t\boldsymbol{\eta},\boldsymbol{\xi})\equiv\mathcal{A}_e^\eta\partial_t\boldsymbol{\eta}\cdot\boldsymbol{\xi}$ (also equivalent to $\partial_t\mathcal{A}_e^\eta\boldsymbol{\eta}\cdot\boldsymbol{\xi}$ since all the bilinear forms have constant coefficients in time).

Now, we can write the coupled problem (4.12) and (4.15) as follows: given initial conditions $p(0)=p_0$ and $\boldsymbol{\eta}(0)=\boldsymbol{\eta}_0$, for any $t\in(0,T]$, find $\mathbb{X}(t)=(\boldsymbol{\eta},\boldsymbol{q},\boldsymbol{U},P,p)\in\mathcal{W}^D$ such that

$$
s_0(\partial_tp,\varphi)+\mathcal{A}(\mathbb{X}(t),\mathbb{Y})=\mathcal{L}(\mathbb{Y}),\quad\forall\mathbb{Y}\in\mathcal{W}=\boldsymbol{\mathcal{V}}^\eta\times\boldsymbol{\mathcal{V}}^p\times\boldsymbol{\mathcal{V}}^f\times\mathcal{Q}^f\times\mathcal{Q}^p,\tag{4.18}
$$

where $\mathcal{A}(\cdot,\cdot)$ is the bilinear form corresponding to the operator $\mathcal{A}$ in (4.17).

4.1. The semi-discrete formulation

We focus only on the spatial discretization of the coupled problem, since the presence of different regions with different spatial discretizations and interface conditions requires careful stability and convergence analysis. The extension of the analysis to the fully-discrete formulation with Backward Euler time discretization is relatively straightforward. To discretize the problem in space, we use the finite element method. Let $\mathcal{T}_h$ be a shape-regular finite element partition [11] of Ω_p with maximum element diameter h such that the traces of the partition on Γ_1 and Γ_2 coincide. These traces define a one dimensional mesh on γ. To simplify the notation, assume that $\boldsymbol{U}^D=0$.

We introduce conforming finite element spaces $\boldsymbol{\mathcal{V}}_h^\eta \subset \boldsymbol{\mathcal{V}}^\eta, \boldsymbol{\mathcal{V}}_h^p \subset \boldsymbol{\mathcal{V}}^p, \mathcal{Q}_h^p \subset \mathcal{Q}^p, \boldsymbol{\mathcal{V}}_h^f \subset \boldsymbol{\mathcal{V}}^f$, and $\mathcal{Q}_h^f \subset \mathcal{Q}^f$ based on $\mathcal{T}_h$. Let $\mathcal{W}_h = \boldsymbol{\mathcal{V}}_h^\eta \times \boldsymbol{\mathcal{V}}_h^p \times \boldsymbol{\mathcal{V}}_h^f \times \mathcal{Q}_h^f \times \mathcal{Q}_h^p$. More precisely, let $\boldsymbol{\mathcal{V}}_h^\eta$ consists of continuous Lagrangian elements of polynomial order $r_1 \geq 1$, let $\boldsymbol{\mathcal{V}}_h^p \times \mathcal{Q}_h^p$ be an inf-sup stable pair of Darcy mixed finite element spaces containing polynomials of degree $r_2 \geq 0$ and $l_2 \geq 0$, respectively, and let $\boldsymbol{\mathcal{V}}_h^f \times \mathcal{Q}_h^f$ be an inf-sup stable pair of Stokes elements containing at least polynomials of degree $r_3 \geq 1$ and $r_3 - 1$, respectively. Examples of admissible Darcy elements include the Raviart−Thomas and the Brezzi−Douglas−Marini spaces, and examples of Stokes elements include the Taylor−Hood elements, the MINI elements, and the Crouzeix−Raviart elements, see, *e.g.* [7].

Since the finite element spaces $\boldsymbol{\mathcal{V}}_h^f \times \mathcal{Q}_h^f$ are inf-sup stable, they satisfy the Fortin criterion, see [14] (Lem. 4.19), *i.e.*, there exists an interpolation operator $\Pi_h^f : (H^1(\gamma))^2 \to \boldsymbol{\mathcal{V}}_h^f$ such that for all $\boldsymbol{V} \in \boldsymbol{\mathcal{V}}^f$,

$$b_f(\boldsymbol{V} - \Pi_h^f \boldsymbol{V}, R_h) = 0 \quad \forall\, R_h \in \mathcal{Q}_h^f, \quad \|\Pi_h^f \boldsymbol{V}\|_{H^1(\gamma)} \lesssim \|\boldsymbol{V}\|_{H^1(\gamma)}, \tag{4.19}$$

where $a \lesssim b$ denotes $a \leq Cb$ with the positive constant C being unspecified, but uniformly independent on the characteristic mesh size h. Similarly, for inf-sup stable Darcy mixed finite elements $\boldsymbol{\mathcal{V}}_h^p \times \mathcal{Q}_h^p$, it is known *e.g.* [7], that there exists an interpolation operator $\Pi_h^p : H(\mathrm{div}; \Omega_p) \cap (H^s(\Omega_p))^2 \to \boldsymbol{\mathcal{V}}_h^p$, $s > 0$, such that for all $\boldsymbol{r} \in H(\mathrm{div}; \Omega_p) \cap (H^s(\Omega_p))^2$,

$$b_p(\boldsymbol{r} - \Pi_h^p \boldsymbol{r}, \varphi_h) = 0, \ \int_{\partial\Omega_p} (\boldsymbol{r} - \Pi_h^p \boldsymbol{r}) \cdot \boldsymbol{n}_p \, \varphi_h \, \mathrm{d}x = 0 \ \ \forall\, \varphi_h \in \mathcal{Q}_h^p, \quad \|\Pi_h^p \boldsymbol{r}\|_{L^2(\Omega_p)} \lesssim \|\boldsymbol{r}\|_{H^s(\Omega_p)} + \|\nabla \cdot \boldsymbol{r}\|_{L^2(\Omega_p)}. \tag{4.20}$$

The semi-discrete problem is given as follows: given initial conditions $p_h(0)$ and $\boldsymbol{\eta}_h(0)$, find $\mathbb{X}_h(t) = (\boldsymbol{\eta}_h, \boldsymbol{q}_h, \boldsymbol{U}_h, P_h, p_h) \in \mathcal{W}_h$ such that for any $t \in (0, T]$,

$$s_0(\partial_t p_h(t), \varphi_h) + \mathcal{A}(\mathbb{X}_h(t), \mathbb{Y}_h) = \mathcal{L}(\mathbb{Y}_h), \quad \forall \mathbb{Y}_h \in \mathcal{W}_h. \tag{4.21}$$

Since (4.21) is based on a conforming approximation, namely $\mathcal{W}_h \subset \mathcal{W}$, the discrete problem is strongly consistent with the continuous problem (4.18), *i.e.*, (4.21) is also satisfied by $\mathbb{X}(t)$, the solution of (4.18).

Let us group the unknowns as $\mathbb{X}_h = [\mathbb{U}_h, \mathbb{P}_h]$, $\mathbb{U}_h = [\boldsymbol{\eta}_h, \boldsymbol{q}_h, \boldsymbol{U}_h] \in \boldsymbol{\mathcal{V}}_h := \boldsymbol{\mathcal{V}}_h^\eta \times \boldsymbol{\mathcal{V}}_h^p \times \boldsymbol{\mathcal{V}}_h^f$, $\mathbb{P}_h = [P_h, p_h] \in \mathcal{Q}_h = \mathcal{Q}_h^f \times \mathcal{Q}_h^p$, as well as the test functions $\mathbb{Y}_h = [\mathbb{V}_h, \mathbb{Q}_h]$, $\mathbb{V}_h = [\boldsymbol{\xi}_h, \boldsymbol{r}_h, \boldsymbol{V}_h] \in \boldsymbol{\mathcal{V}}_h$, $\mathbb{Q}_h = [R_h, \varphi_h] \in \mathcal{Q}_h$. It is convenient to rewrite the operator $\mathcal{A}$ in the compact matrix form

$$\mathcal{A} = \begin{bmatrix} \widetilde{\mathcal{A}} + \widetilde{\mathcal{A}}^\eta \partial_t^\eta & -\big(\widetilde{\mathcal{B}}\big)^T \\ \widetilde{\mathcal{B}} \partial_t^\eta & \widetilde{\mathcal{C}} \end{bmatrix},$$

where the matrix blocks are defined as

$$\widetilde{\mathcal{A}} := \begin{bmatrix} \mathcal{A}_e & 0 & 0 \\ 0 & \mathcal{A}_q & 0 \\ 0 & 0 & \mathcal{A}_f \end{bmatrix}, \quad \widetilde{\mathcal{A}}^\eta := \begin{bmatrix} \mathcal{A}_e^\tau + \mathcal{A}_e^\eta & 0 & -\big(\mathcal{B}_\gamma^\eta\big)^T \\ 0 & 0 & 0 \\ -\mathcal{B}_\gamma^\eta & 0 & \mathcal{A}_f^\eta \end{bmatrix},$$

$$\widetilde{\mathcal{B}} := \begin{bmatrix} 0 & 0 & \mathcal{B}_f \\ \alpha\mathcal{B}_p - \mathcal{M}_\gamma & \mathcal{B}_p - \mathcal{M}_\gamma & \mathcal{M}_\gamma \end{bmatrix}, \quad \widetilde{\mathcal{C}} := \begin{bmatrix} \mathcal{C}_P & -\mathcal{C}_\gamma^T \\ -\mathcal{C}_\gamma & \mathcal{C}_p \end{bmatrix},$$

and the operator ∂_t^η denotes the time derivative applied only to the variable $\boldsymbol{\eta}$, *i.e.*

$$\widetilde{\mathcal{A}}^\eta \partial_t^\eta \equiv \widetilde{\mathcal{A}}^\eta \begin{bmatrix} \partial_t & 0 & 0 \\ 0 & 1 & 0 \\ 0 & 0 & 1 \end{bmatrix} = \begin{bmatrix} \big(\mathcal{A}_e^\tau + \mathcal{A}_e^\eta\big)\partial_t & 0 & -\big(\mathcal{B}_\gamma^\eta\big)^T \\ 0 & 0 & 0 \\ -\mathcal{B}_\gamma^\eta \partial_t & 0 & \mathcal{A}_f^\eta \end{bmatrix}.$$

In what follows, we utilize notational equivalence between matrices and discrete bilinear forms, for example $\mathbb{V}_h^T\widetilde{\mathcal{A}}\mathbb{U}_h = \widetilde{\mathcal{A}}(\mathbb{U}_h, \mathbb{V}_h)$.

We pursue the analysis of problem (4.21) in the general case where the parameter $s_0 \geq 0$. We make the restrictive assumption $p^D = 0$, because bounding the term $L_{\boldsymbol{q}}\boldsymbol{r} = -\int_{\Gamma_p^p} p^D \boldsymbol{r}\cdot\boldsymbol{n}_p \mathrm{d}x$ requires control of $\|\nabla\cdot\boldsymbol{q}\|_{L^2(\Omega_p)}$. This can be done by establishing a bound on $\|\partial_t p\|_{L^2(\Omega_p)}$ (see for example [36]), but we choose not to consider it here in order to keep the paper focused.

For any $\mathbb{Y}_h = [\boldsymbol{\xi}_h, \boldsymbol{r}_h, \boldsymbol{V}_h, R_h, \varphi_h] \in \mathcal{W}_h$ we define the following norms,

$$|||\mathbb{Y}_h|||_{\mathcal{A}}^2 := \|\boldsymbol{\xi}_h\|_{H^1(\Omega_p)}^2 + \|\boldsymbol{r}_h\|_{L^2(\Omega_p)}^2 + \|\sqrt{\delta}\boldsymbol{V}_h\|_{H^1(\gamma)}^2 + \|\sqrt{\delta}R_h\|_{L^2(\gamma)}^2 + \|\varphi_h\|_{L^2(\Omega_p)}^2 + \|\varphi_h\|_{L^2(\gamma)}^2,$$

where $\|\varphi_h\|_{L^2(\gamma)}^2$ is a shorthand notation for $\sum_{i=1,2}\|\varphi_h|_{\Gamma_i}^*\|_{L^2(\gamma)}^2$. Given the decomposition $\mathbb{Y}_h = [\mathbb{V}_h, \mathbb{Q}_h]$, we split the norm $|||\mathbb{Y}_h|||_{\mathcal{A}}$ into its velocity and pressure parts,

$$|||\mathbb{V}_h|||_{\mathcal{V}}^2 := \|\boldsymbol{\xi}_h\|_{H^1(\Omega_p)}^2 + \|\boldsymbol{r}_h\|_{L^2(\Omega_p)}^2 + \|\sqrt{\delta}\boldsymbol{V}_h\|_{H^1(\gamma)}^2,$$
$$|||\mathbb{Q}_h|||_{\mathcal{Q}}^2 := \|\sqrt{\delta}R_h\|_{L^2(\gamma)}^2 + \|\varphi_h\|_{L^2(\Omega_p)}^2 + \|\varphi_h\|_{L^2(\gamma)}^2.$$

It is convenient to introduce the time dependent versions of the above norms, for any $t \in [0,T]$,

$$|||\mathbb{V}_h|||_{\mathcal{V},t}^2 := \|\boldsymbol{\xi}_h(t)\|_{H^1(\Omega_p)}^2 + \int_0^t \left(\|\boldsymbol{r}_h\|_{L^2(\Omega_p)}^2 + \|\sqrt{\delta}\boldsymbol{V}_h\|_{H^1(\gamma)}^2\right)\mathrm{d}\tau,$$
$$|||\mathbb{Q}_h|||_{\mathcal{Q},t}^2 := \int_0^t \left(\|\sqrt{\delta}R_h\|_{L^2(\gamma)}^2 + \|\varphi_h\|_{L^2(\Omega_p)}^2 + \|\varphi_h\|_{L^2(\gamma)}^2\right)\mathrm{d}\tau,$$
$$|||\mathbb{Y}_h|||_{\mathcal{A},t}^2 := |||\mathbb{V}_h|||_{\mathcal{V},t}^2 + |||\mathbb{Q}_h|||_{\mathcal{Q},t}^2.$$

We also set the following norms on $[0,T]\times\Upsilon$ (where Υ stands for Ω_p or γ and the usual notation for Bochner spaces is adopted)

$$\|\cdot\|_{\mathcal{L}^2(L^2(\Upsilon))}^2 := \int_0^T \|\cdot\|_{L^2(\Upsilon)}^2; \quad \|\cdot\|_{\mathcal{L}^2(H^1(\Upsilon))}^2 := \int_0^T \|\cdot\|_{H^1(\Upsilon)}^2; \quad \|\cdot\|_{\mathcal{L}^\infty(H^1(\Upsilon))}^2 := \sup_{t\in[0,T]}\|\cdot\|_{H^1(\Upsilon)}^2,$$

and define

$$|||\mathbb{Y}_h|||_{\mathcal{A},T}^2 := \|\boldsymbol{\xi}_h\|_{\mathcal{L}^\infty(H^1(\Omega_p))}^2 + \|\boldsymbol{r}_h\|_{\mathcal{L}^2(L^2(\Omega_p))}^2 + \|\sqrt{\delta}\boldsymbol{V}_h\|_{\mathcal{L}^2(H^1(\gamma))}^2$$
$$+ \|\sqrt{\delta}R_h\|_{\mathcal{L}^2(L^2(\gamma))}^2 + \|\varphi_h\|_{\mathcal{L}^2(L^2(\Omega_p))}^2 + \|\varphi_h\|_{\mathcal{L}^2(L^2(\gamma))}^2.$$

In the analysis we will employ the Young's inequality

$$\forall\, a,b\in\mathbb{R},\ \forall\,\epsilon>0,\ ab \leq \frac{\epsilon}{2}a^2 + \frac{1}{2\epsilon}b^2. \tag{4.22}$$

Lemma 4.2. *The following properties hold with constants independent of h for all $t\in(0,T]$:*

(i) *Positivity of $\widetilde{\mathcal{A}}$:* $\exists a>0$, $a_0>0$ *such that* $\forall\,\mathbb{V}_h(t)\in\boldsymbol{\mathcal{V}}_h$,

$$\int_0^t \widetilde{\mathcal{A}}(\mathbb{V}_h, \partial_t^\eta\mathbb{V}_h)\mathrm{d}\tau \geq a|||\mathbb{V}_h|||_{\mathcal{V},t}^2 - a_0\|\boldsymbol{\xi}_h(0)\|_{H^1(\Omega_p)}^2. \tag{4.23}$$

(ii) *Non-negativity of $\widetilde{\mathcal{C}}$:* $\widetilde{\mathcal{C}}(\mathbb{Q}_h,\mathbb{Q}_h)\geq 0,\ \forall\mathbb{Q}_h\in\mathcal{Q}_h$.

(iii) *Continuity of* $\widetilde{\mathcal{A}}$: $\exists A > 0$ *such that* $\forall \mathbb{U}_h(t), \mathbb{V}_h(t) \in \boldsymbol{\mathcal{V}}_h$,

$$\widetilde{\mathcal{A}}(\mathbb{U}_h, \mathbb{V}_h) \leq A|||\mathbb{U}_h|||_{\mathcal{V}} |||\mathbb{V}_h|||_{\mathcal{V}}, \tag{4.24}$$

$$\int_0^t \widetilde{\mathcal{A}}(\mathbb{U}_h, \partial_t^\eta \mathbb{V}_h)\mathrm{d}\tau \leq A \left(|||\mathbb{U}_h|||_{\mathcal{V},t} |||\mathbb{V}_h|||_{\mathcal{V},t} + \int_0^t \|\partial_t \boldsymbol{\eta}_h\|_{H^1(\Omega_p)} \|\boldsymbol{\xi}_h\|_{H^1(\Omega_p)} \mathrm{d}\tau \right.$$
$$\left. + \|\boldsymbol{\eta}_h(0)\|_{H^1(\Omega_p)} \|\boldsymbol{\xi}_h(0)\|_{H^1(\Omega_p)} \right). \tag{4.25}$$

(iv) *Continuity of* $\mathcal{L}$: $\exists C^{\mathcal{L}} \geq 0$ *such that* $\forall \mathbb{Y}_h(t) \in \mathcal{W}_h$,

$$\int_0^t \mathcal{L}(\partial_t^\eta \mathbb{Y}_h)\mathrm{d}\tau \leq C^{\mathcal{L}} \left(|||\mathbb{Y}_h|||_{\mathcal{A},t} + \left(\int_0^t \|\boldsymbol{\xi}_h\|^2_{H^1(\Omega_p)} \mathrm{d}\tau \right)^{1/2} + \|\boldsymbol{\xi}_h(0)\|_{L^2(\Omega_p)} \right), \tag{4.26}$$

where

$$C^{\mathcal{L}} = C^{\mathcal{L}}(\|\partial_t \boldsymbol{f}_p\|_{\mathcal{L}^2(L^2(\Omega_p))}, \|\boldsymbol{f}_p\|_{\mathcal{L}^\infty(L^2(\Omega_p))}, \|\partial_t \boldsymbol{s}_p^N\|_{\mathcal{L}^2(L^2(\Gamma_p^N))}, \|\boldsymbol{s}_p^N\|_{\mathcal{L}^\infty(L^2(\Gamma_p^N))},$$
$$\|\sqrt{\delta}\boldsymbol{F}\|_{\mathcal{L}^2(L^2(\gamma))}, \|\sqrt{\delta}H\|_{\mathcal{L}^2(L^2(\gamma))}, \|g\|_{\mathcal{L}^2(L^2(\Omega_p))}).$$

Proof.

(i) For any $\mathbb{V}_h \in \boldsymbol{\mathcal{V}}_h$ we have, using (2.4) and (2.7),

$$\widetilde{\mathcal{A}}(\mathbb{V}_h, \partial_t^\eta \mathbb{V}_h) = a_e(\boldsymbol{\xi}_h, \partial_t \boldsymbol{\xi}_h) + a_q(\boldsymbol{r}_h, \boldsymbol{r}_h) + a_f(\boldsymbol{V}_h, \boldsymbol{V}_h)$$
$$\geq \frac{1}{2}\partial_t a_e(\boldsymbol{\xi}_h, \boldsymbol{\xi}_h) + k_1^{-1}\|\boldsymbol{r}_h\|^2_{L^2(\Omega_p)} + k_{f,1}^{-1}\|\sqrt{\delta}\boldsymbol{V}_h\|^2_{L^2(\gamma)} + \mu_f \left\| \sqrt{\delta}\frac{\partial \boldsymbol{V}_h}{\partial s} \right\|^2_{L^2(\gamma)}. \tag{4.27}$$

Property (i) follows by integrating over $[0, t]$ and employing the Poincaré−Friedrichs and Korn inequalities, see for example [14]. These hold since $|\Gamma_p^D| > 0$ (or $|\partial\Omega_{p,i} \cap \Gamma_p^D| > 0$) and imply the existence of a constant $C_{PFK} > 0$ such that

$$\|\boldsymbol{D}(\boldsymbol{\xi}_h)\|^2_{L^2(\Omega_p)} \geq C_{PFK}\|\boldsymbol{\xi}_h\|^2_{H^1(\Omega_p)}.$$

(ii) Consider first the case $\theta_n \in [1/2, 1]$. For any $\mathbb{Q}_h \in \mathcal{Q}_h$, $\widetilde{\mathcal{C}}(\mathbb{Q}_h, \mathbb{Q}_h) = c_P(R_h, R_h) + c_p(\varphi_h, \varphi_h) - 2c_\gamma(R_h, \varphi_h)$. In this case $\chi_0 = 0$ and we have

$$c_P(R_h, R_h) + c_p(\varphi_h, \varphi_h) = \frac{1}{\mu_f}\|\sqrt{\delta}R_h\|^2_{L^2(\gamma)} + \frac{(1-\theta_n)}{2\mu_f}\|\sqrt{\delta}(\varphi_{1,h}|^*_{\Gamma_1} + \varphi_{2,h}|^*_{\Gamma_2})\|^2_{L^2(\gamma)}$$
$$+ \frac{(2\theta_n - 1)}{2\mu_f}\left(\|\sqrt{\delta}\varphi_{1,h}|^*_{\Gamma_1}\|^2_{L^2(\gamma)} + \|\sqrt{\delta}\varphi_{2,h}|^*_{\Gamma_2}\|^2_{L^2(\gamma)} \right). \tag{4.28}$$

Furthermore, using the Cauchy−Schwarz and Young's inequalities with $\epsilon = 1/2$ we have

$$2c_\gamma(R_h, \varphi_h) = \int_\gamma \frac{\delta}{\mu_f}\left(\varphi_{1,h}|^*_{\Gamma_1} + \varphi_{2,h}|^*_{\Gamma_2} \right) R_h \mathrm{d}s$$
$$\leq \frac{1}{4\mu_f}\left\| \sqrt{\delta}(\varphi_{1,h}|^*_{\Gamma_1} + \varphi_{2,h}|^*_{\Gamma_2}) \right\|^2_{L^2(\gamma)} + \frac{1}{\mu_f}\|\sqrt{\delta}R_h\|^2_{L^2(\gamma)}. \tag{4.29}$$

Combining equation (4.28) with (4.29), we get

$$\widetilde{\mathcal{C}}(\mathbb{Q}_h, \mathbb{Q}_h) \geq \frac{1}{4\mu_f}(1 - 2\theta_n)\|\sqrt{\delta}(\varphi_{1,h}|^*_{\Gamma_1} + \varphi_{2,h}|^*_{\Gamma_2})\|^2_{L^2(\gamma)}$$
$$+ \frac{(2\theta_n - 1)}{2\mu_f}\left(\|\sqrt{\delta}\varphi_{1,h}|^*_{\Gamma_1}\|^2_{L^2(\gamma)} + \|\sqrt{\delta}\varphi_{2,h}|^*_{\Gamma_2}\|^2_{L^2(\gamma)} \right). \tag{4.30}$$

Now using the triangle inequality, it is easy to check that

$$\widetilde{\mathcal{C}}(\mathbb{Q}_h,\mathbb{Q}_h)\geq\frac{(2\theta_n-1)}{4\mu_f}\left(\|\sqrt{\delta}\varphi_{1,h}|^*_{\Gamma_1}\|_{L^2(\gamma)}-\|\sqrt{\delta}\varphi_{2,h}|^*_{\Gamma_1}\|_{L^2(\gamma)}\right)^2\geq 0.$$

We next consider the case $\theta_n\in[0,1/2)$, where $\chi_0=1-2\theta_n$. A direct calculation shows that

$$\widetilde{\mathcal{C}}(\mathbb{Q}_h,\mathbb{Q}_h)=\frac{(1-2\theta_n)}{4\mu_f}\|\sqrt{\delta}(\varphi_{1,h}|^*_{\Gamma_1}+\varphi_{2,h}|^*_{\Gamma_1}-2R_h)\|^2_{L^2(\gamma)}\geq 0.$$

(iii) Inequality (4.24) follows easily from the Cauchy−Schwarz inequality. To prove (4.25), we note that

$$\int_0^t\widetilde{\mathcal{A}}(\mathbb{U}_h,\partial_t^\eta\mathbb{V}_h)\mathrm{d}\tau=\int_0^t\left(a_e(\boldsymbol{\eta}_h,\partial_t\boldsymbol{\xi}_h)+a_q(\boldsymbol{q}_h,\boldsymbol{r}_h)+a_f(\boldsymbol{U}_h,\boldsymbol{V}_h)\right)\mathrm{d}\tau \tag{4.31}$$

and focus on the first term on the right. Integration by parts gives

$$\int_0^t a_e(\boldsymbol{\eta}_h,\partial_t\boldsymbol{\xi}_h)\mathrm{d}\tau=-\int_0^t a_e(\partial_t\boldsymbol{\eta}_h,\boldsymbol{\xi}_h)\mathrm{d}\tau+a_e(\boldsymbol{\eta}_h,\boldsymbol{\xi}_h)\Big|_0^t. \tag{4.32}$$

Bound (4.25) follows from applying the Cauchy−Schwarz inequality to the terms on the right in (4.32) and the last two terms on the right in (4.31).

(iv) Assuming sufficient smoothness of the data, the continuity bound (4.26) follows by integration by parts in time in the terms $\int_{\Omega_p}\boldsymbol{f}_p\cdot\partial_t\boldsymbol{\xi}_h$ and $\int_{\Gamma_p^N}\boldsymbol{s}_p^N\cdot\partial_t\boldsymbol{\xi}_h$, and then applying the Cauchy−Schwarz inequality for all terms, using also the trace inequality [14]

$$\|\xi\|_{L^2(\partial\Omega_p)}\lesssim\|\xi\|_{H^1(\Omega_p)},\quad\forall\,\xi\in H^1(\Omega_p). \tag{4.33}$$

□

In the following we use the shorthand notation

$$\|\boldsymbol{\xi}_h\cdot\boldsymbol{\tau}\|^2_{L^2(\gamma)}:=\sum_{i=1,2}\|(\boldsymbol{\xi}_{i,h}\cdot\boldsymbol{\tau}_i)^*_{\Gamma_i}\|^2_{L^2(\gamma)},$$

as well as the jump notation $[\boldsymbol{\xi}_h\cdot\boldsymbol{\tau}]=(\boldsymbol{\xi}_{1,h}\cdot\boldsymbol{\tau}_1)|^*_{\Gamma_1}+(\boldsymbol{\xi}_{2,h}\cdot\boldsymbol{\tau}_2)|^*_{\Gamma_2}$

Lemma 4.3. *The following properties of $\widetilde{\mathcal{A}}^\eta$ are satisfied. When $\theta_\tau=0$, $\widetilde{\mathcal{A}}^\eta=0$. When $\theta_\tau=1/2$,*

$$\widetilde{\mathcal{A}}^\eta(\mathbb{V}_h,\mathbb{V}_h)=\frac{C^\tau}{4}\|[\boldsymbol{\xi}_h\cdot\boldsymbol{\tau}]\|^2_{L^2(\gamma)}, \tag{4.34}$$

$$\widetilde{\mathcal{A}}^\eta(\mathbb{U}_h,\mathbb{V}_h)\leq\frac{C^\tau}{4}\|[\boldsymbol{\eta}_h\cdot\boldsymbol{\tau}]\|_{L^2(\gamma)}\|[\boldsymbol{\xi}_h\cdot\boldsymbol{\tau}]\|_{L^2(\gamma)}. \tag{4.35}$$

When $\theta_\tau=2/3$, provided that $\delta>0$, there exist a positive constant A^η such that

$$\widetilde{\mathcal{A}}^\eta(\mathbb{V}_h,\mathbb{V}_h)+10\delta^{-1}c_{BJS}\|\sqrt{\delta}\boldsymbol{V}_h\|^2_{L^2(\gamma)}\geq\frac{1}{6}C^\eta\|\boldsymbol{\xi}_h\cdot\boldsymbol{\tau}\|^2_{L^2(\gamma)}, \tag{4.36}$$

$$\begin{aligned}\widetilde{\mathcal{A}}^\eta(\mathbb{U}_h,\mathbb{V}_h)\leq A^\eta\Big(&C^\eta\|\boldsymbol{\eta}_h\cdot\boldsymbol{\tau}\|_{L^2(\gamma)}\|\boldsymbol{\xi}_h\cdot\boldsymbol{\tau}\|_{L^2(\gamma)}+\delta^{-1}c_{BJS}\|\sqrt{\delta}\boldsymbol{U}_h\|_{L^2(\gamma)}\|\sqrt{\delta}\boldsymbol{V}_h\|_{L^2(\gamma)}\\&+\delta^{-\frac{1}{2}}\sqrt{c_{BJS}}\sqrt{C^\eta}\left(\|\sqrt{\delta}\boldsymbol{U}_h\|_{L^2(\gamma)}\|\boldsymbol{\xi}_h\cdot\boldsymbol{\tau}\|_{L^2(\gamma)}+\|\sqrt{\delta}\boldsymbol{V}_h\|_{L^2(\gamma)}\|\boldsymbol{\eta}_h\cdot\boldsymbol{\tau}\|_{L^2(\gamma)}\right)\Big).\end{aligned} \tag{4.37}$$

Proof. When $\theta_\tau = 0, 1/2$ only the term $\mathcal{A}_e^\tau$ of $\widetilde{\mathcal{A}}^\eta$ is active, *i.e.* $\widetilde{\mathcal{A}}^\eta(\mathbb{V}_h, \mathbb{V}_h) = a_e^\tau(\boldsymbol{\xi}_h, \boldsymbol{\xi}_h)$, and (4.34) follows directly from the definition of $a_e^\tau(\boldsymbol{\xi}_h, \boldsymbol{\xi}_h)$, since it is non-negative. The upper bound (4.35) follows from the Cauchy−Schwarz inequality.

In the case $\theta_\tau = \frac{2}{3}$, the coefficient in $a_e^\tau(\cdot,\cdot)$ is negative and all entries of $\widetilde{\mathcal{A}}^\eta$ are active. Using Young's inequality (4.22) for $b_\gamma^\eta(\boldsymbol{V}_h, \boldsymbol{\xi}_h)$, we obtain

$$\begin{aligned}\widetilde{\mathcal{A}}^\eta(\mathbb{V}_h, \mathbb{V}_h) &= a_e^\eta(\boldsymbol{\xi}_h, \boldsymbol{\xi}_h) + a_f^\eta(\boldsymbol{V}_h, \boldsymbol{V}_h) + a_e^\tau(\boldsymbol{\xi}_h, \boldsymbol{\xi}_h) - 2b_\gamma^\eta(\boldsymbol{V}_h, \boldsymbol{\xi}_h)\\ &\geq 2\left(\frac{\epsilon-1}{\epsilon}\right) C^\eta \|V_{\tau,h}\|^2_{L^2(\gamma)} + (1-\epsilon)C^\eta \sum_{i=1,2} \|\boldsymbol{\xi}_{i,h}\cdot\boldsymbol{\tau}_i\|^2_{L^2(\gamma)} - \frac{4}{9}C^\tau \sum_{i=1,2} \|\boldsymbol{\xi}_{i,h}\cdot\boldsymbol{\tau}_i\|^2_{L^2(\gamma)}\\ &\geq 2\left(\frac{\epsilon-1}{\epsilon}\right) C^\eta \|V_{\tau,h}\|^2_{L^2(\gamma)} + (\frac{1}{3}-\epsilon)C^\eta \sum_{i=1,2} \|\boldsymbol{\xi}_{i,h}\cdot\boldsymbol{\tau}_i\|^2_{L^2(\gamma)},\end{aligned}$$

where we have used (3.56) and the fact that $1 - \frac{2\delta c_{BJS}}{3c_{BJS}\delta + 6\mu_f} \geq \frac{1}{3}$ in the last inequality. Inequality (4.36) follows by taking $\epsilon = 1/6$ and using (3.57) and the assumption $\delta > 0$. The continuity bound (4.37) is obtained using the Cauchy−Schwarz inequality. □

Lemma 4.4. *The operator $(\widetilde{\mathcal{B}})^T$ is inf-sup stable, that is: there exists $\beta > 0$ independent of h such that $\forall \mathbb{Q}_h = [R_h, \varphi_h] \in \mathcal{Q}_h$, there exists $\mathbb{V}_h = [\boldsymbol{0}, \boldsymbol{r}_h, \boldsymbol{V}_h] \in \boldsymbol{\mathcal{V}}_h$ such that*

$$(\widetilde{\mathcal{B}})^T(\mathbb{Q}_h, \mathbb{V}_h) \geq |||\mathbb{Q}_h|||^2_{\mathcal{Q}}, \quad |||\mathbb{V}_h|||_{\mathcal{V}} \leq \beta |||\mathbb{Q}_h|||_{\mathcal{Q}}. \tag{4.38}$$

Proof. We first note that for any $R_h \in \mathcal{Q}_h^f$, there exists $\boldsymbol{V} = (0, V_\tau) \in \boldsymbol{\mathcal{V}}^f$ such that

$$b_f(\boldsymbol{V}, R_h) \geq \|\sqrt{\delta} R_h\|^2_{L^2(\gamma)}, \quad \|\sqrt{\delta}\boldsymbol{V}\|_{H^1(\gamma)} \lesssim \|\sqrt{\delta} R_h\|_{L^2(\gamma)},$$

which can be achieved by noting that $b_f(\boldsymbol{V}, R_h) = \int_\gamma \delta \frac{\partial V_\tau}{\partial s} R_h \, \mathrm{d}s$, and choosing $V_\tau = \int_0^s R_h(\zeta) d\zeta$. Taking $\boldsymbol{V}_h = \mathit{\Pi}_h^f \boldsymbol{V}$ and using the properties (4.19) of $\mathit{\Pi}_h^f$, we conclude that

$$b_f(\boldsymbol{V}_h, R_h) \geq \|\sqrt{\delta} R_h\|^2_{L^2(\gamma)}, \quad \|\sqrt{\delta}\boldsymbol{V}_h\|_{H^1(\gamma)} \lesssim \|\sqrt{\delta} R_h\|_{L^2(\gamma)}. \tag{4.39}$$

Next, for any $\varphi_h \in \mathcal{Q}_h^p$, there exists $\boldsymbol{r} \in \boldsymbol{\mathcal{V}}^p$ such that, for some $s > 0$,

$$b_p(\boldsymbol{r}, \varphi_h) - m_\gamma(\boldsymbol{r}, \varphi_h) \geq \|\varphi_h\|^2_{L^2(\Omega_p)} + \|\varphi_h\|^2_{L^2(\gamma)}, \quad \|\boldsymbol{r}\|_{H^s(\Omega_p)} + \|\nabla\cdot\boldsymbol{r}\|_{L^2(\Omega_p)} \lesssim \|\varphi_h\|_{L^2(\Omega_p)} + \|\varphi_h\|_{L^2(\gamma)}, \tag{4.40}$$

which can be achieved by taking $\boldsymbol{r} = \nabla\psi$, where ψ is the solution to the problem

$$\begin{aligned} &\Delta\psi = \varphi_h && \text{in } \mathit{\Omega}_p,\\ &\nabla\psi\cdot\boldsymbol{n}_i = -\varphi_{i,h} && \text{on } \mathit{\Gamma}_i,\ i = 1,2,\\ &\psi = 0 && \text{on } \mathit{\Gamma}_p^p,\\ &\nabla\psi\cdot\boldsymbol{n}_p = 0 && \text{on } \mathit{\Gamma}_p^q. \end{aligned} \tag{4.41}$$

The above problem is well posed, since $|\mathit{\Gamma}_p^p| > 0$ (or $|\partial\mathit{\Omega}_{p,i} \cap \mathit{\Gamma}_p^p| > 0$). The first part of (4.40) is satisfied by construction, while the second part is guaranteed by the elliptic regularity of problem (4.41) [23, 29]. We now choose $\boldsymbol{r}_h = \mathit{\Pi}_h^p \boldsymbol{r}$ and, using the properties (4.20) of $\mathit{\Pi}_h^p$, we conclude that

$$b_p(\boldsymbol{r}_h, \varphi_h) - m_\gamma(\boldsymbol{r}_h, \varphi_h) \geq \|\varphi_h\|^2_{L^2(\Omega_p)} + \|\varphi_h\|^2_{L^2(\gamma)}, \quad \|\boldsymbol{r}_h\|_{L^2(\Omega_p)} \lesssim \|\varphi_h\|_{L^2(\Omega_p)} + \|\varphi_h\|_{L^2(\gamma)}. \tag{4.42}$$

Finally, we note that $V_{n,h} = 0$ implies that $m_\gamma(\boldsymbol{V}_h, \varphi_h) = 0$. Combining (4.39) and (4.42) we obtain

$$\begin{aligned}(\widetilde{\mathcal{B}})^T(\mathbb{Q}_h, \mathbb{V}_h) &= b_f(\boldsymbol{V}_h, R_h) + b_p(\boldsymbol{r}_h, \varphi_h) - m_\gamma(\boldsymbol{r}_h - \boldsymbol{V}_h, \varphi_h)\\ &\geq \|\sqrt{\delta} R_h\|^2_{L^2(\gamma)} + \|\varphi_h\|^2_{L^2(\Omega_p)} + \|\varphi_h\|^2_{L^2(\gamma)} = |||\mathbb{Q}_h|||^2_{\mathcal{Q}}\end{aligned}$$

and

$$|||\mathbb{V}_h|||_{\mathcal{V}}^2 = \|\sqrt{\delta}\boldsymbol{V}_h\|_{H^1(\gamma)}^2 + \|\boldsymbol{r}_h\|_{L^2(\Omega_p)}^2 \lesssim \|\sqrt{\delta}R_h\|_{L^2(\gamma)}^2 + \|\varphi_h\|_{L^2(\Omega_p)}^2 + \|\varphi_h\|_{L^2(\gamma)}^2 = |||\mathbb{Q}_h|||_{\mathcal{Q}}^2.$$

□

We are now ready to prove the following stability result.

Theorem 4.5. *Under the assumptions of Lemma 4.3 and under the additional condition that when $\theta_\tau = 2/3$, c_{BJS} is small enough such that $a - 10\delta^{-1}c_{BJS} \geq \alpha_1 > 0$, then the solution of (4.21) satisfies*

$$\begin{aligned} s_0\|p_h\|_{\mathcal{L}^\infty(L^2(\Omega_p))}^2 + |||\mathbb{X}_h|||_{\mathcal{A},T}^2 + \chi_{\theta_{\tau,1}}C^\tau\|[\partial_t\boldsymbol{\eta}_h\cdot\boldsymbol{\tau}]\|_{\mathcal{L}^2(L^2(\gamma))}^2 + \chi_{\theta_{\tau,2}}C^\eta\|\partial_t\boldsymbol{\eta}_h\cdot\boldsymbol{\tau}\|_{\mathcal{L}^2(L^2(\gamma))}^2 \\ \lesssim (C^{\mathcal{L}})^2 + \|\boldsymbol{\eta}_h(0)\|_{H^1(\Omega_p)}^2 + \|p_h(0)\|_{L^2(\Omega_p)}^2, \end{aligned} \tag{4.43}$$

where $\chi_{\theta_{\tau,1}} = 1$ when $\theta_\tau = 1/2$, $\chi_{\theta_{\tau,1}} = 0$ otherwise, and $\chi_{\theta_{\tau,2}} = 1$ when $\theta_\tau = 2/3$, $\chi_{\theta_{\tau,2}} = 0$ otherwise.

Proof. Let us take in (4.21) $\mathbb{Y}_{\mathbb{P},h} = [\partial_t^\eta\mathbb{U}_h - \epsilon_1\mathbb{V}_{\mathbb{P},h}, \mathbb{P}_h]$, where $\mathbb{V}_{\mathbb{P},h} \in \boldsymbol{\mathcal{V}}_h$ is the velocity field constructed in Lemma 4.4 with data $\mathbb{P}_h$ and $\epsilon_1 > 0$ is a small parameter to be determined. Integration in time gives

$$\int_0^t \left(s_0(\partial_t p_h, p_h) + \mathcal{A}(\mathbb{X}_h, \mathbb{Y}_{\mathbb{P},h})\right)\mathrm{d}\tau = \int_0^t \mathcal{L}(\mathbb{Y}_{\mathbb{P},h})\mathrm{d}\tau. \tag{4.44}$$

We have

$$\begin{aligned} \mathcal{A}(\mathbb{X}_h, \mathbb{Y}_{\mathbb{P},h}) =& \widetilde{\mathcal{A}}(\mathbb{U}_h, \partial_t^\eta\mathbb{U}_h - \epsilon_1\mathbb{V}_{\mathbb{P},h}) + \widetilde{\mathcal{A}}^\eta\partial_t^\eta(\mathbb{U}_h, \partial_t^\eta\mathbb{U}_h - \epsilon_1\mathbb{V}_{\mathbb{P},h}) \\ &- (\widetilde{\mathcal{B}})^T(\mathbb{P}_h, \partial_t^\eta\mathbb{U}_h - \epsilon_1\mathbb{V}_{\mathbb{P},h}) + \widetilde{\mathcal{B}}\partial_t^\eta(\mathbb{U}_h, \mathbb{P}_h) + \widetilde{\mathcal{C}}(\mathbb{P}_h, \mathbb{P}_h) \\ =& \widetilde{\mathcal{A}}(\mathbb{U}_h, \partial_t^\eta\mathbb{U}_h) - \epsilon_1\widetilde{\mathcal{A}}(\mathbb{U}_h, \mathbb{V}_{\mathbb{P},h}) + \widetilde{\mathcal{A}}^\eta(\partial_t^\eta\mathbb{U}_h, \partial_t^\eta\mathbb{U}_h) - \epsilon_1\widetilde{\mathcal{A}}^\eta(\partial_t^\eta\mathbb{U}_h, \mathbb{V}_{\mathbb{P},h}) \\ &+ \epsilon_1(\widetilde{\mathcal{B}})^T(\mathbb{P}_h, \mathbb{V}_{\mathbb{P},h}) + \widetilde{\mathcal{C}}(\mathbb{P}_h, \mathbb{P}_h). \end{aligned} \tag{4.45}$$

We next estimate each of the terms on the right in the above equality. Lemma 4.2 (i), (ii), and Lemma 4.4 imply, respectively,

$$\int_0^t \widetilde{\mathcal{A}}(\mathbb{U}_h, \partial_t^\eta\mathbb{U}_h)\mathrm{d}\tau \geq a|||\mathbb{U}_h|||_{\mathcal{V},t}^2 - a_0\|\boldsymbol{\eta}_h(0)\|_{H^1(\Omega_p)}^2, \tag{4.46}$$

$$\int_0^t \widetilde{\mathcal{C}}(\mathbb{P}_h, \mathbb{P}_h)\mathrm{d}\tau \geq 0, \tag{4.47}$$

and

$$\int_0^t (\widetilde{\mathcal{B}})^T(\mathbb{P}_h, \mathbb{V}_{\mathbb{P},h})\mathrm{d}\tau \geq |||\mathbb{P}_h|||_{\mathcal{Q},t}^2. \tag{4.48}$$

Recalling that $\mathbb{V}_{\mathbb{P},h} = [\boldsymbol{0}, \boldsymbol{r}_h, \boldsymbol{V}_h]$, we have

$$\begin{aligned} \int_0^t \widetilde{\mathcal{A}}(\mathbb{U}_h, \mathbb{V}_{\mathbb{P},h})\mathrm{d}\tau = \int_0^t \left(a_q(\boldsymbol{q}_h, \boldsymbol{r}_h) + a_f(\boldsymbol{U}_h, \boldsymbol{V})\right)\mathrm{d}\tau \leq A|||\mathbb{U}_h|||_{\mathcal{V},t}\,|||\mathbb{V}_{\mathbb{P},h}|||_{\mathcal{V},t} \\ \leq (4\epsilon_1')^{-1}A|||\mathbb{U}_h|||_{\mathcal{V},t}^2 + \epsilon_1' A\beta^2|||\mathbb{P}_h|||_{\mathcal{Q},t}^2, \end{aligned} \tag{4.49}$$

where A is the constant from (4.24) and we have used (4.38) and Young's inequality (4.22) with $\epsilon = 2\epsilon_1'$.

We next estimate the terms involving $\widetilde{\mathcal{A}}^\eta$. These terms are zero when $\theta_\tau = 0$. Let us consider the case $\theta_\tau = 1/2$. Thanks to Lemma 4.3 and using that $\mathbb{V}_{\mathbb{P},h} = [\boldsymbol{0}, \boldsymbol{r}_h, \boldsymbol{V}_h]$, the following properties hold true,

$$\widetilde{\mathcal{A}}^\eta(\partial_t^\eta\mathbb{U}_h, \partial_t^\eta\mathbb{U}_h) = \frac{C^\tau}{4}\|[\partial_t\boldsymbol{\eta}_h]\|_{L^2(\gamma)}^2, \tag{4.50}$$

$$\widetilde{\mathcal{A}}^\eta(\partial_t^\eta\mathbb{U}_h, \mathbb{V}_{\mathbb{P},h}) = a_e^\tau(\partial_t\boldsymbol{\eta}_h, \boldsymbol{0}) = 0. \tag{4.51}$$

Combining (4.45)–(4.51), we obtain

$$\begin{aligned}
&\int_0^t \left(s_0(\partial_t p_h, p_h) + \mathcal{A}(\mathbb{X}_h, \mathbb{Y}_{\mathbb{P},h})\right) \mathrm{d}\tau + a_0 \|\boldsymbol{\eta}_h(0)\|^2_{H^1(\Omega_p)} + \frac{s_0}{2}\|p_h(0)\|^2_{L^2(\Omega_p)} \\
&\geq \left(a - \epsilon_1 (4\epsilon_1')^{-1} A\right) |||\mathbb{U}_h|||^2_{\mathcal{V},t} + \epsilon_1 \left(1 - \epsilon_1' A \beta^2\right) |||\mathbb{P}_h|||^2_{\mathcal{Q},t} + \frac{s_0}{2}\|p_h(t)\|^2_{L^2(\Omega_p)} \\
&\quad + \chi_{\theta_{\tau,1}} \frac{C^\tau}{4} \int_0^t \|[\partial_t \boldsymbol{\eta}_h \cdot \boldsymbol{\tau}]\|^2_{L^2(\gamma)} \mathrm{d}\tau. \qquad (4.52)
\end{aligned}$$

We next consider the case $\theta_\tau = 2/3$. Owing to Lemma 4.3 and in particular (4.36), we have

$$\begin{aligned}
\int_0^t \widetilde{\mathcal{A}}^\eta(\partial_t^\eta \mathbb{U}_h, \partial_t^\eta \mathbb{U}_h) \mathrm{d}\tau &\geq \int_0^t \left(\frac{1}{6} C^\eta \|\partial_t \boldsymbol{\eta}_h \cdot \boldsymbol{\tau}\|^2_{L^2(\gamma)} - 10\delta^{-1} c_{BJS} \|\sqrt{\delta}\boldsymbol{U}_h\|^2_{L^2(\gamma)}\right) \mathrm{d}\tau \\
&\geq \int_0^t \frac{1}{6} C^\eta \|\partial_t \boldsymbol{\eta}_h \cdot \boldsymbol{\tau}\|^2_{L^2(\gamma)} \mathrm{d}\tau - 10\delta^{-1} c_{BJS} |||\mathbb{U}_h|||^2_{\mathcal{V},t}. \qquad (4.53)
\end{aligned}$$

We note that the last term in the previous inequality does not involve ∂_t^η, because this operator is the identity for variables on Ω_f. Using (4.37) and recalling that $\mathbb{V}_{\mathbb{P},h} = [\mathbf{0}, \boldsymbol{r}_h, \boldsymbol{V}_h]$ the upper bound of $\widetilde{\mathcal{A}}^\eta(\partial_t^\eta \mathbb{U}_h, \mathbb{V}_{\mathbb{P},h})$ reads as follows,

$$\begin{aligned}
&\int_0^t \widetilde{\mathcal{A}}^\eta(\partial_t^\eta \mathbb{U}_h, \mathbb{V}_{\mathbb{P},h}) \mathrm{d}\tau \\
&\leq A^\eta \int_0^t \left(\delta^{-1} c_{BJS} \|\sqrt{\delta}\boldsymbol{U}_h\|_{L^2(\gamma)} \|\sqrt{\delta}\boldsymbol{V}_h\|_{L^2(\gamma)} + \delta^{-1/2}\sqrt{c_{BJS}}\sqrt{C^\eta} \|\sqrt{\delta}\boldsymbol{V}_h\|_{L^2(\gamma)} \|\partial_t \boldsymbol{\eta}_h \cdot \boldsymbol{\tau}\|_{L^2(\gamma)}\right) \mathrm{d}\tau \\
&\leq A^\eta \left(\delta^{-1/2}\sqrt{c_{BJS}} |||\mathbb{U}_h|||_{\mathcal{V},t} + \left(\int_0^t \sqrt{C^\eta} \|\partial_t \boldsymbol{\eta}_h \cdot \boldsymbol{\tau}\|^2_{L^2(\gamma)} \mathrm{d}\tau\right)^{1/2}\right) \delta^{-1/2}\sqrt{c_{BJS}} |||\mathbb{V}_{\mathbb{P},h}|||_{\mathcal{V},t} \\
&\leq A^\eta \delta^{-1} c_{BJS} (4\epsilon_1')^{-1} |||\mathbb{U}_h|||^2_{\mathcal{V},t} + A^\eta (4\epsilon_1')^{-1} \int_0^t \sqrt{C^\eta} \|\partial_t \boldsymbol{\eta}_h \cdot \boldsymbol{\tau}\|^2_{L^2(\gamma)} \mathrm{d}\tau + 2A^\eta \epsilon_1' \delta^{-1} c_{BJS} \beta^2 |||\mathbb{P}_h|||^2_{\mathcal{Q},t}, \qquad (4.54)
\end{aligned}$$

where we have used (4.38) and Young's inequality (4.22) with $\epsilon = 2\epsilon_1'$. Combining (4.45)–(4.49) and (4.53)–(4.54), we obtain

$$\begin{aligned}
&\int_0^t \left(s_0(\partial_t p_h, p_h) + \mathcal{A}(\mathbb{X}_h, \mathbb{Y}_{\mathbb{P},h})\right) \mathrm{d}\tau + a_0 \|\boldsymbol{\eta}_h(0)\|^2_{H^1(\Omega_p)} + \frac{s_0}{2}\|p_h(0)\|^2_{L^2(\Omega_p)} \\
&\quad \geq \left(a - 10\delta^{-1} c_{BJS} - \epsilon_1 (4\epsilon_1')^{-1} (A + A^\eta \delta^{-1} c_{BJS})\right) |||\mathbb{U}_h|||^2_{\mathcal{V},t} \\
&\qquad + \left(\frac{1}{6} - \epsilon_1 (4\epsilon_1')^{-1} A^\eta\right) \int_0^t C^\eta \|\partial_t \boldsymbol{\eta}_h \cdot \boldsymbol{\tau}\|^2_{L^2(\gamma)} \mathrm{d}\tau \\
&\qquad + \epsilon_1 \left(1 - \epsilon_1' \left(A + 2A^\eta \delta^{-1} c_{BJS}\right) \beta^2\right) |||\mathbb{P}_h|||^2_{\mathcal{Q},t} + \frac{s_0}{2}\|p_h(t)\|^2_{L^2(\Omega_p)}. \qquad (4.55)
\end{aligned}$$

We now consider (4.52) for $\theta_\tau = 0, 1/2$ and (4.55) for $\theta_\tau = 2/3$. First we fix ϵ_1' sufficiently small so that the coefficient of $|||\mathbb{P}_h|||^2_{\mathcal{Q},t}$ is strictly positive. Then we take ϵ_1 small enough so that the rest of the coefficients on the right hand sides are strictly positive. To be able to do this in the case of $\theta_\tau = 2/3$, we need to assume that $a - 10\delta^{-1} c_{BJS} \geq \alpha_1 > 0$. Then in both cases we conclude that

$$\begin{aligned}
&s_0 \|p_h\|^2_{L^2(\Omega_p)} + |||\mathbb{X}_h|||^2_{\mathcal{A},t} + \chi_{\theta_{\tau,1}} \int_0^t C^\tau \|[\partial_t \boldsymbol{\eta}_h \cdot \boldsymbol{\tau}]\|^2_{L^2(\gamma)} \mathrm{d}\tau + \chi_{\theta_{\tau,2}} \int_0^t C^\eta \|\partial_t \boldsymbol{\eta}_h \cdot \boldsymbol{\tau}\|^2_{L^2(\gamma)} \mathrm{d}\tau \\
&\quad \lesssim \int_0^t \left(s_0(\partial_t p_h(t), p_h) + \mathcal{A}(\mathbb{X}_h, \mathbb{Y}_{\mathbb{P},h})\right) \mathrm{d}\tau + \|\boldsymbol{\eta}_h(0)\|^2_{H^1(\Omega_p)} + \|p_h(0)\|^2_{L^2(\Omega_p)}, \qquad (4.56)
\end{aligned}$$

which provides a coercivity bound for the left hand side in (4.44). The upper bound on the right hand side in (4.44) follows from Lemma 4.2 (iv):

$$\int_0^t \mathcal{L}(\mathbb{Y}_{\mathbb{P},h})\mathrm{d}\tau = \int_0^t \mathcal{L}([\partial_t^\eta \mathbb{U}_h - \epsilon_1 \mathbb{V}_{\mathbb{P},h}, \mathbb{P}_h])\mathrm{d}\tau$$
$$\leq (1+\epsilon_1\beta)C^{\mathcal{L}}\left(|||\mathbb{X}_h|||_{\mathcal{A},t} + \left(\int_0^t \|\boldsymbol{\eta}_h\|^2_{H^1(\Omega_p)}\mathrm{d}\tau\right)^{1/2} + \|\boldsymbol{\eta}_h(0)\|_{L^2(\Omega_p)}\right), \tag{4.57}$$

where we have also used (4.38). The statement of the theorem follows from combining (4.44), (4.56), and (4.57), and employing Young's inequality (4.22) with sufficiently small ϵ for the first term on the right in (4.57) and Gronwall's inequality for the second term. □

4.2. Error analysis

The error introduced in the approximation of (4.18) with (4.21) requires particular attention because we are dealing with a coupled problem on dimensionally heterogeneous domains. More precisely, the transmission conditions between the fracture and the reservoir involve traces of the reservoir pressure p on the fracture edges. As a result the natural pressure space on Ω_p, namely $\mathcal{Q}^p$, requires additional regularity for the traces on the interface between the reservoir and the fracture. Moreover, the discrete space $\mathcal{Q}_h^p \subset \mathcal{Q}^p$ can not provide optimal approximation properties on Ω_p and Γ_i, $i = 1, 2$ simultaneously. As a result, some degree of suboptimality is expected in the approximation properties of the scheme.

In addition to the velocity mixed finite element interpolants Π_h^p and Π_h^f defined in the previous section, let I_h^η and I_h^f be the Scott–Zhang interpolants for H^1 functions into the finite element spaces $\boldsymbol{\mathcal{V}}_h^\eta$ and $\mathcal{Q}_h^f$, respectively [43], and let I_h^p be the L^2-projection into $\mathcal{Q}_h^p$. The interpolants satisfy the approximation bounds [7, 43]

$$\|\boldsymbol{\eta} - I_h^\eta \boldsymbol{\eta}\|_{H^1(\Omega_p)} \lesssim h^{r_1}|\boldsymbol{\eta}|_{H^{r_1+1}(\Omega_p)}, \tag{4.58}$$
$$\|\boldsymbol{q} - \Pi_h^p \boldsymbol{q}\|_{L^2(\Omega_p)} \lesssim h^{r_2+1}|\boldsymbol{q}|_{H^{r_2+1}(\Omega_p)}, \tag{4.59}$$
$$\|p - I_h^p p\|_{L^2(\Omega_p)} + h^{1/2}\|p - I_h^p p\|_{L^2(\gamma)} \lesssim h^{l_2+1}|p|_{H^{l_2+1}(\Omega_p)}, \tag{4.60}$$
$$\|\boldsymbol{U} - \Pi_h^f \boldsymbol{U}\|_{H^1(\Omega_f)} \lesssim h^{r_3}|\boldsymbol{U}|_{H^{r_3+1}(\gamma)}, \tag{4.61}$$
$$\|P - I_h^f P\|_{L^2(\Omega_f)} \lesssim h^{r_3}|P|_{H^{r_3}(\gamma)}. \tag{4.62}$$

The bound on $\|p - I_h^p p\|_{L^2(\gamma)}$ in (4.60) follows from the local trace inequality [14], for all $E \in \mathcal{T}_h$,

$$\|\xi\|_{L^2(\partial E)} \lesssim h_E^{-1/2}\|\xi\|_{L^2(E)} + h_E^{1/2}|\xi|_{H^1(E)}, \quad \forall\, \xi \in H^1(E) \tag{4.63}$$

as follows. Letting $\tilde{I}_h^p$ be the Scott–Zhang interpolant into $\mathcal{Q}_h^p$, we have, for all $E \in \mathcal{T}_h$,

$$\begin{aligned}\|p - I_h^p p\|_{L^2(\partial E)} &\lesssim h_E^{-1/2}\|p - I_h^p p\|_{L^2(E)} + h_E^{1/2}|p - I_h^p p|_{H^1(E)} \\ &\lesssim h_E^{-1/2}\|p - I_h^p p\|_{L^2(E)} + h_E^{1/2}(|p - \tilde{I}_h^p p|_{H^1(E)} + |\tilde{I}_h^p - I_h^p p|_{H^1(E)}) \\ &\lesssim h_E^{-1/2}(\|p - I_h^p p\|_{L^2(E)} + \|\tilde{I}_h^p - I_h^p p\|_{L^2(E)}) + h_E^{1/2}|p - \tilde{I}_h^p p|_{H^1(E)} \\ &\lesssim h_E^{l_2+1/2}|p|_{H^{l_2+1}(\tilde{E})},\end{aligned}$$

where we have also used a local inverse inequality for finite element functions [11] and $\tilde{E}$ is the neighborhood of E used in the definition of $\tilde{I}_h^p$.

Let us denote the *global error* as $\mathbb{E}(t) = \mathbb{X}(t) - \mathbb{X}_h(t) = [\boldsymbol{e}_\eta, \boldsymbol{e}_q, \boldsymbol{e}_U, e_P, e_p]$. We next state and prove the main convergence result.

Theorem 4.6. *Let $p_h(0) = I_h^p p_0$ and $\boldsymbol{\eta}_h(0) = I_h^\eta \boldsymbol{\eta}_0$. Under the assumptions of Theorem 4.5, assuming that $\delta > 0$ and that the solution $\mathbb{X}(t)$ of (4.18) is sufficient regular, the solution $\mathbb{X}_h(t)$ of (4.21) satisfies*

$$\begin{aligned}
&\sqrt{s_0}\|e_p\|_{\mathcal{L}^\infty(L^2(\Omega_p))} + |||\mathbb{E}|||_{\mathcal{A},T} \lesssim h^{r_1}\Big(\|\partial_t\boldsymbol{\eta}\|_{\mathcal{L}^2(H^{r_1+1}(\Omega_p))} + \|\boldsymbol{\eta}\|_{\mathcal{L}^\infty(H^{r_1+1}(\Omega_p))} + \|\partial_t\boldsymbol{\eta}\|_{\mathcal{L}^\infty(H^{r_1+1}(\Omega_p))}\Big)\\
&+ h^{r_2+1}\|\boldsymbol{q}\|_{\mathcal{L}^2(H^{r_2+1}(\Omega_p))} + h^{l_2+1}\big(\|p\|_{\mathcal{L}^2(H^{l_2+1}(\Omega_p))} + \|\partial_t p\|_{\mathcal{L}^2(H^{l_2+1}(\Omega_p))} + \|p\|_{\mathcal{L}^\infty(H^{l_2+1}(\Omega_p))}\big)\\
&+ h^{l_2+1/2}\big(\delta^{-1/2}\|p\|_{\mathcal{L}^2(H^{l_2+1}(\Omega_p))} + \|\partial_t p\|_{\mathcal{L}^2(H^{l_2+1}(\Omega_p))} + \|p\|_{\mathcal{L}^\infty(H^{l_2+1}(\Omega_p))}\big) + h^{l_2}\|p\|_{\mathcal{L}^2(H^{l_2+1}(\Omega_p))}\\
&+ h^{r_3}\|P\|_{\mathcal{L}^2(H^{r_3}(\gamma))} + h^{r_3}\|\boldsymbol{U}\|_{\mathcal{L}^2(H^{r_3+1}(\gamma))}.
\end{aligned} \tag{4.64}$$

Proof. To study the space discretization error, we first derive the error equation for (4.21) and combine it with the stability properties of the scheme. In this way, we bound the total error in terms of the finite element approximation error. Problem (4.21) is strongly consistent with (4.18), so the error equation follows from testing (4.18) with the test functions from the finite element space $\mathcal{W}_h$ and subtracting it from the semi-discrete problem (4.21):

$$s_0(\partial_t e_p(t), \varphi_h) + \mathcal{A}(\mathbb{E}(t), \mathbb{Y}_h) = 0, \quad \forall \mathbb{Y}_h \in \mathcal{W}_h. \tag{4.65}$$

Let Π_h denote a collection of projectors, such that $\Pi_h\mathbb{X} = [I_h^\eta\boldsymbol{\eta}, \Pi_h^p\boldsymbol{q}, \Pi_h^f\boldsymbol{U}, I_h^f P, I_h^p p]$, one for each component of $\mathbb{X}$. We define the *approximation error* as

$$\mathbb{F} = \mathbb{X} - \Pi_h\mathbb{X} = [\boldsymbol{f}_\eta, \boldsymbol{f}_q, \boldsymbol{f}_U, f_P, f_p]$$

and we exploit the decomposition of the global error into approximation error and *error residual*,

$$\mathbb{E} = \mathbb{F} + \mathbb{G}_h \text{ where } \mathbb{G}_h = \Pi_h\mathbb{X} - \mathbb{X}_h = [\boldsymbol{g}_{\eta,h}, \boldsymbol{g}_{q,h}, \boldsymbol{g}_{U,h}, g_{P,h}, g_{p,h}].$$

As a result, the error equation can be easily rewritten in the following form, more suitable for pursuing the error analysis

$$s_0(\partial_t g_{p,h}(t), \varphi_h) + \mathcal{A}(\mathbb{G}_h(t), \mathbb{Y}_h) = -s_0(\partial_t f_p(t), \varphi_h) - \mathcal{A}(\mathbb{F}(t), \mathbb{Y}_h) \quad \forall \mathbb{Y}_h \in \mathcal{W}_h. \tag{4.66}$$

The error estimate (4.64) is obtained following the approach in the stability Theorem 4.5. Let us denote

$$\mathbb{G}_h = [\mathbb{G}_{\mathbb{U}_h}, \mathbb{G}_{\mathbb{P}_h}],\ \mathbb{G}_{\mathbb{U}_h} = [\boldsymbol{g}_{\eta,h}, \boldsymbol{g}_{q,h}, \boldsymbol{g}_{U,h}],\ \mathbb{G}_{\mathbb{P}_h} = [g_{P,h}, g_{p,h}];\ \mathbb{F} = [\mathbb{F}_{\mathbb{U}}, \mathbb{F}_{\mathbb{P}}],\ \mathbb{F}_{\mathbb{U}} = [\boldsymbol{f}_\eta, \boldsymbol{f}_q, \boldsymbol{f}_U],\ \mathbb{F}_{\mathbb{P}} = [f_P, f_p].$$

Similarly to Theorem 4.5, we take in (4.66) $\mathbb{Y}_h = \mathbb{W}_h := [\partial_t^\eta\mathbb{G}_{\mathbb{U}_h} - \epsilon_2\mathbb{V}_h, \mathbb{G}_{\mathbb{P}_h}]$, where $\mathbb{V}_h = [\boldsymbol{0}, \boldsymbol{r}_h, \boldsymbol{V}_h]$ is the velocity field constructed in Lemma 4.4 associated to $\mathbb{G}_{\mathbb{P}_h}$ and satisfying for all $t \in (0, T]$

$$\int_0^t (\widetilde{\mathcal{B}})^T(\mathbb{G}_{\mathbb{P}_h}, \mathbb{V}_h)\,\mathrm{d}\tau \geq |||\mathbb{G}_{\mathbb{P}_h}|||^2_{\mathcal{Q},t}, \quad |||\mathbb{V}_h|||_{\mathcal{V},t} \leq \beta|||\mathbb{G}_{\mathbb{P}_h}|||_{\mathcal{Q},t}. \tag{4.67}$$

The above inequalities follow from time integration in (4.38). The second inequality is true, since the first component of $\mathbb{V}_h$ is zero. Integration in time on $[0, T]$ in (4.66) with the choice $\mathbb{Y}_h = \mathbb{W}_h$ gives

$$\int_0^T \left(s_0(\partial_t g_{p,h}, g_{p,h}) + \mathcal{A}(\mathbb{G}_h, \mathbb{W}_h)\right)\,\mathrm{d}\tau = \int_0^T \left(-s_0(\partial_t f_p, g_{p,h}) - \mathcal{A}(\mathbb{F}, \mathbb{W}_h)\right)\mathrm{d}\tau. \tag{4.68}$$

As in Theorem 4.5, the error estimate (4.64) is obtained through two fundamental steps. The first is a lower bound of the left hand side of (4.68). The second is an upper bound of the right hand side, featuring terms that can be either hidden into the left hand side or depend on the approximation error.

The argument in Theorem 4.5 leading to (4.56) implies that for sufficiently small ϵ_2, we obtain

$$\begin{aligned}
&s_0\|g_{p,h}\|^2_{\mathcal{L}^\infty(L^2(\Omega_p))} + |||\mathbb{G}_h|||^2_{\mathcal{A},T} + \chi_{\theta_{\tau,1}}C^\tau\|[\partial_t\boldsymbol{g}_{\eta,h}\cdot\boldsymbol{\tau}]\|^2_{\mathcal{L}^2(L^2(\gamma))} + \chi_{\theta_{\tau,2}}C^\eta\|\partial_t\boldsymbol{g}_{\eta,h}\cdot\boldsymbol{\tau}\|^2_{\mathcal{L}^2(L^2(\gamma))}\\
&\qquad\lesssim \int_0^T \left(s_0(\partial_t g_{p,h}, g_{p,h}) + \mathcal{A}(\mathbb{G}_h, \mathbb{W}_h)\right)\mathrm{d}\tau,
\end{aligned} \tag{4.69}$$

using that $g_{p,h}(0) = 0$ and $\boldsymbol{g}_{\eta,h}(0) = 0$.

We continue with the second step, derivation of an upper bound for the right hand side of (4.68). For each term we will be employing the Cauchy−Schwarz and Young's inequalities, placing a small weight ϵ_3 in the terms that will be absorbed by the left hand side of (4.69). Some of the bounds will involve $\|\boldsymbol{g}_{\eta,h}\|_{\mathcal{L}^2(H^1(\Omega_p))}$, which will be controlled *via* Gronwall's inequality.

For the first term on the right in (4.68) we have

$$\int_0^T s_0(\partial_t f_p, g_{p,h})\mathrm{d}\tau \lesssim \epsilon_3\|g_{p,h}\|^2_{\mathcal{L}^2(L^2(\Omega_p))} + \epsilon_3^{-1}\|\partial_t f_p\|^2_{\mathcal{L}^2(L^2(\Omega_p))}. \tag{4.70}$$

Using the definition (4.17) of $\mathcal{A}$ we have

$$\begin{aligned}\mathcal{A}(\mathbb{F},\mathbb{W}_h) = \widetilde{\mathcal{A}}(\mathbb{F}_\mathbb{U}, \partial_t^\eta\mathbb{G}_{\mathbb{U}_h} - \epsilon_2\mathbb{V}_h) + \widetilde{\mathcal{A}}^\eta(\partial_t^\eta\mathbb{F}_\mathbb{U}, \partial_t^\eta\mathbb{G}_{\mathbb{U}_h} - \epsilon_2\mathbb{V}_h)\\ - (\widetilde{\mathcal{B}})^T(\mathbb{F}_\mathbb{P}, \partial_t^\eta\mathbb{G}_{\mathbb{U}_h} - \epsilon_2\mathbb{V}_h) + \widetilde{\mathcal{B}}(\partial_t^\eta\mathbb{F}_\mathbb{U}, \mathbb{G}_{\mathbb{P}_h}) + \widetilde{\mathcal{C}}(\mathbb{F}_\mathbb{P}, \mathbb{G}_{\mathbb{P}_h})\end{aligned} \tag{4.71}$$

We next bound each of the terms in (4.71). Using (4.25), we have

$$\begin{aligned}\int_0^T \widetilde{\mathcal{A}}(\mathbb{F}_\mathbb{U}, \partial_t^\eta\mathbb{G}_{\mathbb{U}_h})\,\mathrm{d}\tau &\le A\left(|||\mathbb{F}_\mathbb{U}|||_{\mathcal{V},T}\,|||\mathbb{G}_{\mathbb{U}_h}|||_{\mathcal{V},T} + \int_0^T \|\partial_t\boldsymbol{f}_\eta\|_{H^1(\Omega_p)}\|\boldsymbol{g}_{\eta,h}\|_{H^1(\Omega_p)}\mathrm{d}\tau\right)\\ &\lesssim \epsilon_3|||\mathbb{G}_{\mathbb{U}_h}|||^2_{\mathcal{V},T} + \epsilon_3^{-1}|||\mathbb{F}_\mathbb{U}|||^2_{\mathcal{V},T} + \|\boldsymbol{g}_{\eta,h}\|^2_{\mathcal{L}^2(H^1(\Omega_p))} + \|\partial_t\boldsymbol{f}_\eta\|^2_{\mathcal{L}^2(H^1(\Omega_p))}.\end{aligned} \tag{4.72}$$

Recalling that $\mathbb{V}_h = [\boldsymbol{0}, \boldsymbol{r}_h, \boldsymbol{V}_h]$, similarly to (4.49) we obtain

$$\int_0^T \widetilde{\mathcal{A}}(\mathbb{F}_\mathbb{U}, \mathbb{V}_h)\mathrm{d}\tau \le A|||\mathbb{F}_\mathbb{U}|||_{\mathcal{V},T}\,|||\mathbb{V}_h|||_{\mathcal{V},T} \lesssim \epsilon_3|||\mathbb{G}_{\mathbb{P}_h}|||^2_{\mathcal{Q},T} + \epsilon_3^{-1}|||\mathbb{F}_\mathbb{U}|||^2_{\mathcal{V},T}, \tag{4.73}$$

where we have also used (4.67). We continue with the bounds on the terms involving $\widetilde{\mathcal{A}}^\eta$. These terms are zero when $\theta_\tau = 0$. Let us consider $\theta_\tau = 1/2$. Using (4.35) we have

$$\begin{aligned}\int_0^T \widetilde{\mathcal{A}}^\eta(\partial_t^\eta\mathbb{F}_\mathbb{U}, \partial_t^\eta\mathbb{G}_{\mathbb{U}_h})\,\mathrm{d}\tau &\le \frac{1}{4}\int_0^T C^\tau\|[\partial_t\boldsymbol{f}_\eta\cdot\boldsymbol{\tau}]\|_{L^2(\gamma)}\|[\partial_t\boldsymbol{g}_{\eta,h}\cdot\boldsymbol{\tau}]\|_{L^2(\gamma)}\mathrm{d}\tau\\ &\lesssim \epsilon_3 C^\tau\|[\partial_t\boldsymbol{g}_{\eta,h}\cdot\boldsymbol{\tau}]\|^2_{\mathcal{L}^2(L^2(\gamma))} + \epsilon_3^{-1}C^\tau\|[\partial_t\boldsymbol{f}_\eta\cdot\boldsymbol{\tau}]\|^2_{\mathcal{L}^2(L^2(\gamma))}.\end{aligned} \tag{4.74}$$

Since $\mathbb{V}_h = [\boldsymbol{0}, \boldsymbol{r}_h, \boldsymbol{V}_h]$,

$$\widetilde{\mathcal{A}}^\eta(\partial_t^\eta\mathbb{F}_\mathbb{U}, \mathbb{V}_h) = a_e^\tau(\partial_t\boldsymbol{f}_\eta, \boldsymbol{0}) = 0. \tag{4.75}$$

Next consider $\theta_\tau = 2/3$, in which case all terms of $\widetilde{\mathcal{A}}^\eta$ are active. Using (4.37), we have

$$\begin{aligned}\int_0^T \widetilde{\mathcal{A}}^\eta(\partial_t^\eta\mathbb{F}_\mathbb{U}, \partial_t^\eta\mathbb{G}_{\mathbb{U}_h} - \epsilon_2\mathbb{V}_h)\,\mathrm{d}\tau &\lesssim \epsilon_3(|||\mathbb{G}_{\mathbb{U}_h}|||^2_{\mathcal{V},T} + C^\eta\|\partial_t\boldsymbol{g}_{\eta,h}\cdot\boldsymbol{\tau}\|^2_{\mathcal{L}^2(L^2(\gamma))} + |||\mathbb{G}_{\mathbb{P}_h}|||^2_{\mathcal{Q},T})\\ &\quad + \epsilon_3^{-1}\big(|||\partial_t^\eta\mathbb{F}_\mathbb{U}|||^2_{\mathcal{V},T} + C^\eta\|\partial_t\boldsymbol{f}_\eta\cdot\boldsymbol{\tau}\|^2_{\mathcal{L}^2(L^2(\gamma))}\big),\end{aligned} \tag{4.76}$$

where we have also used (4.67). Using the definition of $\widetilde{\mathcal{C}}$, we obtain

$$\int_0^T \widetilde{\mathcal{C}}(\mathbb{F}_\mathbb{P}, \mathbb{G}_{\mathbb{P}_h})\mathrm{d}\tau \lesssim \epsilon_3|||\mathbb{G}_{\mathbb{P}_h}|||^2_{\mathcal{Q},T} + \epsilon_3^{-1}|||\mathbb{F}_\mathbb{P}|||^2_{\mathcal{Q},T}. \tag{4.77}$$

We proceed with the off-diagonal terms. We consider $-(\widetilde{\mathcal{B}})^T(\mathbb{F}_\mathbb{P}, \partial_t^\eta\mathbb{G}_{\mathbb{U}_h}) + \widetilde{\mathcal{B}}(\partial_t^\eta\mathbb{F}_\mathbb{U}, \mathbb{G}_{\mathbb{P}_h})$ and bound its various components.

• Estimate on $\big(\alpha\mathcal{B}_p-\mathcal{M}_\gamma\big)\partial_t-\big(\alpha\mathcal{B}_p-\mathcal{M}_\gamma\big)^T$:

$$\int_0^T\Big(\big(\alpha\mathcal{B}_p-\mathcal{M}_\gamma\big)(\partial_t\boldsymbol{f}_\eta,g_{p,h})-\big(\alpha\mathcal{B}_p-\mathcal{M}_\gamma\big)^T(f_p,\partial_t\boldsymbol{g}_{\eta,h})\Big)\,\mathrm{d}\tau$$
$$=\alpha\int_0^T\int_{\Omega_p}g_{p,h}\nabla\cdot\partial_t\boldsymbol{f}_\eta\mathrm{d}\boldsymbol{x}\,\mathrm{d}t-\alpha\int_0^T\int_{\Omega_p}f_p\nabla\cdot\partial_t\boldsymbol{g}_{\eta,h}\mathrm{d}\boldsymbol{x}\,\mathrm{d}t$$
$$-\sum_i\Big(\int_0^T\int_\gamma g_{p,h,i}\big|^*_{\Gamma_i}(\partial_t\boldsymbol{f}_\eta\cdot\boldsymbol{n}_i)|^*_{\Gamma_i}\mathrm{d}s\,\mathrm{d}t-\int_0^T\int_\gamma f_{p,i}\big|^*_{\Gamma_i}(\partial_t\boldsymbol{g}_{\eta,h}\cdot\boldsymbol{n}_i)|^*_{\Gamma_i}\mathrm{d}s\,\mathrm{d}t\Big).$$

Then, proceeding term by term, we get

$$\left|\int_0^T\int_{\Omega_p}g_{p,h}\nabla\cdot\partial_t\boldsymbol{f}_\eta\mathrm{d}\boldsymbol{x}\,\mathrm{d}t\right|\lesssim\epsilon_3\|g_{p,h}\|^2_{\mathcal{L}^2(L^2(\Omega_p))}+\epsilon_3^{-1}\|\partial_t\boldsymbol{f}_\eta\|^2_{\mathcal{L}^2(H^1(\Omega_p))},$$

$$\left|\int_0^T\int_{\Omega_p}f_p\nabla\cdot\partial_t\boldsymbol{g}_{\eta,h}\mathrm{d}\boldsymbol{x}\,\mathrm{d}t\right|=\left|-\int_0^T\int_{\Omega_p}\partial_tf_p\nabla\cdot\boldsymbol{g}_{\eta,h}\mathrm{d}\boldsymbol{x}\,\mathrm{d}t+\int_{\Omega_p}f_p\nabla\cdot\boldsymbol{g}_{\eta,h}\mathrm{d}\boldsymbol{x}\Big|_0^T\right|$$
$$\lesssim\epsilon_3\|\boldsymbol{g}_{\eta,h}\|^2_{\mathcal{L}^\infty(H^1(\Omega_p))}+\epsilon_3^{-1}\|f_p\|^2_{\mathcal{L}^\infty(L^2(\Omega_p))}+\|\boldsymbol{g}_{\eta,h}\|^2_{\mathcal{L}^2(H^1(\Omega_p))}+\|\partial_tf_p\|^2_{\mathcal{L}^2(L^2(\Omega_p))},$$

$$\left|\sum_i\int_0^T\int_\gamma g_{p,h,i}\big|^*_{\Gamma_i}(\partial_t\boldsymbol{f}_\eta\cdot\boldsymbol{n}_i)|^*_{\Gamma_i}\mathrm{d}s\,\mathrm{d}t\right|\lesssim\epsilon_3\|g_{p,h}\|^2_{\mathcal{L}^2(L^2(\gamma))}+\epsilon_3^{-1}\|\partial_t\boldsymbol{f}_\eta\|^2_{\mathcal{L}^2(H^1(\Omega_p))},$$

$$\left|\sum_i\int_0^T\int_\gamma f_{p,i}\big|^*_{\Gamma_i}(\partial_t\boldsymbol{g}_{\eta,h}\cdot\boldsymbol{n}_i)|^*_{\Gamma_i}\mathrm{d}s\,\mathrm{d}t\right|$$
$$=\left|-\sum_i\int_0^T\int_\gamma\partial_tf_{p,i}\big|^*_{\Gamma_i}(\boldsymbol{g}_{\eta,h}\cdot\boldsymbol{n}_i)|^*_{\Gamma_i}\mathrm{d}s\,\mathrm{d}t+\int_\gamma f_{p,i}\big|^*_{\Gamma_i}(\boldsymbol{g}_{\eta,h}\cdot\boldsymbol{n}_i)|^*_{\Gamma_i}\mathrm{d}s\Big|_0^T\right|$$
$$\lesssim\epsilon_3\|\boldsymbol{g}_{\eta,h}\|^2_{\mathcal{L}^\infty(H^1(\Omega_p))}+\epsilon_3^{-1}\|f_p\|^2_{\mathcal{L}^\infty(L^2(\gamma))}+\|\boldsymbol{g}_{\eta,h}\|^2_{\mathcal{L}^2(H^1(\Omega_p))}+\|\partial_tf_p\|^2_{\mathcal{L}^2(L^2(\gamma))}.$$

As a result we obtain

$$\left|\int_0^T\Big(\big(\alpha\mathcal{B}_p-\mathcal{M}_\gamma\big)(\partial_t\boldsymbol{f}_\eta,g_{p,h})-\big(\alpha\mathcal{B}_p-\mathcal{M}_\gamma\big)^T(f_p,\partial_t\boldsymbol{g}_{\eta,h})\Big)\,\mathrm{d}\tau\right|$$
$$\lesssim\epsilon_3\big(\|\boldsymbol{g}_{\eta,h}\|^2_{\mathcal{L}^\infty(H^1(\Omega_p))}+\|g_{p,h}\|^2_{\mathcal{L}^2(L^2(\Omega_p))}+\|g_{p,h}\|^2_{\mathcal{L}^2(L^2(\gamma))}\big)$$
$$+\epsilon_3^{-1}\big(\|\partial_t\boldsymbol{f}_\eta\|^2_{\mathcal{L}^2(H^1(\Omega_p))}+\|f_p\|^2_{\mathcal{L}^\infty(L^2(\Omega_p))}+\|f_p\|^2_{\mathcal{L}^\infty(L^2(\gamma))}\big)$$
$$+\|\boldsymbol{g}_{\eta,h}\|^2_{\mathcal{L}^2(H^1(\Omega_p))}+\|\partial_tf_p\|^2_{\mathcal{L}^2(L^2(\Omega_p))}+\|\partial_tf_p\|^2_{\mathcal{L}^2(L^2(\gamma))}\tag{4.78}$$

• Estimate on $\big(\mathcal{B}_p-\mathcal{M}_\gamma\big)-\big(\mathcal{B}_p-\mathcal{M}_\gamma\big)^T$:

$$\int_0^T\Big(\big(\mathcal{B}_p-\mathcal{M}_\gamma\big)(\boldsymbol{f}_q,g_{p,h})-\big(\mathcal{B}_p-\mathcal{M}_\gamma\big)^T(f_p,\boldsymbol{g}_{q,h})\Big)\,\mathrm{d}\tau=\int_0^T\int_{\Omega_p}g_{p,h}\nabla\cdot\boldsymbol{f}_q\mathrm{d}\boldsymbol{x}\,\mathrm{d}t-\int_0^T\int_{\Omega_p}f_p\nabla\cdot\boldsymbol{g}_{q,h}\mathrm{d}\boldsymbol{x}\,\mathrm{d}t$$
$$-\sum_i\Big(\int_0^T\int_\gamma g_{p,h,i}\big|^*_{\Gamma_i}(\boldsymbol{f}_{q,i}\cdot\boldsymbol{n}_i)|^*_{\Gamma_i}\mathrm{d}s\,\mathrm{d}t-\int_0^T\int_\gamma f_{p,i}\big|^*_{\Gamma_i}(\boldsymbol{g}_{q,h,i}\cdot\boldsymbol{n}_i)|^*_{\Gamma_i}\mathrm{d}s\,\mathrm{d}t\Big).$$

Using the property (4.20) of Π_h^p, we have that

$$\int_0^T \int_{\Omega_p} g_{p,h} \nabla \cdot \boldsymbol{f}_q \mathrm{d}\boldsymbol{x}\,\mathrm{d}t = 0, \qquad \sum_i \int_0^T \int_\gamma g_{p,h,i}|_{\Gamma_i}^*(\boldsymbol{f}_{q,i}\cdot\boldsymbol{n}_i)|_{\Gamma_i}^* \mathrm{d}s\,\mathrm{d}t = 0.$$

The orthogonality of the L^2-projection I_h^p and the property $\nabla\cdot\boldsymbol{\mathcal{V}}_h^p = \mathcal{Q}_h^p$ of the Darcy mixed finite element spaces implies that

$$\int_0^T \int_{\Omega_p} f_p \nabla\cdot \boldsymbol{g}_{q,h} \mathrm{d}\boldsymbol{x}\,\mathrm{d}t = 0.$$

For the remaining term we have

$$\left|\sum_i \int_0^T \int_\gamma f_{p,i}|_{\Gamma_i}^*(\boldsymbol{g}_{q,h,i}\cdot\boldsymbol{n}_i)|_{\Gamma_i}^* \mathrm{d}s\,\mathrm{d}t\right| \lesssim \epsilon_3 \|\boldsymbol{g}_{q,h}\|^2_{\mathcal{L}^2(L^2(\Omega_p))} + \epsilon_3^{-1}h^{-1}\|f_p\|^2_{\mathcal{L}^2(L^2(\gamma))},$$

where we used the discrete trace inequality (4.63). In conclusion, we obtain that

$$\left|\int_0^T \Big((\mathcal{B}_p - \mathcal{M}_\gamma)(\boldsymbol{f}_q, g_{p,h}) - (\mathcal{B}_p - \mathcal{M}_\gamma)^T(f_p, \boldsymbol{g}_{q,h})\Big)\mathrm{d}\tau\right| \lesssim \epsilon_3\|\boldsymbol{g}_{q,h}\|^2_{\mathcal{L}^2(L^2(\Omega_p))} + \epsilon_3^{-1}h^{-1}\|f_p\|^2_{\mathcal{L}^2(L^2(\gamma))}. \quad (4.79)$$

- Estimate on $\mathcal{M}_\gamma - (\mathcal{M}_\gamma)^T$:

$$\begin{aligned}
&\left|\int_0^T \big(\mathcal{M}_\gamma(\boldsymbol{f}_U, g_{p,h}) - \mathcal{M}_\gamma^T(f_p, \boldsymbol{g}_{U,h})\big)\,\mathrm{d}\tau\right| \\
&\quad = \left|\int_0^T\int_\gamma (g_{p,h,1}|_{\Gamma_1}^* - g_{p,h,2}|_{\Gamma_2}^*)(\boldsymbol{f}_U)_n \mathrm{d}s\,\mathrm{d}t - \int_0^T\int_\gamma (f_{p,1}|_{\Gamma_1}^* - f_{p,2}|_{\Gamma_2}^*)(\boldsymbol{g}_{U,h})_n \mathrm{d}s\,\mathrm{d}t\right| \\
&\quad \lesssim \epsilon_3\big(\|g_{p,h}\|^2_{\mathcal{L}^2(L^2(\gamma))} + \|\sqrt{\delta}\boldsymbol{g}_{U,h}\|^2_{\mathcal{L}^2(L^2(\gamma))}\big) + \epsilon_3^{-1}\big(\|\delta^{-1/2}f_p\|^2_{\mathcal{L}^2(L^2(\gamma))} + \|\boldsymbol{f}_U\|^2_{\mathcal{L}^2(L^2(\gamma))}\big). \quad (4.80)
\end{aligned}$$

- Estimate on $\mathcal{B}_f - (\mathcal{B}_f)^T$:

$$\begin{aligned}
&\left|\int_0^T \big((\mathcal{B}_f(\boldsymbol{f}_U, g_{P,h}) - \mathcal{B}_f^T(f_P, \boldsymbol{g}_{U,h})\big)\,\mathrm{d}\tau\right| = \left|\int_0^T\int_\gamma \delta\,\partial_s(\boldsymbol{g}_{U,h})_\tau f_P\,\mathrm{d}s\,\mathrm{d}t - \int_0^T\int_\gamma \delta\,\partial_s(\boldsymbol{f}_U)_\tau g_{P,h}\,\mathrm{d}s\,\mathrm{d}t\right| \\
&\quad \lesssim \epsilon_3\big(\|\sqrt{\delta}\boldsymbol{g}_{U,h}\|^2_{\mathcal{L}^2(H^1(\gamma))} + \|\sqrt{\delta}g_{P,h}\|^2_{\mathcal{L}^2(L^2(\gamma))}\big) + \epsilon_3^{-1}\big(\|\sqrt{\delta}\boldsymbol{f}_U\|^2_{\mathcal{L}^2(H^1(\gamma))} + \|\sqrt{\delta}f_P\|^2_{\mathcal{L}^2(L^2(\gamma))}\big). \quad (4.81)
\end{aligned}$$

Combining (4.78)–(4.81), we obtain

$$\begin{aligned}
\left|\int_0^T \Big(-(\widetilde{\mathcal{B}})^T(\mathbb{F}_\mathbb{P}, \partial_t^\eta \mathbb{G}_{\mathbb{U}_h}) + \widetilde{\mathcal{B}}(\partial_t^\eta \mathbb{F}_\mathbb{U}, \mathbb{G}_{\mathbb{P}_h})\Big)\mathrm{d}\tau\right| &\lesssim \epsilon_3 |||\mathbb{G}_h|||^2_{\mathcal{A},T} + \|\boldsymbol{g}_{\eta,h}\|^2_{\mathcal{L}^2(H^1(\Omega_p))} \\
&+ \epsilon_3^{-1}\big(\|\partial_t \boldsymbol{f}_\eta\|^2_{\mathcal{L}^2(H^1(\Omega_p))} + \|f_p\|^2_{\mathcal{L}^\infty(L^2(\Omega_p))} + \|f_p\|^2_{\mathcal{L}^\infty(L^2(\gamma))} + h^{-1}\|f_p\|^2_{\mathcal{L}^2(L^2(\gamma))} \\
&+ \|\delta^{-1/2}f_p\|^2_{\mathcal{L}^2(L^2(\gamma))} + \|\boldsymbol{f}_U\|^2_{\mathcal{L}^2(H^1(\gamma))} + \|f_P\|^2_{\mathcal{L}^2(L^2(\gamma))}\big) \\
&+ \|\partial_t f_p\|^2_{\mathcal{L}^2(L^2(\Omega_p))} + \|\partial_t f_p\|^2_{\mathcal{L}^2(L^2(\gamma))}. \quad (4.82)
\end{aligned}$$

where a factor proportional to $1+\delta$ has been absorbed in the generic constant, without loss of generality. Recalling that $\mathbb{V}_h = [\boldsymbol{0}, \boldsymbol{r}_h, \boldsymbol{V}_h]$, we obtain in a similar way

$$\left|\int_0^T (\widetilde{\mathcal{B}})^T(\mathbb{F}_\mathbb{P}, \mathbb{V}_h)\mathrm{d}\tau\right| \lesssim \epsilon_3 |||\mathbb{G}_{\mathbb{P}_h}|||^2_{\mathcal{Q},T} + \epsilon_3^{-1}\big(h^{-1}\|f_p\|^2_{\mathcal{L}^2(L^2(\gamma))} + \|\delta^{-1/2}f_p\|^2_{\mathcal{L}^2(L^2(\gamma))} + \|f_P\|^2_{\mathcal{L}^2(L^2(\gamma))}\big), \quad (4.83)$$

where we have also used (4.67). Combining (4.68)–(4.83), taking ϵ_3 sufficiently small, and employing Gronwall's inequality, we obtain

$$s_0\|g_{p,h}\|^2_{\mathcal{L}^\infty(L^2(\Omega_p))} + |||\mathbb{G}_h|||^2_{\mathcal{A},T} \lesssim \mathcal{H}(\mathbb{F})^2, \tag{4.84}$$

where $\mathcal{H}(\mathbb{F})^2 = \mathcal{H}_{\boldsymbol{f}_\eta}(\mathbb{F})^2 + \mathcal{H}_{\boldsymbol{f}_q}(\mathbb{F})^2 + \mathcal{H}_{f_p}(\mathbb{F})^2 + \mathcal{H}_{\boldsymbol{f}_U}(\mathbb{F})^2 + \mathcal{H}_{f_P}(\mathbb{F})^2$,

$$\begin{aligned}
\mathcal{H}_{\boldsymbol{f}_\eta}(\mathbb{F})^2 &:= \|\partial_t \boldsymbol{f}_\eta\|^2_{\mathcal{L}^2(H^1(\Omega_p))} + \|\boldsymbol{f}_\eta\|^2_{\mathcal{L}^\infty(H^1(\Omega_p))} + \|\partial_t \boldsymbol{f}_\eta\|^2_{\mathcal{L}^\infty(H^1(\Omega_p))},\\
\mathcal{H}_{\boldsymbol{f}_q}(\mathbb{F})^2 &:= \|\boldsymbol{f}_q\|^2_{\mathcal{L}^2(L^2(\Omega_p))},\\
\mathcal{H}_{f_p}(\mathbb{F})^2 &:= \|\partial_t f_p\|^2_{\mathcal{L}^2(L^2(\Omega_p))} + \|f_p\|^2_{\mathcal{L}^\infty(L^2(\Omega_p))} + \|\partial_t f_p\|^2_{\mathcal{L}^2(L^2(\gamma))}\\
&\qquad + \|f_p\|^2_{\mathcal{L}^\infty(L^2(\gamma))} + \|f_p\|^2_{\mathcal{L}^2(L^2(\Omega_p))} + \big(1 + h^{-1} + \delta^{-1}\big)\|f_p\|^2_{\mathcal{L}^2(L^2(\gamma))},\\
\mathcal{H}_{\boldsymbol{f}_U}(\mathbb{F})^2 &:= \|\boldsymbol{f}_U\|^2_{\mathcal{L}^2(H^1(\gamma))},\\
\mathcal{H}_{f_P}(\mathbb{F})^2 &:= \|f_P\|^2_{\mathcal{L}^2(L^2(\gamma))}.
\end{aligned}$$

Using the approximation bounds (4.58)–(4.62) and observing that $1 + \delta^{-1} \lesssim \delta^{-1}$, we obtain

$$\begin{aligned}
\mathcal{H}_{\boldsymbol{f}_\eta}(\mathbb{F}) &\lesssim h^{r_1}\big(\|\partial_t \boldsymbol{\eta}\|_{\mathcal{L}^2(H^{r_1+1}(\Omega_p))} + \|\boldsymbol{\eta}\|_{\mathcal{L}^\infty(H^{r_1+1}(\Omega_p))} + \|\partial_t \boldsymbol{\eta}\|_{\mathcal{L}^\infty(H^{r_1+1}(\Omega_p))}\big),\\
\mathcal{H}_{\boldsymbol{f}_q}(\mathbb{F}) &\lesssim h^{r_2+1}\|\boldsymbol{q}\|_{\mathcal{L}^2(H^{r_2+1}(\Omega_p))},\\
\mathcal{H}_{f_p}(\mathbb{F}) &\lesssim h^{l_2+1}\big(\|p\|_{\mathcal{L}^2(H^{l_2+1}(\Omega_p))} + \|\partial_t p\|_{\mathcal{L}^2(H^{l_2+1}(\Omega_p))} + \|p\|_{\mathcal{L}^\infty(H^{l_2+1}(\Omega_p))}\big)\\
&\quad + h^{l_2+1/2}\big(\delta^{-1/2}\|p\|_{\mathcal{L}^2(H^{l_2+1}(\Omega_p))} + \|\partial_t p\|_{\mathcal{L}^2(H^{l_2+1}(\Omega_p))} + \|p\|_{\mathcal{L}^\infty(H^{l_2+1}(\Omega_p))}\big)\\
&\quad + h^{l_2}\|p\|_{\mathcal{L}^2(H^{l_2+1}(\Omega_p))},\\
\mathcal{H}_{\boldsymbol{f}_U}(\mathbb{F}) &\lesssim h^{r_3}\|\boldsymbol{U}\|_{\mathcal{L}^2(H^{r_3+1}(\gamma))},\\
\mathcal{H}_{f_P}(\mathbb{F}) &\lesssim h^{r_3}\|P\|_{\mathcal{L}^2(H^{r_3}(\gamma))}.
\end{aligned}$$

The proof of the theorem is completed by combining (4.84) with the above approximation bounds and employing triangle inequality. □

Remark 4.7. The lowest order term of (4.64) is $h^{l_2}\|p\|_{\mathcal{L}^2(H^{l_2+1}(\Omega_p))}$. It entails that the convergence rate of the proposed scheme is one order lower than the optimal one. This is due to the term $h^{-1/2}\|f_p\|_{\mathcal{L}^2(L^2(\gamma))}$, which results from the bound on $\int_\gamma f_{p,i}\big|^*_{\Gamma_i}(\boldsymbol{g}_{q,h,i}\cdot\boldsymbol{n}_i)|^*_{\Gamma_i}\mathrm{d}s$, where half order is lost for each of the two terms. An improved estimate can be obtained by employing a Lagrange multiplier space for the trace of the Darcy pressure p on γ to enforce the continuity of flux. This space can be chosen to be of higher order and an optimal interpolant on the interface can be utilized, see, *e.g.* [3]. This approach is a subject of forthcoming work. We also note that the term involving $\delta^{-1/2}$ results from bounding $\int_\gamma (f_{p,1}\big|^*_{\Gamma_1} - f_{p,2}\big|^*_{\Gamma_2})(\boldsymbol{g}_{U,h})_n\mathrm{d}s$, since only $\|\sqrt{\delta}\boldsymbol{g}_{U,h}\|_{\mathcal{L}^2(H^1(\gamma))}$ is controlled by the method. We note that the use of a Lagrange multiplier space and an interface interpolant would result in this term depending on the norm of $p_1\big|^*_{\Gamma_1} - p_2\big|^*_{\Gamma_2}$ on γ, which goes to zero with δ, due to (4.4).

5. Numerical results

In this section we focus on the numerical verification of the theoretical results and on the application of the proposed scheme to solving a representative problem in geomechanics. For this purpose, we consider four examples. The first one is an academic benchmark problem proposed in [28]. In the second example we consider the same configuration, but we use more realistic physical parameters taken from [18]. The third and fourth examples concern numerical experiments for curved fracture configurations. In all examples we take $\theta_n = \theta_\tau$ and consider only the discrete values $0, \frac{1}{2}, \frac{2}{3}$. The numerical solver for problem (4.21) was implemented in *FreeFem++* [24]. To discretize the problem in time we have adopted the Backward Euler scheme on a uniform partition of the time interval $(0, T]$ in time steps $t^n := n\Delta t$ for $n = 1, \ldots, N$, where $T = N\Delta t$ is the final

time. The time derivative of the displacement is discretized using the first order approximation $\partial_t \boldsymbol{\eta}_h^{n+1} \approx \Delta t^{-1}(\boldsymbol{\eta}_h^{n+1} - \boldsymbol{\eta}_h^n)$. For the space discretization we have used continuous piecewise linears for $\boldsymbol{\mathcal{V}}_h^\eta$ with $r_1 = 1$, the Raviart−Thomas elements RT_1 for $\boldsymbol{\mathcal{V}}_h^p \times \mathcal{Q}_h^p$ with $r_2 = l_2 = 1$, and the $P_2 - P_1$ Taylor−Hood elements for $\boldsymbol{\mathcal{V}}_h^f \times \mathcal{Q}_h^f$ with $r_3 = 2$. The discrete problem is solved using GMRES with a preconditioner consisting of diagonal blocks of the system matrix given in (4.17).

5.1. Example 1: Numerical validation

To validate our numerical scheme, we consider a benchmark problem investigated by Lesinigo et al in [28], Section 7.2. The computational domain consists of two unitary squares separated by a fracture of width δ, with midline γ. The squares represent the poroelastic domains Ω_1 and Ω_2 (see Fig. 2). We assume that there are no external forces or mass sources. On the left and right boundaries, namely Γ_1^4 and Γ_2^2 in Figure 2, we impose homogeneous Dirichlet pressure and homogeneous Dirichlet displacement conditions, while on the remaining external boundaries we impose zero normal flux and zero normal poroelastic stress. In the fracture, on the bottom boundary $\Gamma_1^1 \cap \Gamma_2^1$ we impose the Dirichlet boundary condition (3.15) for the tangential velocity, $U_\tau^D = 10$ (m/s), and the homogeneous Neumann boundary condition (3.16) for the normal velocity, $\mu_f \frac{\partial U_n}{\partial s} = 0$. On the top boundary $\Gamma_1^3 \cap \Gamma_2^3$, we impose the homogeneous Neumann conditions (3.16) for the normal stress. Values of parameters used in this example are given in Table 2. The problem is solved over the time interval $[0, 1]$(s) with time step $\Delta t = 0.01$(s). The space discretization step is $h = 0.05$ (m).

We compare the results obtained by the reduced model with $\theta_n = \theta_\tau = 1/2$ to the ones obtained using a non-reduced model, where the flow in the fracture is fully resolved on Ω_f using the Brinkman equation. The full model was solved using a scheme based on Nitsche's approach presented in [8]. Figure 3 shows a comparison of the average pressure P (left) along the fracture midline γ and the average tangential velocity U_τ (right) obtained using the two models at time T=1 (s). In particular, for the full model pressure and velocity profiles

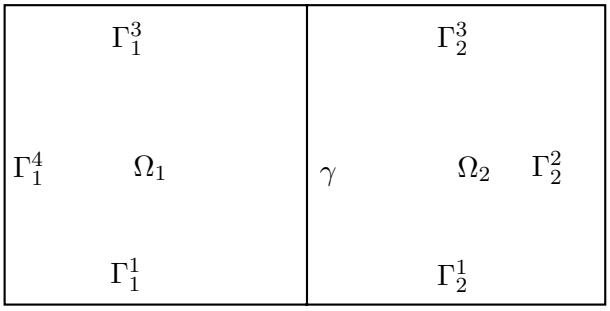

FIGURE 2. Example 1: Reference domain for the test problem.

TABLE 2. Example 1: Poroelasticity and fluid parameters.

Parameter	Symbol	Units	Values
Young's modulus	E	(KPa)	10^3
Poisson's ratio	σ		0.3
Hydraulic conductivity	$\boldsymbol{K}$	(m^2/KPa s)	$\boldsymbol{I}$
Mass storativity coeff.	s_0	(KPa^{-1})	1
Biot–Willis constant	α		1
Friction coefficient	c_{BJS}		10^{-4}
Hydraulic conductivity	$\boldsymbol{K}_f$	(m^2/KPa s)	$0.1\boldsymbol{I}$
Fracture width	δ	(m)	0.1
Brinkman viscosity	μ_f	(KPa s)	1

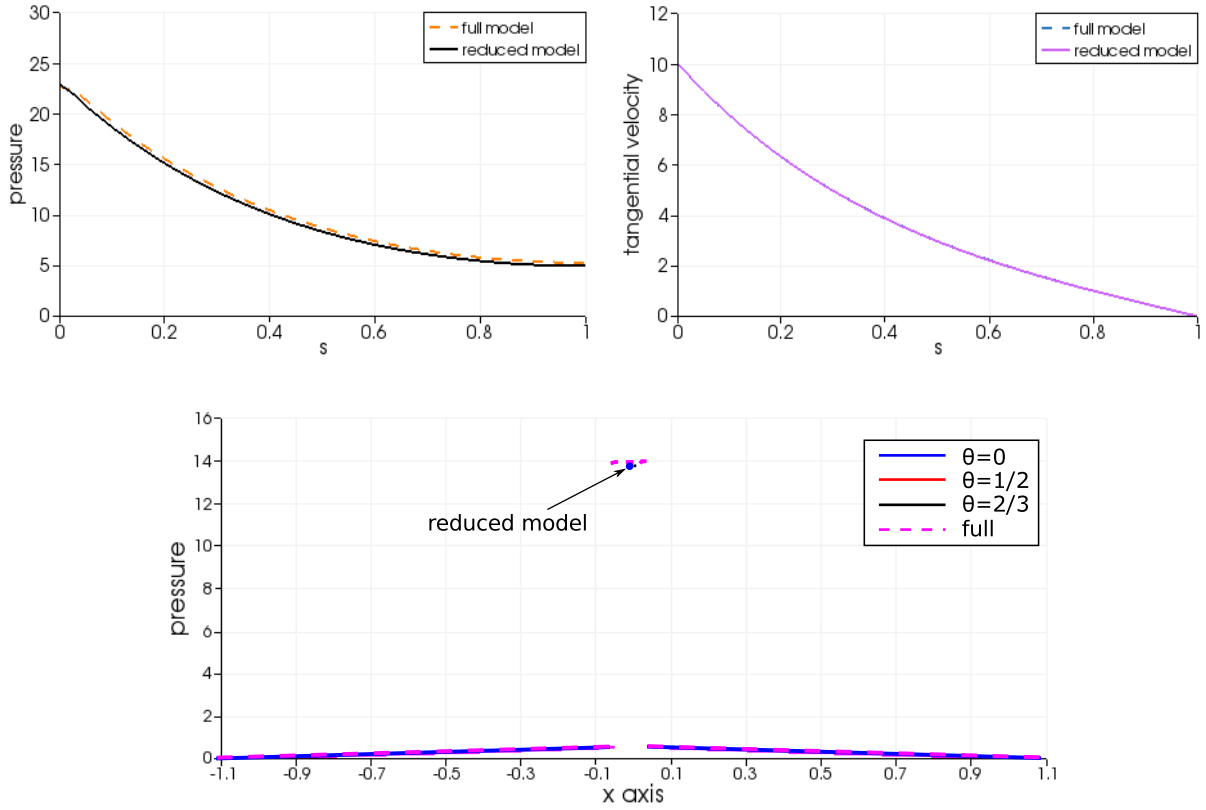

FIGURE 3. Example 1. *Top left panel*: Average pressure P along the midline γ. *Top right panel*: Average tangential velocity U_τ along the fracture midline γ. The values of the reduced model in the top panel are obtained with $\theta_n = \theta_\tau = \frac{1}{2}$. *Bottom panel*: Pressure profiles for the full and reduced model (calculated using different values of $\theta_n = \theta_\tau =: \theta$) along a transversal section of the domain at height $y = 0.25$ (m). The results are shown at $T = 1$ (s).

are plotted along the meanline of the fluid domain Ω_f. In the bottom panel of Figure 3 we show the pressure in the transversal direction, visualized along the line $y = 0.25$ (m). We observe a significant jump between the pressure in the fracture and pressure in the reservoir. For all values of $\theta_n = \theta_\tau$, a good comparison with the full model is achieved. Figure 4 shows a comparison of the pressure and displacement of the porous medium. The pressure is superimposed to the Darcy velocity vector field, while the displacement modulus is superimposed to the displacement vector field. In both figures we observe an excellent agreement between the results obtained using the reduced model and the results obtained using a full model. Furthermore, the computed pressure and velocity are in agreement with the results in [28].

On the same benchmark problem we test the spatial convergence of the scheme. Table 3 shows the convergence in space for the Darcy pressure and velocity, the displacement, and the fracture fluid velocity, where we have used the numerical solution with $h = 1/80$ (m) as a reference solution. According to (4.64), the convergence rate with $r_1 = 1$, $r_2 = l_2 = 1$, and $r_3 = 2$ should be at least linear. Higher orders of convergence are actually observed in some cases. All the convergence tests have been performed for the three admissible values of $\theta_n = \theta_\tau = 0, 1/2, 2/3$ and no significant differences have been detected among these variants of the model.

Finally, we study the accuracy of the reduced model with in the approximation of the interface conditions. We focus in particular on the flow balance in the direction orthogonal to the interface, *i.e.* equation (2.8). In the case of the full model, we define the following residual on each side of the fracture $\Gamma_i = \Omega_f \cap \Omega_{p,i}$, $i = 1, 2$,

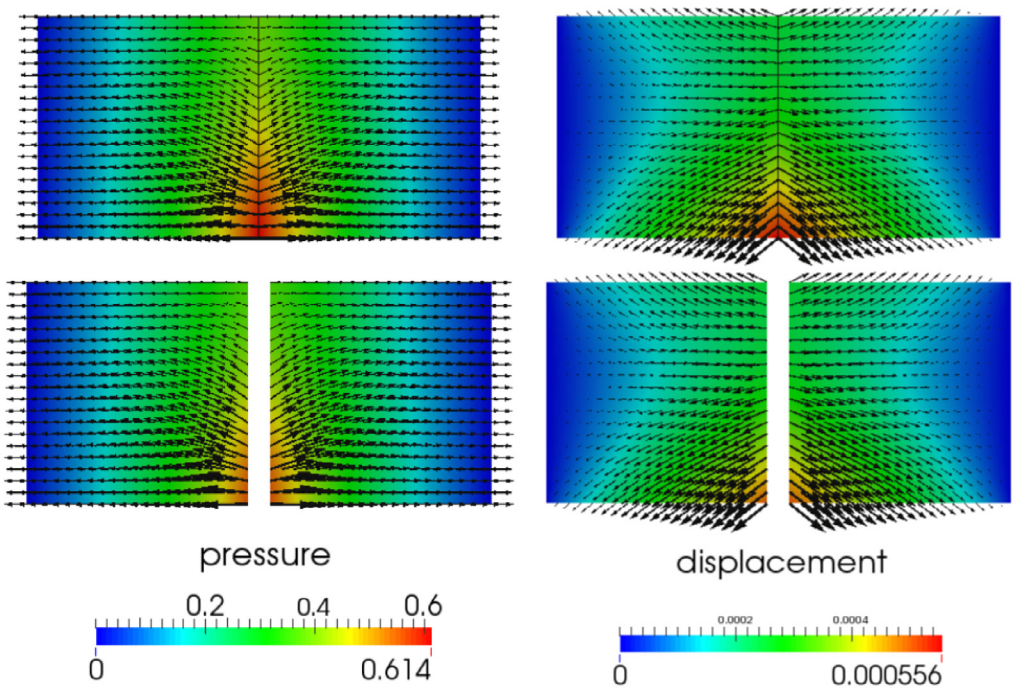

FIGURE 4. Example 1. *Left*: Pressure p in the pores obtained using the reduced model (*top*) and the full model (*bottom*). The Darcy velocity field $\boldsymbol{q}$ is superimposed to the pressure. *Right*: Magnitude of the displacement $\boldsymbol{\eta}$ obtained using the reduced model with $\theta_n = \theta_\tau = 1/2$ (*top*) and the full model (*bottom*). The displacement vector field is superimposed to the displacement magnitude. The results are shown at $T = 1$ (s).

TABLE 3. Example 1: Convergence in space for different values of the parameters $\theta_n = \theta_\tau$.

Test case $\delta = 0.1,\ \theta_n = \theta_\tau = 0, \frac{1}{2}, \frac{2}{3}$.

h	$\|e_p\|_{l^\infty(L^2(\Omega_p))}$	Rate	$\|e_{\boldsymbol{\eta}}\|_{l^\infty(H^1(\Omega_p))}$	Rate	$\|e_{\boldsymbol{q}}\|_{l^2(L^2(\Omega_p))}$	Rate	$\|e_{\boldsymbol{U}}\|_{l^2(H^1(\gamma))}$	Rate
1/10	3.4e − 2	–	1.0e − 1	–	2.6e − 2	–	9.2e − 4	–
1/20	8.9e − 3	1.9	5.3e − 2	0.9	9.8e − 3	1.4	3.2e − 4	1.5
1/40	2.2e − 3	2.0	2.7e − 2	1.0	3.3e − 3	1.6	1.7e − 4	0.9

for $i, j = 1, 2, i \neq j$:

$$\mathcal{R}_{\Gamma_i}(\boldsymbol{u}_i, \boldsymbol{\eta}_i, \boldsymbol{q}_i) := \int_{\Gamma_i} \left(\boldsymbol{u}_i \cdot \boldsymbol{n}_i - \left(\frac{\partial \boldsymbol{\eta}_i}{\partial t} + \boldsymbol{q}_i \right) \cdot \boldsymbol{n}_i \right),$$

while for the reduced model the previous definition must be modified as

$$\mathcal{R}_{\gamma,i}(\boldsymbol{U}_i, \boldsymbol{\eta}_i, \boldsymbol{q}_i) := \int_\gamma \left(\frac{\delta\theta_n}{2\mu_f} p_i|^*_{\Gamma_i} + \frac{\delta(1-\theta_n)}{2\mu_f} p_j|^*_{\Gamma_j} - \frac{\delta}{2\mu_f} P - \left(\frac{\partial \boldsymbol{\eta}_i}{\partial t} \cdot \boldsymbol{n}_i + \boldsymbol{q}_i \cdot \boldsymbol{n}_i - \boldsymbol{U} \cdot \boldsymbol{n}_i \right) \Big|^*_{\Gamma_i} \right).$$

The results of Table 4 show that the reduced model asymptotically satisfies the kinematic conditions, however it is less accurate than the full model. We have calculated the residuals for all values $\theta_n = \theta_\tau = 0, 1/2, 2/3$ and for two values of $\delta = 0.1, 0.2$ (m). It appears that the accuracy of the model is insensitive to θ_n, θ_τ, while it is affected by δ. More precisely, Table 4 confirms that the reduced model is more accurate for fractures with smaller aperture.

TABLE 4. Example 1: The behavior of the indicators $\mathcal{R}_{\Gamma_i}$ and $\mathcal{R}_{\gamma,i}$ when varying the characteristic mesh size at time $T = 1$ (s).

	Full model			Reduced model		
h, $\delta = 0.1$, $\theta_n = \theta_\tau = 0, \frac{1}{2}, \frac{2}{3}$	$\mathcal{R}_{\Gamma_1}$	$\mathcal{R}_{\Gamma_2}$	rate	$\mathcal{R}_{\gamma,1}$	$\mathcal{R}_{\gamma,2}$	rate
1/10	5.63e − 3	5.63e − 3	–	1.98e − 2	1.98e − 2	–
1/20	1.44e − 3	1.44e − 3	1.97	1.13e − 2	1.13e − 2	0.81
1/40	3.63e − 4	3.63e − 4	1.99	6.08e − 3	6.08e − 3	0.89
h, $\delta = 0.2$, $\theta_n = \theta_\tau = 0, \frac{1}{2}, \frac{2}{3}$	$\mathcal{R}_{\Gamma_1}$	$\mathcal{R}_{\Gamma_2}$	rate	$\mathcal{R}_{\gamma,1}$	$\mathcal{R}_{\gamma,2}$	rate
1/10	3.78e − 2	3.78e − 2	–	3.95e − 2	3.95e − 2	–
1/20	1.22e − 2	1.22e − 2	1.63	2.25e − 2	2.25e − 2	0.81
1/40	3.07e − 3	3.07e − 3	1.99	1.21e − 2	1.21e − 2	0.89

5.2. Example 2: Model response to parameters

In this section we investigate the behavior of the reduced model with $\theta_n = \theta_\tau = 1/2$ when the parameters are modified, moving towards the values that resemble the characteristic ones for flow in a fractured reservoir. In particular, we progressively update the parameters δ, $\boldsymbol{K}$, s_0, $p|_{t=0}$ and the Young's modulus E, starting from the reference values considered in the previous section for numerical validation. The corresponding grid of new parameters is reported in Table 5. As in the previous example, we take $\alpha = 1$ and $\mu_f = 1$ (KPa s). The reservoir boundary conditions are modified to be suitable for a typical case of hydraulic fracturing. In particular, we enforce no flow on the entire reservoir boundary, while we prescribe zero displacement on Γ_1^4, Γ_2^2 and zero normal stresses on Γ_1^1, Γ_1^3, Γ_2^1, Γ_2^3. As in the previous example, on the bottom boundary of the fracture $\Gamma_1^1 \cap \Gamma_2^1$ we impose the Dirichlet boundary condition (3.15) for the tangential velocity, $U_\tau^D = 10$ (m/s), and the homogeneous Neumann boundary condition (3.16) for the normal velocity, $\mu_f \frac{\partial U_n}{\partial s} = 0$. On the top boundary of the fracture $\Gamma_1^3 \cap \Gamma_2^3$, we impose the homogeneous Neumann conditions (3.16) for mean stress. The final simulation time is $T = 100$ (s).

The results of cases A, B, C, D, E in Table 5 are reported in Figure 5 at the final time. On the left panels we show pressure, flow and displacement fields in the reservoir, on the right panel we show the pressure and velocity profile in the fracture. These results confirm that the scheme responds correctly to large changes in the parameter values as discussed below. We observe that in all cases, the flow and deformations are generated by injection of $Q = \delta U_\tau = 10^{-3}$ (m^3/s) of fluid into the fracture.

Flow analysis:

Case A. Due to the large value of hydraulic conductivity in equation (2.2), the pressure gradient is small, as confirmed by the pressure surface plot. Under the assumption of the uniform pressure field and small displacements, the mass balance equation (2.3) reduces to $Q = |\Omega| s_0 \partial_t p$, which entails that $\partial_t p = 5 \times 10^{-4}$.

TABLE 5. Example 2: Grid of parameters used in the numerical simulations of cases A,B,C,D,E.

	δ (m)	$\boldsymbol{K}$ (m^2/KPa s)	s_0 (KPa^{-1})	$p(0)$ (KPa)	E (KPa)
A	10^{-4}	1	1	0	10^3
B	10^{-4}	10^{-3}	1	0	10^3
C	10^{-4}	10^{-3}	10^{-2}	0	10^3
D	10^{-4}	10^{-3}	10^{-2}	10^3	10^3
E	10^{-4}	10^{-3}	10^{-2}	10^3	10^{10}

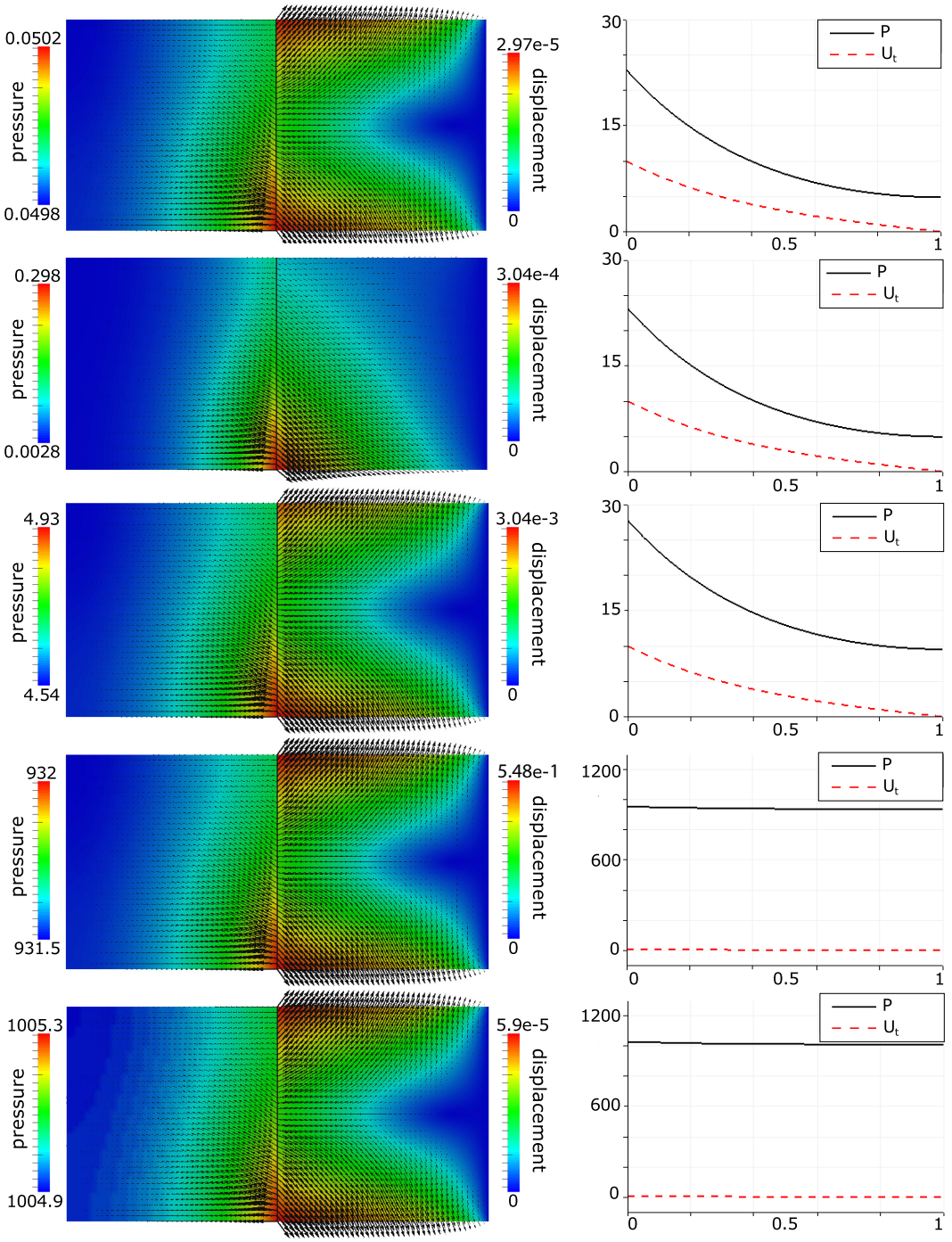

FIGURE 5. Example 2: Response of the model to variations of its parameters. Cases A, B, C, D, E of Table 5 are shown at the final time $T = 100$ (s) from top to bottom. Contour and vector plots on the left show the pressure p superimposed to the reservoir flow $\boldsymbol{q}$ depicted in Ω_1 combined with displacement magnitude and orientation in Ω_2. On the right we show the pressure and flow profile along the fracture γ.

As a result, at the final time $T = 100$ (s) we expect that $p \simeq 5 \times 10^{-2}$, which is confirmed by the numerical simulation.

Case B. Since the permeability decreases by three orders of magnitude, we expect to observe larger pressure gradients. From a visual inspection of the results, we notice that $(\max p - \min p) = 0.3$ for case B, while $(\max p - \min p) = 0.4 \times 10^{-3}$ in case A, which is consistent with the prescribed perturbation.

Case C. We superimpose to the previous effects a small mass storativity, which increases the pressure rate of change due to injection, according to equation (2.3). Proceeding as in case A we conclude that $\partial_t p = 5 \times 10^{-2}$ and after 100 s we expect to see $p(T) - p(0) \simeq 5$, which is indeed the case.

Case D, E. We analyze here the sensitivity of the model to the pressure initial conditions, which are increased to the level of 1000 (KPa) (*i.e.* 1 (MPa)) to mimic the high pressure conditions of a real reservoir. For a very stiff material, as in case E, we notice that the pressure field turns out to be the superposition of pressure fields B, C on top of a baseline pressure equal to 1000 (KPa), giving rise to $\max p \simeq 1005.3$. The linear superposition of pressure fields is not exactly satisfied for case D, which corresponds to a soft material. We believe that this effect depends on the interaction of the pressure and displacement governed by equation (2.3). More precisely, the pressure time derivative is not only affected by flow $\nabla \cdot \boldsymbol{q}$, but also by the volumetric deformation rates $\alpha \nabla \cdot \partial_t \boldsymbol{\eta}$.

Mechanical analysis:

Cases A, B, C. We notice that the displacement directly increases with the magnitude of the pressure. The displacement field of case B is different from A and C. We attribute this effect to the relative pressure gradient (*i.e.* the pressure gradient normalized with respect to the pressure magnitude), which is non negligible only for case B, leading to a non-symmetric distribution of stresses and deformations with respect to the layout of the boundary conditions. In all these cases, the displacement to pressure ratio is almost equivalent to the Young's modulus. As a result, we infer that for low pressure values, the poroelastic effects are governed by the coupling of the flow with the pressure time derivative, namely by equation (2.3), as illustrated in case C, while the mechanical deformations are mostly determined by the elastic stresses, namely $\boldsymbol{\sigma}_E$.

Cases D, E. The behavior of the system changes considerably for high pressures, as shown by cases D and E. In this regime, the fluid pressure and elastic mechanical stresses are comparable and they interact by means of the constitutive law $\boldsymbol{\sigma}_p = \boldsymbol{\sigma}_E - \alpha p \boldsymbol{I}$. This justifies why for large pressure values the displacement to pressure ratio and the Young's modulus are no longer directly related. In particular, we observe that the Young modulus of cases D and E differ by seven orders of magnitude, while the displacement changes by a factor two only, suggesting that in this case the component $\alpha p \boldsymbol{I}$ dominates over $\boldsymbol{\sigma}_E$. For test case D we have run simulations with $\alpha = 0$ instead of $\alpha = 1$, with the purpose of investigating the impact of poroelastic coupling on the displacement and flow fields. The results (not reported here) show that the variation of the parameter α has a noticeable effect on the orientation of the displacement field and we also observe a small variation in the pressure field.

5.3. Curved fracture configurations

We finally test our approach to model curved fractures. We consider two test cases. In the former we compare the flow and displacement fields calculated using the dimensionally reduced model with the full model for a curved fracture configuration where the fracture represents a preferential way for flow, namely its permeability is significantly higher than the one of the surrounding reservoir. In the latter, we address a fracture featuring a variable hydraulic conductivity and test different fracture boundary conditions, including a fracture that is completely confined into the reservoir.

5.3.1. Example 3: Comparison of the dimensionally reduced with the full model

The model parameters are $\delta = 0.1$ (m), $\boldsymbol{K} = 10^{-3}$ (m^2/KPa s), $s_0 = 10^{-2}$ (KPa^{-1}), $p(0) = 0$ (KPa), E=10^{10} (KPa), $\sigma = 0.3$, $\boldsymbol{K}_f = \boldsymbol{I}$, $c_{BJS} = 10^{-4}$, $\alpha = 1$ and $\mu_f = 1$ (KPa s). The computational domain is obtained from the one of Figure 2, after modifying the profile of γ to be curved. The extrema of the fracture

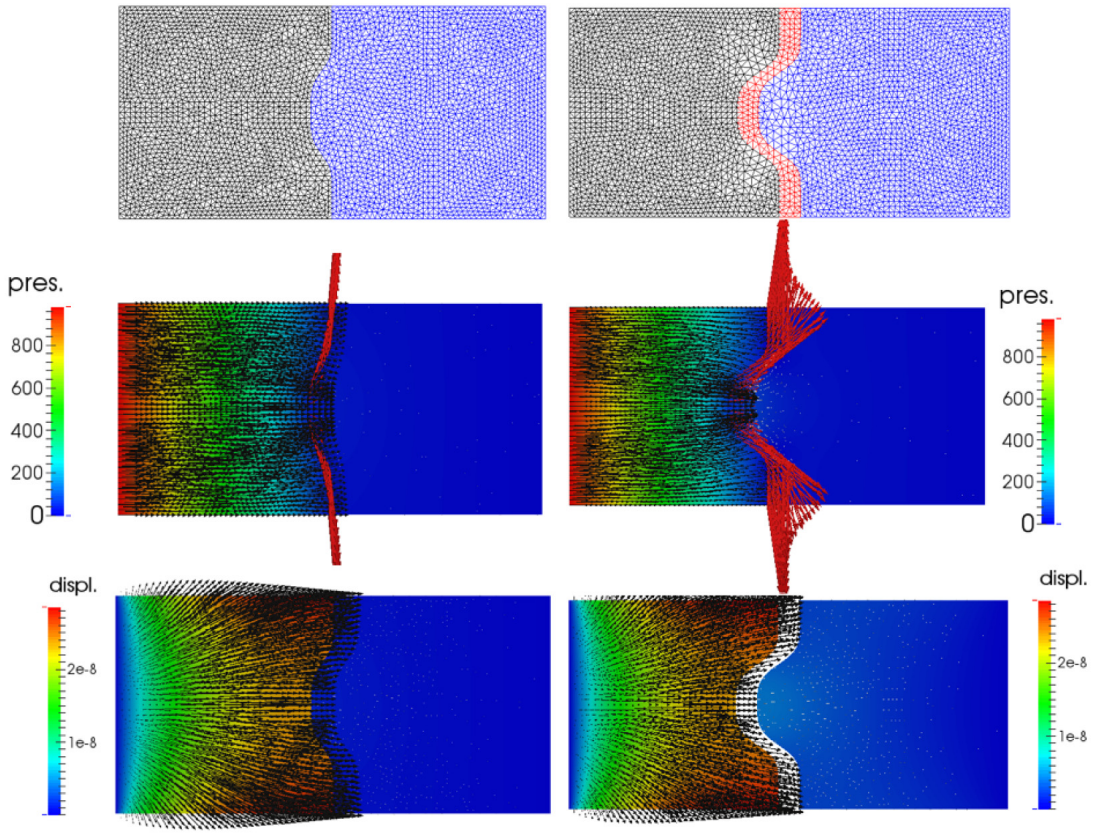

FIGURE 6. Example 3: Comparison of simulations for dimensionally reduced fracture model (*left*) and thick fracture model (*right*) at at $T = 100$ (s). Computational meshes, pressure contour plot and velocity fields, displacement magnitude and orientation are shown from top to bottom. Vector fields in Ω_1 are visualized in black, those in Ω_2 in white and those in Ω_f or γ in red. (Color online)

are however unchanged. On the boundary Γ_1^4 we enforce a uniform flow $\boldsymbol{q} \cdot \boldsymbol{n} = -1$ (m/s), on the horizontal sides we set $\boldsymbol{q} \cdot \boldsymbol{n} = 0$ and on Γ_2^2 null pressure is imposed. As in the previous example, we prescribe zero displacement on Γ_1^4, Γ_2^2 and zero normal stress on Γ_1^1, Γ_1^3, Γ_2^1, Γ_2^3. At the fracture boundaries we impose zero normal stress (3.16). As a result, this test case represents the flow through a reservoir that is cut by a fracture open at both endpoints. We expect the fracture to act as a gateway for flow, by carrying out the fluid injected from the left side of the domain. The final simulation time is $T = 100$ (s). We used $\Delta t = 1$ (s) and $h = 0.042$ (m).

The results for both the dimensionally reduced and the thick fracture models at T=100s are shown in Figure 6. They confirm a very good qualitative agreement of the full and dimensionally reduced models. As expected, in both cases most of the flow penetrating from the left side escapes through the fracture. Only a negligible amount of fluid extravasates to the right side of the domain. We observe that the flow direction in the neighborhood of the fracture deviates from the horizontal, because it is sensitive to the fracture configuration.

For a more quantitative comparison, we analyze mass conservation and the pressure variation across the interface. A flow rate $Q_{in} = \int_{\Gamma_1^4} \boldsymbol{q} \cdot \boldsymbol{n} = -1$ (m/s) is injected into the reservoir from the left. The peak velocity at both fracture endpoints is about $|\boldsymbol{U}| \simeq 5$ (m/s) in the vertical direction. Then we get $Q_{out} \simeq 2\delta|\boldsymbol{U}| = 1$ (m^2/s), confirming that the computed velocity field along the fracture is physically reasonable. In Figure 7 we study the

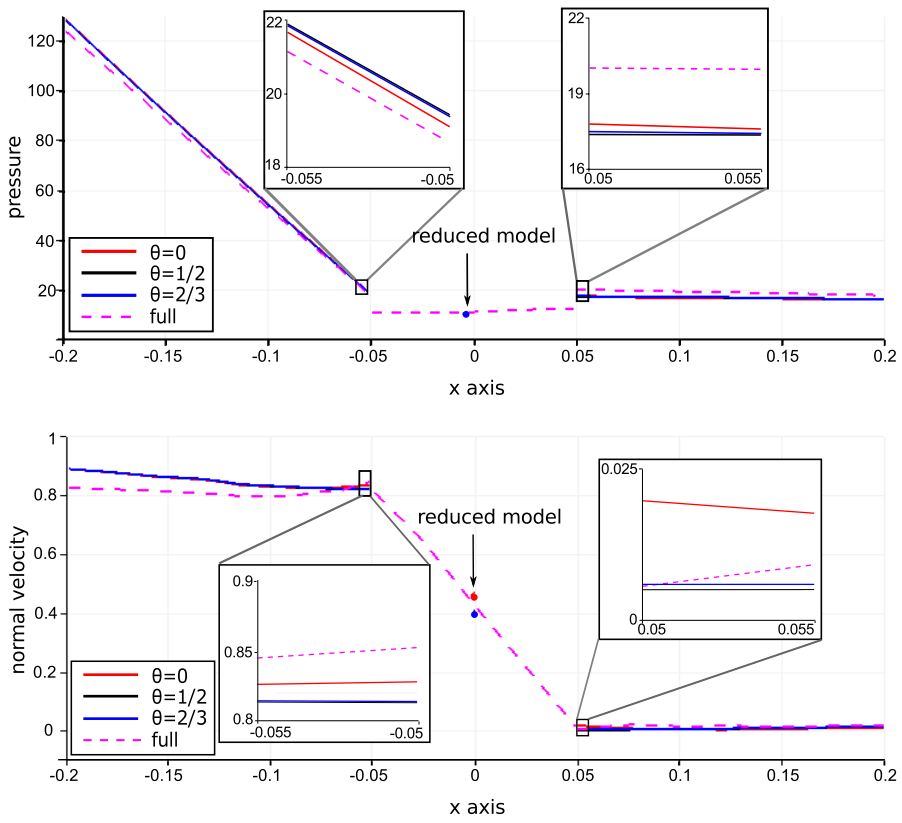

FIGURE 7. Example 3: Comparison of pressure profiles (*top*) and normal velocity (*bottom*) for $\theta_n = \theta_\tau = 0, 1/2, 2/3$ along a horizontal line $x \in (-0.2, 0.2)$, $y = 0.1$ in the fracture and reservoir at $T = 100$ (s).

comparison of the pressure profile (*top*) and the normal velocity (*bottom*) of the dimensionally reduced model and the full model, along a horizontal line cutting the interface γ from left to right. For visualization purposes only the interval $x \in (-0.2, 0.2)$, $y = 0.1$ is considered, in order to restrict the range of variation of the pressure. As expected, the pressure varies linearly on the left of the interface (located at $x = 0$), corresponding to a uniform flow towards the fracture, while the pressure profile is flat on the right, because there is almost no flow on the right. We observe that there is a small pressure jump across the fracture, according to the interface conditions (4.10)–(4.11). The pressure profiles corresponding the parameters values $\theta_n = \theta_\tau = 0, \frac{1}{2}, \frac{2}{3}$, are also compared. Small differences are observed in the values obtained using different closure conditions. In particular, the case $\theta_n = \theta_\tau = 0$ results in the smallest pressure jump, since the profiles for both pressure and velocity across the fracture are assumed constant. Of the other two cases, the case $\theta_n = \theta_\tau = \frac{1}{2}$ corresponds to a linear pressure profile and thus leads to a larger pressure jump when compared to the case $\theta_n = \theta_\tau = \frac{2}{3}$, even though the latter case assumes a quadratic velocity profile. The profile assumptions have even smaller effect on the normal velocity. Overall, the differences between the values obtained using different closure assumptions do not have a significant influence on the solution.

5.3.2. Example 4: Analysis of a fracture with variable conductivity.

Here we investigate how to adapt the model in order to describe multiple fractures embedded into the reservoir. Indeed, an embedded fracture can be modeled by means of no-flow boundary conditions at the

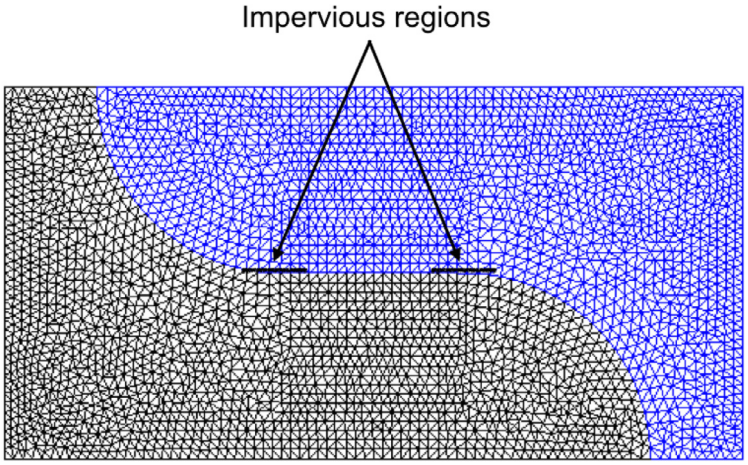

FIGURE 8. Example 4: The profile of the curved fracture where the impervious regions are highlighted with dark bars.

endpoints (3.15) that corresponds to conditions $U_\tau = 0$, $U_n = 0$. Furthermore, multiple (almost independent) embedded fracture segments can be modeled using a small hydraulic conductivity $\boldsymbol{K}_f$ at some regions of a connected fracture. In particular, $\boldsymbol{K}_f$ is equal to the permeability $\boldsymbol{K}$ of the surrounding material in the impervious regions, while it is higher elsewhere. As a result, away from the impervious regions, the fracture is more permeable than the surrounding rock. In this example we consider a curved fracture with hydraulic conductivity profile shown in Figure 8. The model parameters used in the simulation are $\delta = 0.1$ (m), $\boldsymbol{K} = 10^{-3}$ (m^2/KPa s), $s_0 = 10^{-2}$ (KPa^{-1}), $p(0) = 0$ (KPa), E=10^{10} (KPa), $\sigma = 0.3$, $c_{BJS} = 10^{-4}$, $\alpha = 1, \mu_f = 1$ (KPa s) $\boldsymbol{K}_f = \boldsymbol{K} = 10^{-3}$ (m^2/KPa s) in the impervious regions, $\boldsymbol{K}_f = 10^{-1}$ (m^2/KPa s) elsewhere. The boundary conditions are the same as in Example 3.

The results in Figure 9 suggest that the reduced model captures well the behavior of both open and closed (or embedded) fractures. In particular, in all cases it can be observed that the fracture represents a preferential path for the flow either in the longitudinal and transversal directions, in the regions of high conductivity. Conversely, the fracture represents an obstacle in the impervious regions. The comparison of panels A and B or C and D of Figure 9 illustrates the sensitivity of the model with respect to the fracture aperture δ. According to mass conservation law, smaller aperture means higher velocity field in the fracture. However, the total flow rate carried by the fracture decreases.

It is interesting to notice that for this new problem configuration, which features more complex and computationally challenging flow conditions, we observe a dependence of the numerical solution on the parameters θ_n, θ_τ used in the model reduction technique. Panels E and F of Figure 9 show the velocity field in the fracture for $\theta_n = \theta_\tau = 0$ (*color black*), $\theta_n = \theta_\tau = 1/2$ (color blue) and $\theta_n = \theta_\tau = 2/3$ (*color black*). It is apparent that the first case differs from the others, which are almost superposed. In particular, while in the cases $\theta_n = \theta_\tau = 1/2, 2/3$ the flow in the fracture is mostly tangential, it seems that in the case $\theta_n = \theta_\tau = 0$ the normal component of the flow is not negligible. This interpretation is supported by the analysis of the residual of the interface conditions, reported in Table 6. These data suggest that when $\theta_n = \theta_\tau = 0$ is used, the scheme can hardly satisfy the balance of normal components of velocities across the fracture, which is quantified by the indicator $-\int_\gamma (\frac{\partial \boldsymbol{\eta}_i}{\partial t} \cdot \boldsymbol{n}_i + \boldsymbol{q}_i \cdot \boldsymbol{n}_i - \boldsymbol{U} \cdot \boldsymbol{n}_i)|^*_{\Gamma_i}$. This property is more accurately satisfied by the other values of θ, which enable a better approximation of the flow inside the fracture. Although the flow seems to be physically reasonable and almost equivalent for $\theta_n = \theta_\tau = 1/2$ and $2/3$, interestingly, among these values the one with smallest residuals is the former.

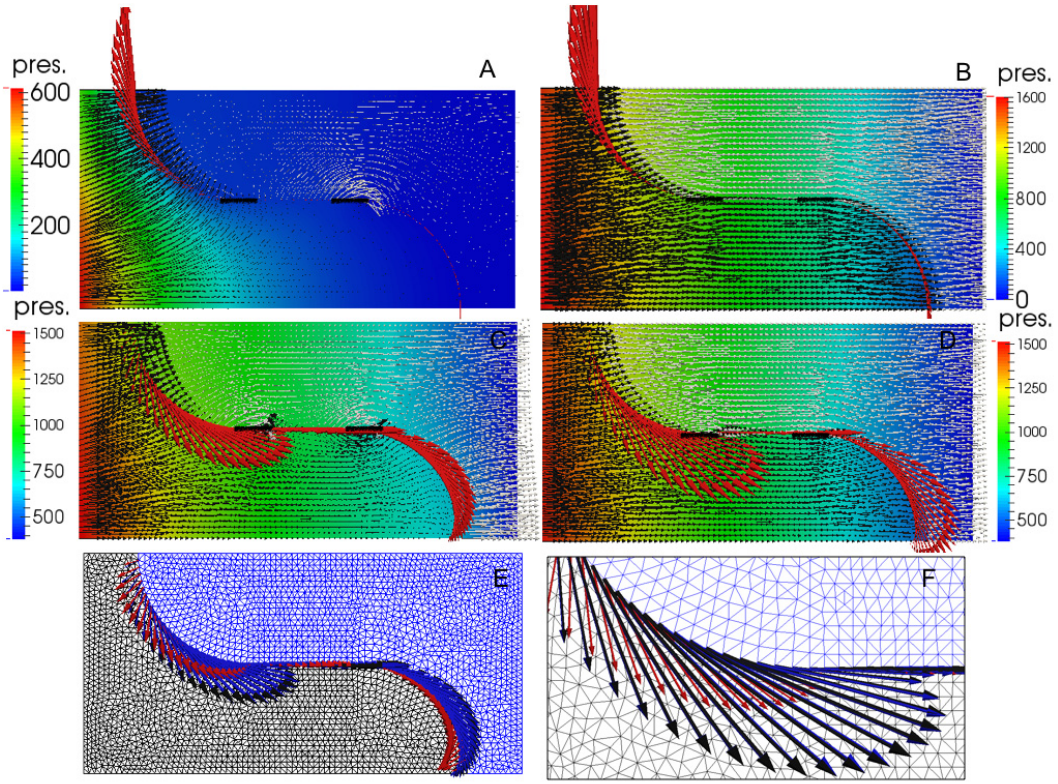

FIGURE 9. Example 4: Comparison of different model configurations for a fracture with variable permeability. Impervious regions are marked with dark bars. In panel A and B the fracture endpoints are open to flow, owing to boundary conditions (3.16), namely $\mu_f \partial_s U_\tau - P = 0,\ \mu_f \partial_s U_n = 0$. The parameters θ_n, θ_τ have been set to $\theta_n = \theta_\tau = 2/3$. For visualization purposes, different scaling factors have been adopted for the vector fields in $\Omega_1, \gamma, \Omega_2$. In panel A the fracture aperture is $\delta = 0.1(m)$ and the velocity in Ω_1 has been scaled by a factor 0.1, the one in γ by a factor 0.05 and the one in Ω_2 by a unit factor. The background color represents the pressure, namely p_p. In panel B the aperture is $\delta = 0.001(m)$ and the velocity in $\Omega_1,\ \Omega_2$ has been scaled by a factor 0.1, the one in γ by a factor 0.003. In panels C and D, we modify the boundary conditions to (3.15), namely $U_\tau = 0,\ U_n = 0$ (m/s) to model a fracture that is completely contained into the reservoir. In this plot, the scaling factor used for visualization of the vector fields is uniform and equal to 0.1. In panel D, for the same boundary conditions as in panel C, we modify the fracture aperture to $\delta = 0.01$ (m). Here, the scaling factor of the velocity in the fracture has been reduced to 0.05. In panel E we fix $\delta = 0.1$ (m) and we vary θ_n, θ_τ. Only the fracture velocity profile is shown. Simulations performed using $\theta_n = \theta_\tau = 0$ are reported in red, those using $\theta_n = \theta_\tau = 1/2$ are blue and the ones with $\theta_n = \theta_\tau = 2/3$ are black. Panel F shows a zoom of these vector fields. (Color online)

Remark 5.1. In Example 4, we also analyzed the response of the model to the friction coefficient c_{BJS} by performing a similar set of simulations using the value $c_{BJS} = \mu_f / \sqrt{\boldsymbol{K}}$, which is five orders of magnitude larger that the former. We observed no significant differences from visual inspection of the results, thus concluding that the model is rather insensitive to changes of the friction coefficient. Results from the simulations with $c_{BJS} = \mu_f / \sqrt{\boldsymbol{K}}$ are not shown.

TABLE 6. Example 4: The residuals of the interface conditions for the reduced model in the case of different values of $\theta_n = \theta_\tau$.

$\theta_n = \theta_\tau$	$-\int_\gamma (\frac{\partial \boldsymbol{\eta}_i}{\partial t} \cdot \boldsymbol{n}_i + \boldsymbol{q}_i \cdot \boldsymbol{n}_i - \boldsymbol{U} \cdot \boldsymbol{n}_i)\vert^*_{\Gamma_i}$	$\mathcal{R}_{\gamma_1}$
0	1.076e+00	8.672e-01
1/2	−5.314e-03	−5.456e-03
2/3	−8.542e-02	−9.919e-03

6. Conclusions

We have addressed the problem of modeling the flow into a fracture surrounded by a permeable poroelastic material. The main application is the simulation of hydraulic fracturing, which is a significant challenge, considering the extreme conditions under which this technology operates. In this work, we have shown that dimensional model reduction is a successful approach to account for the very heterogeneous scales of the problem in a coupled formulation. We have addressed for the first time, to our best knowledge, the topological reduction approach in the case of a poroelastic material coupled with a fracture flow model of Stokes/Brinkman type. Several variants of interface conditions have been analyzed and cast into a unified formulation depending on the parameter θ_n and θ_τ. The model has been complemented with a state of the art numerical scheme that has been analyzed. Numerical experiments confirm the validity of the approach and highlight the importance of using a poroelastic material formulation in hydraulic fracturing. In the three first examples, there were no significant differences between the results obtained using different values of $\theta_n = \theta_\tau$. However, in Example 4, $\theta_n = \theta_\tau = 0$ yields results that seem less accurate than $\theta_n = \theta_\tau = 1/2$ and $\theta_n = \theta_\tau = 2/3$. Furthermore, we did not notice significant differences in the results for different values of the coefficient c_{BJS}. Some considerable difficulties are only partially addressed here, such as modeling the tips of embedded fractures, and modeling the effect of material deformation on the aperture and on the flow into the fracture.

References

[1] P. Angot, Analysis of singular perturbations on the Brinkman problem for fictitious domain models of viscous flows. *Math. Methods Appl. Sci* **22** (1999) 1395–1412.

[2] P. Angot, F. Boyer and F. Hubert, Asymptotic and numerical modelling of flows in fractured porous media. *Math. Model. Numer. Anal.* **43** (2009) 239–275.

[3] T. Arbogast, L. C. Cowsar, M.F. Wheeler and I. Yotov, Mixed finite element methods on non-matching multiblock grids. *SIAM J. Numer. Anal.* **37** (2000) 1295–1315.

[4] S. Badia, A. Quaini and A. Quarteroni, Coupling Biot and Navier–Stokes equations for modelling fluid–poroelastic media interaction. *J. Comput. Phys.* **228** (2009) 7986–8014.

[5] G.S. Beavers and D.D. Joseph, Boundary conditions at a naturally impermeable wall. *J. Fluid. Mech.* **30** (1967) 197–207.

[6] M.A. Biot, Theory of elasticity and consolidation for a porous anisotropic solid. *J. Appl. Phys.* **26** (1955) 182–185.

[7] D. Boffi, F. Brezzi and M. Fortin, Mixed finite element methods and applications. Vol. 44 of *Springer Series in Computational Mathematics*. Springer, Heidelberg (2013).

[8] M. Bukač, I. Yotov, R. Zakerzadeh and P. Zunino, Partitioning strategies for the interaction of a fluid with a poroelastic material based on a Nitsches coupling approach. *Comput. Methods Appl. Mech. Engrg.* **292** (2015) 138–170.

[9] M. Bukač, I. Yotov and P. Zunino, An operator splitting approach for the interaction between a fluid and a multilayered poroelastic structure. *Numer. Methods Partial Differ. Equ.* **31** (2015) 1054–1100.

[10] A.P. Bunger and E. Detournay, Experimental validation of the tip asymptotics for a fluid-driven crack. *J. Mech. Phys. Solids* **56** (2008) 3101–3115.

[11] P. Ciarlet, The finite element method for elliptic problems. Vol. 4. North Holland (1978).

[12] C. D'Angelo and A. Scotti, A mixed finite element method for Darcy flow in fractured porous media with non-matching grids. *ESAIM: M2AN* **46** (2012) 465–489.

[13] M. Discacciati, E. Miglio and A. Quarteroni, Mathematical and numerical models for coupling surface and groundwater flows. *Appl. Numer. Math.* **43** (2002) 57–74.

[14] A. Ern and J.-L. Guermond, Theory and practice of finite elements. Vol. 159 of *Appl. Math. Sci.* Springer-Verlag, New York (2004).

[15] N. Frih, V. Martin, J.E. Roberts and A. Sada, Modeling fractures as interfaces with nonmatching grids. *Comput. Geosci.* **16** (2012) 1043–1060.

[16] N. Frih, J.E. Roberts and A. Saada, Modeling fractures as interfaces: A model for Forchheimer fractures. *Comput. Geosci.* **12** (2008) 91–104.

[17] A. Fumagalli and A. Scotti, Numerical modelling of multiphase subsurface flow in the presence of fractures. *Commun. Appl. Ind. Math.* **3** (2012) e–380, 23.

[18] B. Ganis, V. Girault, M. Mear, G. Singh and M.F. Wheeler, Modeling fractures in a poro-elastic medium. *Oil Gas Sci. Technol.* **69** (2014) 515–528.

[19] B. Ganis, M. E. Mear, A. Sakhaee-Pour, M. F. Wheeler and T. Wick, Modeling fluid injection in fractures with a reservoir simulator coupled to a boundary element method. *Comput. Geosci.* **18** (2014) 613–624.

[20] V. Girault, D. Vassilev and I. Yotov, Mortar multiscale finite element methods for Stokes-Darcy flows. *Numer. Math.* **127** (2014) 93–165.

[21] V. Girault, M.F. Wheeler, B. Ganis and M.E. Mear, A lubrication fracture model in a poro-elastic medium. *Math. Models Methods Appl. Sci.* **25** (2015) 587–645.

[22] E. Gordeliy and A. Peirce, Implicit level set schemes for modeling hydraulic fractures using the XFEM. *Comput. Methods Appl. Mech. Engrg.* **266** (2013) 125–143.

[23] P. Grisvard, Elliptic problems in nonsmooth domains. Pitman, Boston (1985).

[24] F. Hecht, New development in FreeFem++. *J. Numer. Math.* **20** (2012) 251–265.

[25] J. Jaffre, M. Mnejja and J.E. Roberts, A discrete fracture model for two-phase flow with matrix fracture interaction. *Procedia Comput. Sci.* **4** (2011) 967–973.

[26] J. Jaffre and J.E. Roberts, Modeling flow in porous media with fractures; discrete fracture models with matrix-fracture exchange. *Numer. Anal. Appl.* **5** (2012) 162–167.

[27] W. J. Layton, F. Schieweck and I. Yotov, Coupling fluid flow with porous media flow. *SIAM J. Numer. Anal.* **40** (2002) 2195–2218.

[28] M. Lesinigo, C. D'Angelo and A. Quarteroni, A multiscale Darcy–Brinkman model for fluid flow in fractured porous media. *Numer. Math.* **117** (2011) 717–752.

[29] J.L. Lions and E. Magenes, Non-homogeneous boundary value problems and applications, vol. 1. Springer-Verlag (1972).

[30] V. Martin, J. Jaffre and J.E. Roberts, Modeling fractures and barriers as interfaces for flow in porous media. *SIAM J. Sci. Comput.* **26** (2005) 1667–1691.

[31] A. Mikelić and M. F. Wheeler, On the interface law between a deformable porous medium containing a viscous fluid and an elastic body. *Math. Models Methods Appl. Sci.* **22** (2012) 1250031, 32.

[32] A. Mikelić and M. F. Wheeler, Convergence of iterative coupling for coupled flow and geomechanics. *Comput. Geosci.* (2013) **17** 455–461.

[33] A. Mikelic, M.F. Wheeler and T. Wick, A phase-field method for propagating fluid-filled fractures coupled to a surrounding porous medium. *Multiscale Model Simul.* (2015).

[34] F. Morales and R. E. Showalter, The narrow fracture approximation by channeled flow. *J. Math. Anal. Appl.* **365** (2010) 320–331.

[35] Fernando Morales and Ralph E. Showalter, Interface approximation of Darcy flow in a narrow channel. *Math. Methods Appl. Sci.*, 35(2):182–195, 2012.

[36] E.-J. Park, Mixed finite element methods for generalized Forchheimer flow in porous media. *Numer. Methods Partial Differ. Equ.* **21** (2005) 213–228.

[37] P.J. Phillips and M.F. Wheeler, A coupling of mixed and continuous Galerkin finite element methods for poroelasticity I: The continuous in time case. *Comput. Geosci.* **11** (2007) 131–144.

[38] P.J. Phillips and M.F. Wheeler, A coupling of mixed and continuous Galerkin finite element methods for poroelasticity II: The discrete-in-time case. *Comput. Geosci.* **11** (2007) 145–158.

[39] P.J. Phillips and M. F. Wheeler, A coupling of mixed and discontinuous Galerkin finite-element methods for poroelasticity. *Comput. Geosci.* **12** (2008) 417–435.

[40] K. R. Rajagopal, On a hierarchy of approximate models for flows of incompressible fluids through porous solids. *Math. Models Methods Appl. Sci.* **17** (2007) 215–252.

[41] J. Rungamornrat and M.E. Mear, SGBEM-FEM coupling for analysis of cracks in 3D anisotropic media. *Int. J. Numer. Methods Engrg.* **86** (2011) 224–248.

[42] P.G. Saffman, On the boundary condition at the surface of a porous media. *Stud. Appl. Math.* **50** (1971) 93–101.

[43] L.R. Scott and S. Zhang, Finite element interpolation of nonsmooth functions satisfying boundary conditions. *Math. Comput.* **54** (1990) 483–493.

[44] R.E. Showalter, Poroelastic filtration coupled to Stokes flow. In Control theory of partial differential equations. In vol. 242 of of *Lect. Notes Pure Appl. Math.* Chapman & Hall/CRC, Boca Raton, FL (2005) 229–241.

[45] K. Terzaghi, R.B. Peck and G. Mesri, Soil Mechanics in Engineering Practice. Wiley-Interscience publication. Wiley (1996).